NATIONAL TECHNICAL UNIVERSITY OF ATHENS

SCHOOL OF NAVAL ARCHITECTS AND MARINE ENGINEERS

DIPLOMA THESIS

A Probabilistic Analysis of Ship Rolling Under the Influence of Irregular Wave Groups

PANAYIOTIS ANASTOPOULOS

SUPERVISOR: Professor Konstantinos J. Spyrou

ACKNOWLEDGEMENTS

During my studies at the School of Naval Architecture and Marine Engineering, a wide range of scientific fields concerning shipbuilding, ship design and machinery was presented. However, ship stability drew my attention as a field foreseen to offer a lot of scientific knowledge through extended study. Consequently, this thesis represents my research effort in the field of ship stability as well as the knowledge derived from a five-year period of hard study at the School.

I would like to express my sincere gratitude to my supervisor Professor K. Spyrou for his support during the preparation of this thesis. His valuable knowledge provided me with all the necessary background to face the difficulties met on the way to complete this study. Moreover, he gave me the inspiration and encouragement to select ship stability as the field associated with my thesis. Finally, I would like to thank him because through the assignment of the subject analyzed in this thesis, he gave me the opportunity to study ship stability from a very interesting aspect.

Furthermore, of utmost importance was the help, comments and guidance provided by Dr. Nikos Themelis. I feel indebted for the precious time he spent whenever I needed his advice. His contribution to the completion of this thesis is invaluable.

Last but not least, I would like to thank my family as without their help, support and understanding it would be very difficult to finish my studies.

CONTENTS

LIST OF FIGURES

LIST OF TABLES

ABSTRACT

This study deals with the effects of realistic waves (called as “irregular”) on ship stability in beam seas and it is consisted of two parts:

The purpose of the first part is to make an introduction to the principal theory of wave group modeling. The employed theory is Paolo Boccotti’s “Quasi-Determinism theory” and it is presented to the appropriate and sufficient for the purposes of this thesis extent. In this theory the most probable non regular (this term can be considered as equivalent to the potentially more widely used one: “non harmonic”) waveform is modeled when the sea state conditions are defined. In the first formulation of the theory the most probable waveform is developed if a large crest occurs, whilst in the second one when a large crest-to-trough height arises. Because of the fact that Boccotti’s developed theory is exact to the first order in a Stokes expansion, the second-order corrections according to the studies and research of Felice Arena are also displayed. In the end, extended applications of the theory are presented and critical observations are either made or verified. At the end of this part, all the necessary conclusions are outlined and the essential background so as to proceed in further research concerning ship stability is finally obtained.

In the second part, the Quasi-Determinism theory, with all the implied consequences, is used to establish a solid mathematical model concerning ship rolling in beam seas. In this deterministic part of the analysis, ship’s correspondence to irregular excitation is examined and compared to the regular one. Wave groups, regular or not, resulting in critical ship inclination according to the “Weather Criterion” are identified and noted as “critical”. Moreover, two different probabilistic approaches for encountering critical wave groups are introduced. In the first method the waves constituting the wave group are treated as a Markov Chain sequence (“Wave Group theory”), while the second one deals with the probability of occurrence for the central wave of the group (“Central Wave theory”). The latter probabilistic methodology is based on a corollary of the Quasi-Determinism theory presented in Part I. Eventually, after the probabilistic background of this study is obtained, the final probability rate of ship instability is calculated. The final outcome of this thesis is the recommendation of a new modeling method, regarding the phenomenon of ship rolling in a more realistic and applicable way.

CHAPTER I:

INTRODUCTION

In the current chapter a brief introduction is made to the basic concepts and the structural chapters of this thesis.

With the growth of maritime transportations naval society has to face more complex problems than ever before. It is an indisputable fact that the ship's stability is strongly connected with the safety level provided by the ship to its passengers, crew and cargo and eventually the maximization of her survivability.

Definitely, during the last decade, significant progress has been made in the field of ship safety against capsizing. Yet in spite of the rapid progress made, a wide scope of aspects regarding ship dynamics remains to be explored. Whilst numerous scientific and practical challenges continuously arise, widely accepted methods depicting the laws of nature have to be established. Gradually, several remarkable studies have come to light giving the necessary tools to interpret the ocean mechanics. Taking all the advantages deriving from such extended research and experiments, more accurate predictions of extreme motion for intact and damaged vessels can be reached.

As it follows from the previously addressed prevailing conditions, ship stability assessment methods need to be reinforced. Thus, the main purpose of this study will be to develop a new as well as solid probabilistic framework aiming to a settled stability assessment procedure. In this thesis the benefits of a semi-deterministic method for modeling irregular wave groups are reaped. Consequently, the method preludes a more realistic approach on ship stability rather than employing a theory based on harmonic waves, no matter how popular regularity in wave effects is regarded. The differences will be outlined in the following sections inferring critical conclusions.

The analysis made in the next pages targets to point out the discrepancies of the aforementioned approaches dealing with ship rolling. In the first part of the thesis, the concepts of wind generated waves, which will involve the excitation force for ship rolling motions, are introduced, whilst in the second one the new probabilistic assessment methodology in the field of ship stability is developed. In more detail:

In chapter II a brief outline of the aims of the current thesis is given.

In chapter III an introduction is made to the main principals of wind generated waves.

In chapter IV Boccotti's "Quasi-Determinism theory" is presented and finally employed for practical applications.

In chapter V the mathematical model for ship rolling that will be used for further analysis is displayed.

In chapter VI the probabilistic treatment of wave groups is recommended and the stability assessment procedure is eventually settled.

In chapter *VII* application of the assessment methodology has been demonstrated through an extended example. A ROPAX ferry has been investigated if it is prone to capsizing in non regular beam seas for different sea state scenarios. Stability assessment diagrams are displayed and critical comments are eventually made.

I.1 *Wind generated waves*

One of the first things a man will notice by looking at the ocean is the presence of waves. Ancient Greeks were the first to play an important role to the conception of the realistic seaway. The interaction between the air and sea surface in the formation of ocean waves has been observed since then. However, very little progress has been made from the ancient times to the 19th century. It was that period when the scientific outburst of Airy (1801-1892), Stokes (1819-1903) and Rayleigh (1842-1919) gave important contributions to the knowledge of ocean waves.

Undoubtedly, the most important sea waves in a wave spectrum are those generated by the wind. Wind-generated waves are much more complex than the simple monochromatic waves considered in earlier times. The quantification of wind-generated waves for the purposes of various engineering analyses is invaluable only by taking into consideration the stochastic nature of the sea (fig. *1.1*). It is important to be able to predict these waves for a given sea or wind condition - both wave hindcasts for historic wind conditions and wave forecasts for predicted impending wind and sea state conditions. Finally, we also need to look at procedures for extreme wave analysis, i.e., to predict those extreme wind-generated wave conditions that will be used as the limit for engineering design.

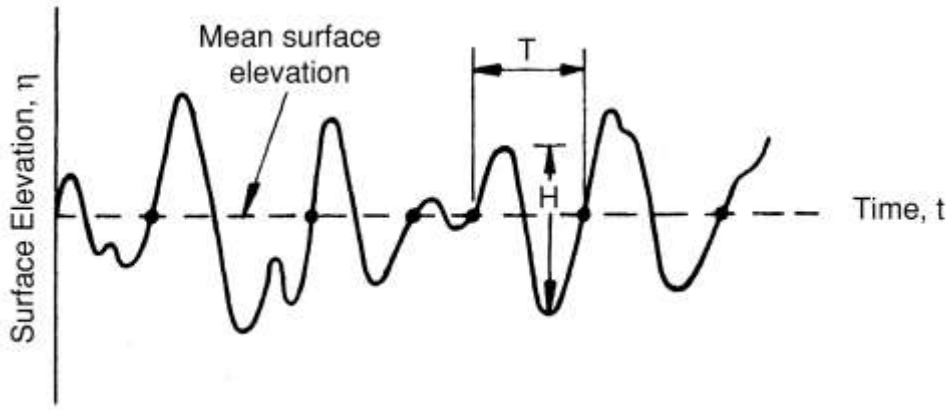

Figure 1.1: Typical water surface elevation versus time record (taken from Boccotti, 2000)

I.2 *Ship stability in beam seas*

Ships, and therefore ship stability, is of vital importance for the transportation of humans, as well as providing the only means of transporting heavy cargoes between the

continents. Thus, it is an essential part of a ship designer's work to obtain all the acquired knowledge so as to proceed in the quantification of ship stability.

Ship stability seems to originate from Archimedes' early times. However, it was not until 1746 when Bouguer introduced the concept of metacentric height as a quantified magnitude of ship stability. Derivation and calculation procedures for the righting lever curves were published by Atwood in 1796. Moseley in 1850 founded quasi dynamic stability over the concept of the energy balance methods. In 1874 William Froude's experimental results on H.M.S. Devastation rolling responses came to the scene. Several proposals for the use of a GM based stability criteria were offered in the late 1800s and proposals for criteria based on righting energy have existed since the early 1900s. The major historical work on the stability of ships was by Rahola in 1939. Rahola's work involved a detailed analysis of Baltic ship capsizing and included a proposal for a GZ based criteria. Wind heel GM requirements have been applied in the US since 1949 and became a US requirement for cargo ships in 1952. Based on recommendations from the 1960 International Conference on the Safety of Life at Sea (SOLAS 60), the IMCO sub-committee on Subdivision and Stability was formed in 1962. The first international stability criterion, Resolution A.167, largely based on Rahola's GZ criteria, was adopted by the IMO in 1968 for ships less than 100m long. The IMO assembly adopted Resolution A.562 in 1985. This resolution is an energy balanced criterion, but also includes a wind heel recommendation, and is to be used as a supplement to A.167.

In general, ships can experience three types of displacement motions (heave, sway or drift, and surge) and three angular motions (yaw, pitch, and roll) as shown in figure *1.2*. Capsizing is related to the extreme motion of the ship in wave phenomena. Of the six motions experienced by a vessel, the roll oscillation is the most critical motion that might lead to the ship capsizing. For small angles of roll motions, the response of ships can be described by a linear equation. However, as the amplitude of oscillation increases, nonlinear effects come into the scene. Generally speaking, the environmental loadings are nonlinear and beyond the control of the designer. For this reason, a critical matter to be investigated is, when nonlinearity can magnify small variations in excitation to the point where the restoring force contributes to capsizing. The nonlinearity is due to the nature of restoring moment and damping and their nonlinearity depends on the shape of the righting arm diagram.

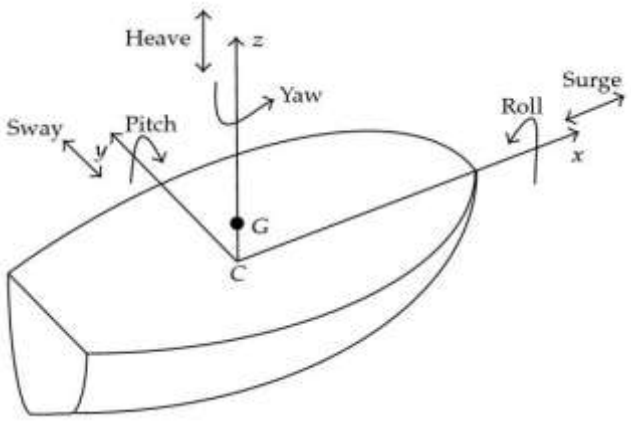

Figure 1.2: Ship schematic diagram showing the six degrees of freedom

CHAPTER II:

OBJECTIVES

The main objectives of this thesis can be stated as:

- To improve probabilistic assessment methodologies that were developed under the consideration of regular wave group effects on ship intact stability.

- To highlight the differences of critical importance between regular and irregular wave group effects on ship rolling motion.

- To study the scientific areas that underlie the methodology; such as, ship dynamic stability, main probabilistic methods of ship rolling, stochastic waves and particularly wave group theory.

- To apply the developed methodology and interpret the final results as far as their rationality is concerned.

PART *I*

On irregular very large sea wave groups

CHAPTER III:

WIND GENERATED WAVES: BASIC CONCEPTS

This chapter aims to present the necessary background and basic concepts of the Quasi-Determinism theory, which will be examined in the next chapter.

III.1 *The theory of sea states (Boccotti, 2000)*

By the term *ideal sea state* we mean an infinitely long stationary stochastic process concerning wind generated waves. To understand this definition, we will follow a simple repetitive procedure: Let us gather a number of sets of N consecutive waves so as to estimate the mean height and period for each of these sets: $\overline{H}_1$, $\overline{T}_1$ will be respectively the mean wave height and the mean wave period of the first set, $\overline{H}_2$, $\overline{T}_2$ will be the mean wave height and the mean wave period of the second set, and so on. For a small N, say $N = 5$, the pairs $(\overline{H}_1, \overline{T}_1)$, $(\overline{H}_2, \overline{T}_2)$, ... will generally be very different from one another. However, as N grows, the differences between these pairs will tend to vanish, and as $N \to \infty$ all the pairs will become equal to each other. This is a simple way to introduce the ideal sea.

On the other hand, by the term *real sea state* we mean a sequence of a few hundred wind-generated waves (typically $100 \div 300$ waves). Such a sequence is sufficiently short to be nearly stationary and it is long enough for its statistical properties to be meaningful. In simple words, we deal with a wave sequence drawn from an ideal sea state with its mean wave height and period verging to the mean wave height and period of this ideal sea state.

At this point, it is of great importance to understand the differences between a *wind generated wave* and a *swell*:

In fluid dynamics, wind waves or, more precisely, wind-generated waves are surface waves that occur on the free surface of oceans, seas, lakes, rivers, and canals or even on small puddles and ponds. They usually result from the wind blowing over a vast enough stretch of fluid surface. Waves in the oceans can travel thousands of miles before reaching land. Wind waves range in size from small ripples to huge waves over 30 meters high.

When directly being generated and affected by the local winds, a wind wave system is called a wind sea. After the wind ceases to blow, wind waves are called *swell*. Or, more generally, a swell consists of wind generated waves that are not - or are hardly - affected by the local wind at that time. They have been generated elsewhere, or some time ago.

Wind waves have a certain amount of randomness: subsequent waves differ in height, duration and shape, with a limited predictability. They can be described as a stochastic process, in combination with the physics governing their generation, growth, propagation and decay - as well as governing the interdependence between flow quantities such as: the water surface movements, flow velocities and water pressure. The key statistics of wind waves (both seas and swells) in evolving sea states can be predicted with wind wave models, one of them will be briefly introduced in the following chapter and described in more detail in chapter VI.

Now, let us choose an arbitrary point (which will be noted as a "node") at sea and record surface elevation $\eta(t)$ at this fixed point. When a sea storm provokes a certain surface elevation in the vicinity of the node, the record $\eta_1(t)$ is obtained. If the same sea storm is repeated in the same way affecting the vicinity of the node with the same manner, a second record $\eta_2(t)$ is obtained. When this procedure is repeated for many times, the records, $\eta_3(t), \dots\dots\dots \eta_n(t)$ are eventually gathered.

According to the theory of the sea states to the first order in a Stokes expansion (Boccotti, 2000), each of the n time series $\eta_1(t)$, $\eta_2(t)$, $\eta_3(t), \dots\dots\dots \eta_n(t)$ is a piece of a new realization of a stationary Gaussian process. Each realization of this process has an infinite duration and thus it represents the ideal sea state introduced in the previous section. The analytical form of the process is:

$$\eta(t) = \sum_{i}^{N} a_i \cos(\omega_i t + \varepsilon_i) \tag{3.1}$$

where it is assumed that frequencies ω_i are different from each other, number N is infinitely large, phase angles ε_i are uniformly distributed into $(0,2\pi)$ and are stochastically independent of each other, and all amplitudes a_i are of the same order. Finally, the frequency spectrum $E(\omega)$, shown in fig. *3.1*, which is defined as:

$$E(\omega)\delta\omega = \sum_i \frac{1}{2} a_i^2 \quad \textit{for } i \textit{ such that } \omega_i \textit{ belongs to the small interval of amplitude } \delta\omega.$$

is assumed to be continuous and to be the same in each realization. Under these hypotheses, eq. (3.1) represents a stationary Gaussian random process which is exact to the first order in a Stokes expansion as it was mentioned before.

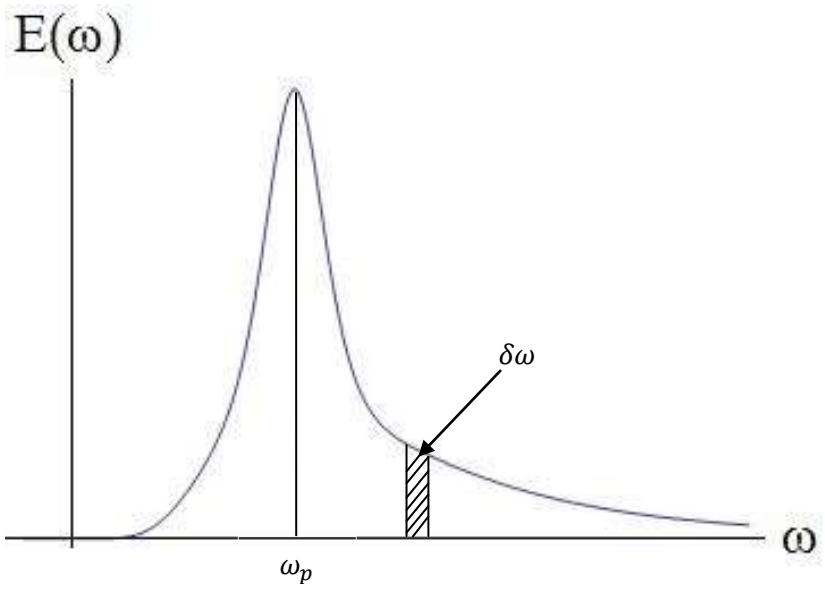

Figure 3.1: Definition of spectrum: the small noted area is equal to the partial sum $\sum_i \frac{1}{2} a_i^2$, for i such that ω_i belongs to the small interval of amplitude $\delta\omega$

III.2 *Basic equations in the theory of sea states*

At this point standard definitions and basic relations regarding the theory of sea states shall be displayed:

- Standard deviation

$$\sigma \equiv \sqrt{< \eta^2(t) >} \tag{3.2}$$

The larger the σ , the higher the waves.

- Significant wave height

$$H_s \equiv 4\sigma \tag{3.3}$$

The first theories (in the 50's) gave H_s, as equal to $H_{1/3}$ that is the average height of the highest one-third of all the waves of a particular sea state. Nowadays, with the growth of modern ocean engineering, we know that $H_{1/3}$ is systematically smaller (of 5÷10%) with respect to 4σ. Nevertheless, H_s is still used for the strength of the wave motion.

- Root Mean Square wave height

$$H_{rms} = 2\sqrt{2m_0} \tag{3.4}$$

where, the symbol m_j denotes the *j*th order moment of the spectrum:

$$m_j = \int_0^\infty \omega^j E(\omega) d\omega \tag{3.5}$$

Other typical statistical quantities can also be expressed in terms of the zero-moment, if we assume a common Rayleigh distribution:

Mean $H = \bar{H} = \sqrt{2\pi m_0}$, Median $= \sqrt{2\pi m_0}$, Mode $H = 2\sqrt{m_0}$.

The temporal structure of waves (i.e., the period) is more difficult to characterize. There are three different definitions, which reach into three different results. They are:

- The peak period is the wave period associated with the peak frequency[1]:

$$T_p = 2\pi/\omega_p \tag{3.6}$$

- Average period between increasing zero-crossings

$$\bar{T}_z = T_{02} = 2\pi\sqrt{m_0/m_2} \tag{3.7}$$

- Average wave period

$$\bar{T} = T_m = T_{10} = 2\pi\, m_0/m_1 \tag{3.8}$$

- Average period between crests

$$\bar{T}_z = 2\pi\sqrt{m_2/m_4} \tag{3.9}$$

After all the necessary statistical quantities related to the theory of sea states are displayed, it should be highlighted that from now on the term “defined sea state conditions” will be equivalent to the definition of the significant wave height and the peak spectral period (H_s, T_p).

III.3 *The autocovariance function*

The definition of the *autocovariance* is

$$\psi(T) \equiv < \eta(t)\eta(t+T) > \tag{3.10}$$

[1] The peak frequency (ω_p) is the frequency of the highest peak of the spectrum.

and thus it is the mean value of the product of the surface displacement at time t and surface displacement at the later time $t+T$.

The definition of autocovariance may look abstract for the time being but we shall see in the following chapter that this specific function takes on a central role in the light of the Quasi-Determinism theory.

The relation between variance and autocovariance of the surface displacement and spectral function are respectively given below:

$$< \eta^2(t) >= \int_0^\infty E(\omega)d\omega \qquad \textit{or equivalently} \qquad \sum_i \frac{1}{2}a_i^2 = \int_0^\infty E(\omega)d\omega \quad (3.11a,b)$$

And

$$< \psi(T) >= \int_0^\infty E(\omega)cos(\omega T)d\omega \quad \textit{or equivalently} \quad \psi(T) = \sum_i \frac{1}{2}a_i^2\, cos(\omega_i T) \quad (3.12a,b)$$

The first equation of the second set of the above given equation (3.12a) is strongly connected with another relation of the form:

$$E(\omega) = \frac{2}{\pi}\int_0^\infty \psi(T)cos(\omega T)dT \tag{3.13}$$

This pair of equations is very well known in literature as the ***Wiener-Khinchin*** equations.

III.4 *A mathematical form of a wind wave spectrum: the JONSWAP spectrum*

When a wind generates waves and hence waves and wind have nearly the same direction, we speak of wind waves. Such waves typically have a spectrum where $E(\omega)$ approaches rapidly zero on the left side and approaches zero more gradually on the right side. A mathematical form suggested for describing this characteristic spectrum shape is (DNV 2002):

$$E(\omega) = \alpha_w g^2 \omega^{-5} exp\left(-\frac{5}{4}\left(\frac{\omega}{\omega_p}\right)^{-4}\right)\gamma^{exp\left(-0.5\left(\frac{\omega-\omega_p}{\sigma\omega_p}\right)^2\right)} \tag{3.14}$$

where

$$\alpha_w = \frac{5}{16}\left(\frac{H_s^2\omega_p^4}{g^2}\right)A_\gamma \tag{3.15}$$

$$A_\gamma = 1 - 0.287\ln(\gamma) \tag{3.16}$$

$$\sigma = \begin{cases} 0.07 & if \quad \omega \le \omega_p \\ 0.09 & if \quad \omega > \omega_p \end{cases} \tag{3.17}$$

The JONSWAP spectrum was the final result of a work developed in the 50's and 60's. Phillips was the first to observe in the 50's that the spectrum approaches zero, for large ω, as ω^{-5}. The term $\alpha_w g^2 \omega^{-5}$ in the above given formula is due to him, and indeed α_w is called the *Phillips parameter.* The form $E(\omega) = \alpha_w g^2 \omega^{-5} exp\left(-\frac{5}{4}\left(\frac{\omega}{\omega_p}\right)^{-4}\right)$ was introduced by Pierson and Moskowitz in the 60's. The last improvement, that is the introduction of the second exponential function, was due to the JONSWAP project in the early 70's. We should note though that this spectrum is effective under the assumption of deep water. The two proposed spectra are given in fig. *3.2*.

According to the researchers of the JONSWAP project, the more characteristic values of the shape parameters γ and σ are:

$$\gamma = 3.3 \quad , \quad \sigma = 0.08$$

If the above given values of shape parameters are considered then we deal with the so called *mean JONSWAP* spectrum.

In the end, it is important to define the relation between T_p and H_s for the JONSWAP spectrum:

$$T_p = \sqrt[4]{\frac{1}{0.305\alpha_w}}\ 2\pi\sqrt{\frac{H_s}{4g}} \tag{3.18}$$

The value of α_w depends on the characteristics of the wave generation. A very usual value for design conditions is $\alpha_w = 0.01$, through which, relation (3.18) is formed as:

$$T_p = 8.5\pi\sqrt{\frac{H_s}{4g}} \tag{3.19}$$

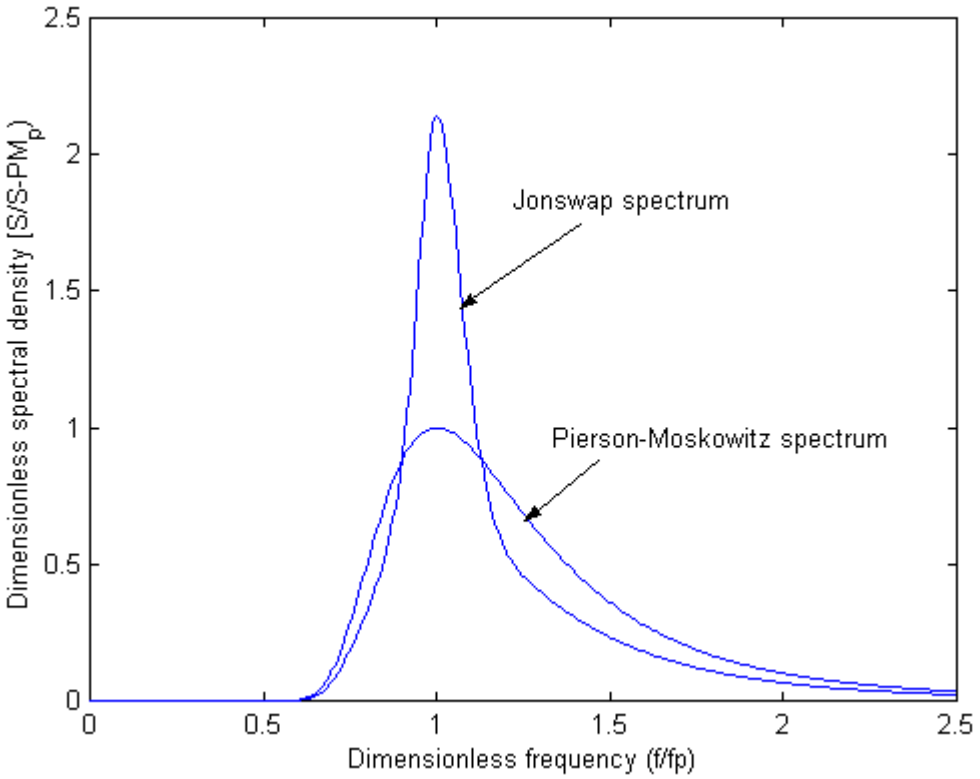

Figure 3.2: The mean JONSWAP spectrum compared to the Pierson-Moskowitz spectrum

III.5 *Inferring the nature of waves from the bandwidth: the concept of an infinitely narrow spectrum*

The practical meaning of a random process to be considered as narrow band or not, will be explained in this paragraph. For a narrow band spectrum, there is great concentration of the so called "spectral mass", around a specific central angular frequency $\bar{\omega}$, as it is shown in fig. *3.3*. So, in this case, a stochastic process $X(t;\beta)$ represents a waveform (though irregularities are possible to be observed due to the introduced elements of randomness) through which it is feasible to define a meaningful mean wave period [see fig. *3.4*]. This mean period can be approximately expressed either through the peak period (T_p) or the mean period (T_m), as they are defined in section III.2. On the other hand, the case of a broad band spectrum [see fig. *3.3*] corresponds to a $X(t;\beta)$ function to which no waveform characteristics can be attributed. All in all, for a narrow band spectrum it can be considered that randomness and waveform characteristics participate evenly.

Briefly, a sea state with an infinitely narrow spectrum tends to be similar to a sequence of periodic waves. However there would be a substantial difference as the wave height would vary largely though very gradually. Clearly, the narrower the spectrum, the closer the waves would be to this ideal condition. Vice versa, the wider the spectrum is the more irregular the waves are, thus greater differences among consecutive waves occur.

As it is obvious, it is a critical matter to establish some kind of index in order to quantify the spectral bandwidth, because the acquired information of a narrow spectrum through a bandwidth parameter will be useful for further analysis.

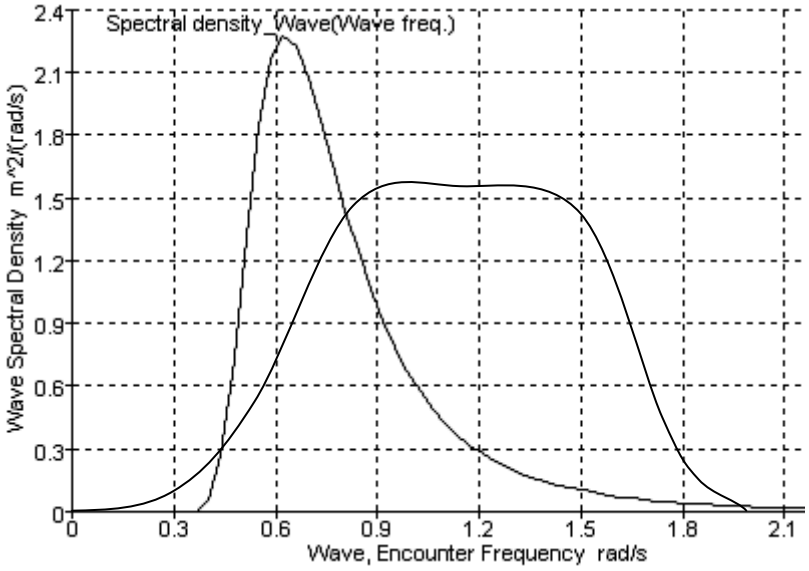

Figure 3.3: Narrow and broad band spectra

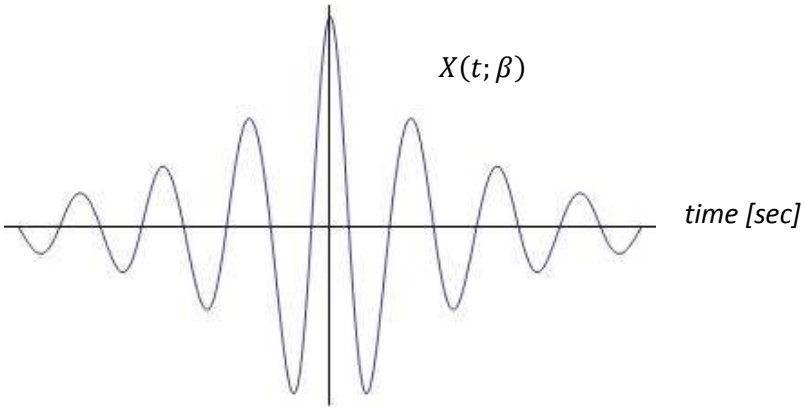

Figure 3.4: Random process $X(t;\beta)$ for the narrow band spectrum of fig.3.3

III.5.1 *Bandwidth Parameters* ε, v

Cartwright and Longuet-Higgins (1956) used the bandwidth parameter:

$$\varepsilon = \sqrt{1 - \frac{m_2^2}{m_0 m_4}} \tag{3.20}$$

which really is not always efficient, in that it is too sensitive to the high frequency noise and is generally not recommended if the JONSWAP spectrum will be used for practical applications. The range for parameter ε is $(0,1)$, where 0 stands for the infinitely narrow spectrum.

In 1975 Longuet-Higgins used a new bandwidth parameter:

$$v = \sqrt{\frac{m_0 m_2}{m_1^2} - 1} \tag{3.21}$$

This new parameter is more effective than ε. However, for the JONSWAP spectrum it sometimes (depending on the spectral parameters) tends to the upper limit of the range $(0,1)$, where 0 stands for the infinitely narrow spectrum.

III.5.2 *Narrow bandedness parameter ψ^**

Let us define:
$\psi^* \equiv$ absolute value of the quotient between the absolute minimum and the absolute maximum of the autocovariance,

that is:

$$\psi^* = |\psi(T^*)/\psi(0)| \tag{3.22}$$

where

T^*= abscissa of the absolute minimum of the autocovariance function

If the spectrum is infinitely narrow, the autocovariance approaches a cosine, and thus ψ^* approaches 1. As the bandwidth grows, ψ^* gets smaller and smaller approaching 0. Therefore ψ^* is a natural narrow bandedness parameter scientifically fitted to the JONSWAP spectrum.

However, ψ^* is efficient if the absolute minimum of the autocovariance is also the first minimum of this function. In the rather rare case that this condition is not satisfied a critical observation was made through small scale experiments in Reggio Calabria. According to the results of these experiments, the case of the first local minimum not being the absolute minimum of the autocovariance is the special case of wind waves superimposed on somewhat higher swells.

The quotient $\psi(T)/\psi(0)$ as a function of T/T_p is shown in fig. *3.5* for the mean JONSWAP spectrum. From this figure it is clarified that $\psi^* \to 0.73$.

The experience, based on a few thousand sea states recorded in the natural laboratory of Reggio Calabria, confirms $(0.65, 0.75)$ as the typical domain of ψ^* for the wind waves. If ψ^* falls below 0.60, we are probably dealing with wind waves superimposed on

swells. Indeed the presence of wind waves and swells leads to a wider spectrum, and consequently to a smaller ψ^*.

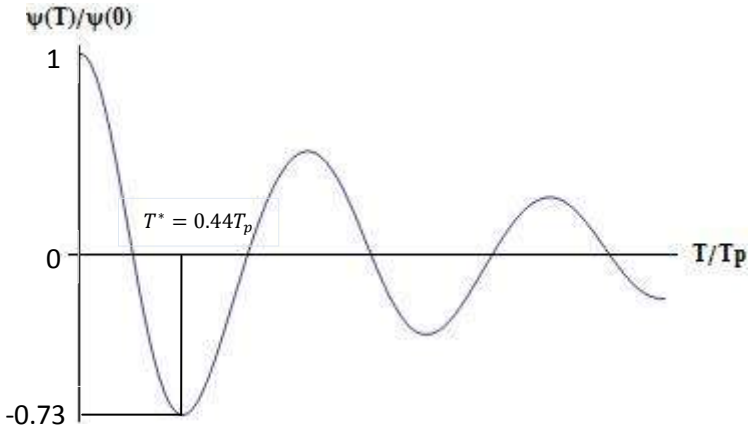

Figure 3.5: Normalized autocovariance obtained from the mean JONSWAP spectrum

At this point, the mean JONSWAP spectrum will be considered for further analysis. Our purpose will be the verification of the previously presented bandwidth parameters' effectiveness. In general, the mean JONSWAP spectrum tends to be considered as narrow band. This will be a settled condition whose verification will be the object of the following paragraph.

For the intentions of our investigation method, the variation of the bandwidth parameters ε, ν and ψ^* with respect to the growth of the significant wave height H_S [2] should be examined. The final outcome would be a diagram like the one shown in fig. *3.6*. A direct result, which crosschecks the hypothesis of the *narrow spectrum*, comes to light.

From the derived diagram of the next page, it is obvious that:

$$\psi^* \to 0.73, \text{ for the mean JONSWAP spectrum}$$

Moreover, the effectiveness of the bandwidth parameters ν and ψ^* is verified in contradiction to the parameter ε, which misses the mark. The fact is that resorting to ε is equivalent to judging by the number of the local maxima (or minima) being present in each wave; the greater this number, the greater the difference from the infinitely narrow spectrum. With the JONSWAP spectrum, each wave has an infinitely large number of local maxima due to the very small noise on the wave surface, and this is why ε gets the upper limit.

[2] The option to display a diagram concerning the variation of the specific bandwidth parameters with respect to the significant wave height was selected, because H_S is a crucial parameter which (in combination with the peak period) defines the sea state conditions.

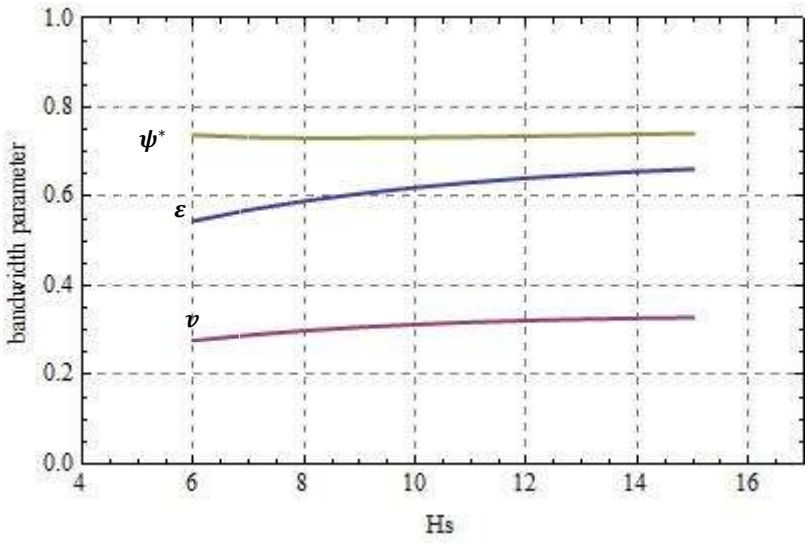

Figure 3.6: Comparative diagram of the spectral bandwidth parameters ε, ν, ψ^* as the significant wave height (H_s) increases (mean JONSWAP spectrum considered)

III.6 *Concluding remarks*

The link between sea state and Gaussian random process was first noticed by Longuet-Higgins (1952). The theory of the sea states then ripened in the 60's, thanks to the contribution of several authors. In general, a sea state will be identified from the definition of the critical parameters H_s and T_p.

In this context, clear distinction of the so called swells and wind generated waves should be made in order to proceed in further analysis. The differences between these two kinds of ocean waves are depicted in the form of the autocovariance function. Certain properties of the autocovariance will play a central role for the establishment of the Quasi-Determinism theory [see next chapter]. In particular the fact that the main statistical properties of a sea state are coded in the first two waves of the autocovariance (the *core* of the autocovariance) is a consequence of the aforesaid theory.

In the following chapter we shall see that the narrow bandedness parameter ψ^* proceeds from a corollary of Boccotti's theory. The parameter's efficiency for the identification of a narrow band spectrum is experimentally verified against other bandwidth parameters of increased sensitivity to high frequency noise, such as ε and ν.

CHAPTER IV:

THE QUASI – DETERMINISM THEORY

This chapter deals with the irregular sea wave groups.

Boccotti's Quasi-Determinism (QD) theory gives the mechanics of sea wave groups when either a very large crest (first formulation of the theory – "New wave"), or a large crest-to-trough wave height (second formulation of the theory) occurs.

In this chapter, the theory, in both formulations, is employed for the generation of two-dimensional irregular semi-random sea waveforms. Afterwards, starting from the linear components of the theory, the second order wave corrections are obtained to model the most probable non-linear time evolution of a wave group if a very large crest or a large crest-to-trough height would occur at some fixed point (Felice Arena, 2004).

IV.1 *Concept of the methodology*

In the 1980s Boccotti developed the QD theory, exact to the first order in a Stokes expansion, in two formulations. The first formulation ("New wave") deals with the crest height, and shows that the space-time profile of an exceptionally high crest is depended on the autocovariance function. The second formulation of the theory deals with the crest-to-trough height; it was derived by obtaining firstly the probability density function of the surface displacement at a point $x_0 + X$, $y_0 + Y$, at time $t_0 + T$, given the condition:

$$\eta(x_0, y_0, t_0) = \frac{1}{2}H, \qquad \eta(x_0, y_0, t_0 + T^*) = -\frac{1}{2}H \tag{4.1}$$

where t_0 is an arbitrary time instant (x_0, y_0) an arbitrary point, H the crest-to-trough wave height and T^* the abscissa of the absolute minimum of the autocovariance function (which is assumed to be also the first local minimum of this function on the positive domain: this condition being always verified for wind waves as explained in the previous chapter).

The basic theorem (see Boccotti, 1989, 1997, 2000) is that, as $H/\sigma \to \infty$, condition (4.1) becomes both sufficient and necessary (in probability) for the occurrence of a wave of given height H in a random wind-generated sea state. A corollary is that a wave of a very large given height H, with a very large probability, belongs to a wave group with the following deterministic form:

$$\eta_1 = (x_0 + X, y_0 + Y, t_0 + T) = \frac{\psi(X, Y, T) - \psi(X, Y, T - T^*)}{\psi(0,0,0) - \psi(0,0,T^*)}\frac{H}{2} \tag{4.2}$$

Where $\psi(X, Y, T)$ is the autocovariance function of the surface displacement.

According to the author's words: "*if a wave with a given height H occurs at a fixed point (x_0, y_0) and H is very large with respect to the mean wave height at this point, we may*

expect the water surface to be very close to the deterministic form (4.2)". More specifically, "*each wave of the set will occupy the centre of a well defined group that is the sum of a deterministic framework and a residual random noise of a smaller order"*. Boccotti's approach is exact to the first order in a Stokes expansion and hence (4.2) represents the linear component of surface displacement.

Let us shed more light to the concept of the theory. The original idea is that the higher the waves, the more negligible the differences between consecutive waves are. So, let us consider a set of waves with a given height H, say $H = 3\sigma$ in a stationary Gaussian process. The waves of this set will be different, even very different, from one another. However, if we fixed a larger H, say $H = 8\sigma$, we should find that the waves contained in the set differ much less from one another and, in the limit as $H/\sigma \to \infty$, all waves of the set, apart from a negligible share, would prove to be equal to one another.

Obviously, the developed formulations (Boccotti, 1989-2000) are applicable and effective for long-crested random waves, in an undisturbed field. The final expressions of the surface displacement are presented in the following sections.

IV.1.1 *First formulation – "New wave"*

If a wave crest with a given exceptionally large height H_c occurs at some point y_0 at a time instant t_0, during a sea storm, with probability approaching to 1, the random free surface displacement around point y_0 for a span of time before and after t_0, will be very close to the following deterministic function:

$$\eta_1 = \frac{H_c}{\sigma^2}\int_0^\infty E(\omega)\cdot\{\cos[\ \varphi(\omega,Y,T)]\}d\omega \tag{4.3}$$

where

$$\sigma^2 = \int_0^\infty E(\omega)d\omega$$

is the variance of the random free surface displacement.

$E(\omega)$: is the frequency spectrum, with

$$\varphi(\omega,Y,T) = kY - \omega T \tag{4.4}$$

From the well-known linear dispersion relation:

$$ktanh(kd) = \frac{\omega^2}{g} \tag{4.5}$$

with g the acceleration due to gravity.

IV.1.2 *Second formulation*

If a wave with a given exceptionally large crest-to-trough height H^* occurs at some point y_0 at a time instant t_0, during a sea storm, with probability approaching to 1, the random free surface displacement around point y_0 for a span of time before and after t_0, will be very close to the following deterministic function:

$$\eta_1 = \frac{H^*/2}{\sigma^2 - \psi(T^*)} \int_0^\infty E(\omega) \cdot \{\cos[\ \varphi(\omega, Y, T)] - \cos[\varphi(\omega, Y, T) + \omega T^*]\} d\omega \tag{4.6}$$

where

$$\sigma^2 = \int_0^\infty E(\omega) d\omega$$

is the variance of the random free surface displacement.

T^* : is the abscissa of the absolute minimum of the autocovariance function (which is assumed to be also the first local minimum of this function on the positive domain).

Note: the origin of the Cartesian co-ordinate system (X, Y) is considered to be at (x_0, y_0).

IV.2 *Quasi – Determinism theory: the consequences*

IV.2.1 *Mean period T_{10} and period T_h of a very large wave*

A common way to estimate the dominating period for a specific wave group, is to follow a simple calculation procedure of the mean period T_m. However, when the "Quasi-determinism (QD) theory" is employed, a different approach would be more appropriate. A very significant observation is mentioned in Boccotti's notes as the first consequence of the QD theory. According to his analysis, a wave of given height H has a *well defined* period, with probability approaching 1, as $H/\sigma \to \infty$. This characteristic period is given as:

T_h= period of the central wave group

Where the subscript h stands for *high waves*. Especially for the uses of the mean JONSWAP spectrum $\boldsymbol{T_h \to 0.92 T_p}$ with probability approaching 1, as $H/\sigma \to \infty$.

In the previous chapter the condition of the narrow band JONSWAP spectrum was verified and thus the discussed random process $X(t;\beta)$ (coincident with the water surface displacement η at a fixed location at sea) approximates satisfactorily a waveform with a meaningful mean wave period.

So, the purpose of this section is to investigate which definition of the characteristic periods displayed in chapter III is most appropriate for characterizing and identifying a specific wave group. For this reason, the variation of these typical characteristic periods with respect to the significant wave height is displayed below [see fig. *4.1*]. The periods that were used in the process are given as follows:

i. The peak period T_p
ii. The central wave period T_h of the quasi-deterministic wavegroup defined in the previous pages
iii. The average-mean period T_m
iv. Average period between increasing zero-crossings $\bar{T}_z$
v. The "mean calculated period" $T_{mean\ calculated}$

As it is commonly known, the spectral peak period (T_p) is the inverse of the frequency at which the value of the frequency spectrum is a maximum, though it cannot be defined satisfactorily in multi-peaked spectra.

Let us suppose that the most likely height of the highest wave in a record of duration 3 hours is H_{max} with period T_{max}. It is often obtained indirectly from $\bar{T}_z$ or T_p using empirical relationships, or from H_{max} and steepness assumptions – usually to obtain a range of possible associated periods. These methods should be applied only in the water depth for which the empirical relationships have been found, usually deep water (i.e. depth >$1/2$ wavelength). It should be possible to use the steepness method in shallow water provided that refraction is minimal and that allowance can be made for shoaling effects. It cannot, however, be derived directly from the wave spectrum. Following such an approach, according to the first consequence of the Quasi-determinism theory we would arrive at the definition of T_h= period of the most probable central wave of the group.

The mean wave period (T_m) is the mean of all wave periods in a time-series representing a certain sea state:

$$\bar{T} = T_m = T_{10} = 2\pi(m_0/m_1) \tag{4.7}$$

When recordings were first taken this was onto charts and simple counts could be made. First the charts were zero meaned (the average and trend calculated and drawn through the plot to provide a new axis for measuring) and then the number of times the wave record crossed the mean going up (or sometimes down) was counted and this gave the number of waves and, as a time measure, the zero-crossing period. The parameter is estimated by taking the mean of these periods for a given wave record. For wave records on paper the mean level is found by eye and T_{visual} is estimated from the record length and

the number of zero up-crossings counted on the record. This method can also be applied to digitized data using a computer but if the wave records are available in machine readable form it is preferable to estimate from the moments of the spectrum using:

$$\bar{T}_z = T_{02} = 2\pi\sqrt{m_0/m_2} \tag{4.8}$$

Finally, the previously referred as "mean calculated period", is the mean calculated period of a Quasi-Deterministic wave group generated according to eq. (4.6) in a time range of 40 seconds. The values of this characteristic period were derived from waveform diagrams (examples will be displayed in the applications section) after simulation runs carried out in a *MATHEMATICA* environment.

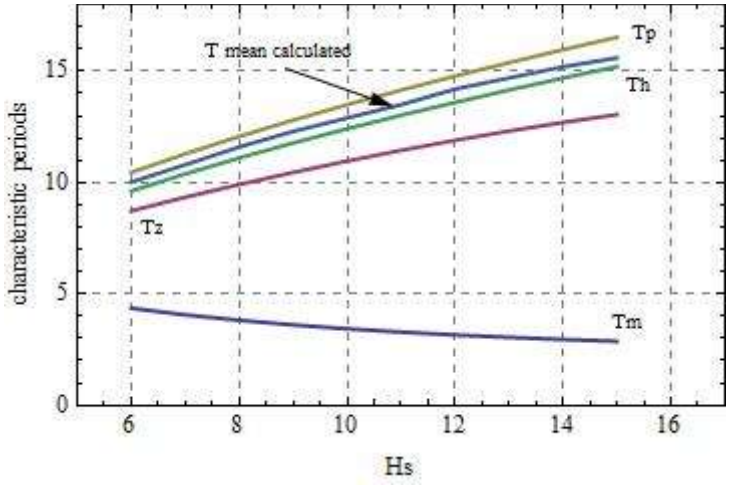

Figure 4.1: Comparative diagram of the characteristic periods $T_p, T_h, T_m, T_z, T_{mean\ calculated}$ as the significant wave height (H_s) increases

As expected, with the growth of the significant wave height H_s , the characteristic periods T_p , T_h and T_{10} grow, too. As it can be seen (fig. *4.1*), T_{10} grows rapidly in contrast to T_h and T_p. Furthermore, T_{10} curve is developed in a different span of period time. Since QD theory estimates that for the central wave period the equation $T_h = 0.92T_p$ prevails and because of the fact that waves composing the wave group are approximately of equal periods, the T_{10} curve is developed in a time range with different practical meaning for the potential of the QD theory. The efficiency of the characteristic period T_h is confirmed from the results of the "mean calculated period".

IV.2.2 *The wave height probability under general bandwidth assumptions*

The second consequence of the Quasi-Determinism theory, in the field of wave statistics, deals with the very wave height probability. Let us see how the presented theory and wave height probability are related to each other.

A wave of given height H necessarily has crest elevation and trough depth between 0 and H. Fig. *4.2a* shows two possible cases lying within the infinite range of sea waveforms. It would be preferable to present each possible wave in the plane $\tau - \xi$[3], so as distinct points to be spotted similar to the case of the noted waveforms (1) and (2) shown in fig. *4.2a-b*.

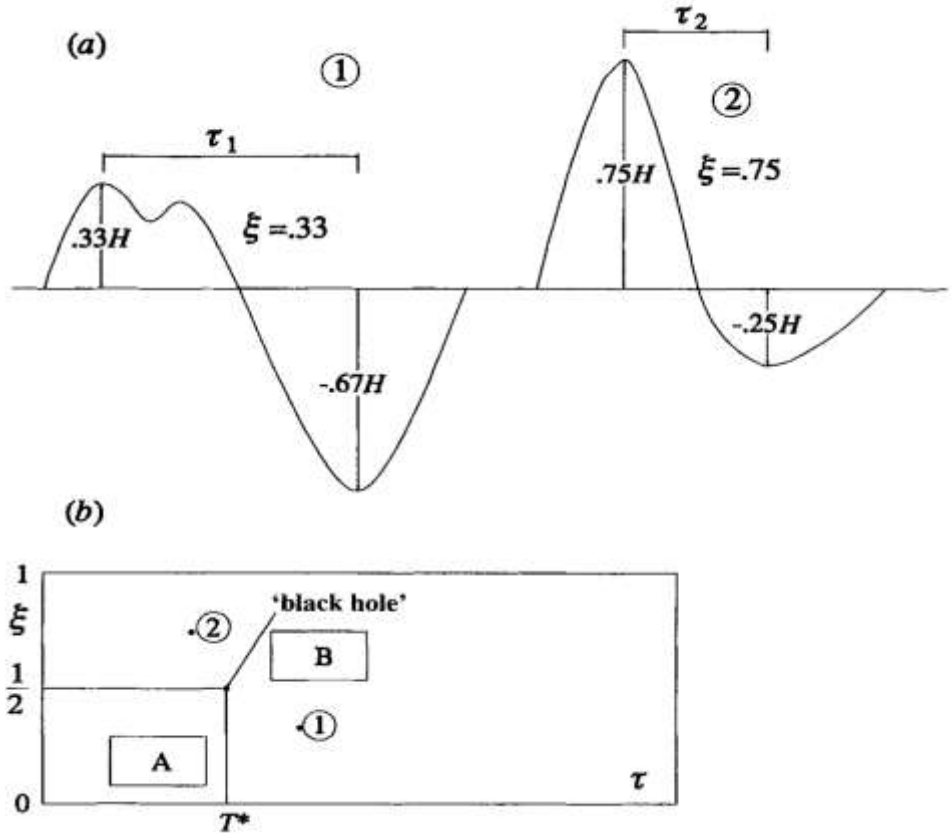

Figure 4.2: a) The waves with a fixed height H generally show a large variety of ξ and τ. b) Plotting ξ vs τ, generally we get a wide cloud of points. Only in the limit as $H/\sigma \to \infty$, all points would gather at a special location, something like a black hole. This special location is at $\tau = T^*$, $\xi = 1/2$ (Boccotti, 2000)

Let us imagine that we examine a very large time interval $\mathcal{T}$. Then, we gather all waves whose height is within a fixed small interval $H, H + dH$, and we mark the points representative of these waves in the plane $\tau - \xi$. For a finite H/σ the marked points will gradually spread over the plane $\tau - \xi$. On the contrary, as $H/\sigma \to \infty$, great point concentration is observed: all the points but a negligible share fall in an open 2-ball with centre at $T^*, 1/2$ and radius of order $(H/\sigma)^{-1}$. The most important fact is that all the points in this small 2-ball are associated with waves whose profile is very close to the deterministic profile (4.2). Moreover, a wave of very large height H, according to (4.2), has crest elevation

[3] Where τ is the crest-trough lag, and ξ is the quotient between the crest elevation and the crest-to-trough wave height.

$H/2$ and crest-trough lag T^*, and thus it is represented by the point $(T^*, 1/2)$ in the plane $\tau - \xi$.

If we associate a mass with each point in the plane $\tau - \xi$ (considering the same mass for each point), in the case of a finite H/σ, uniform mass distribution over the plane $\tau - \xi$ appears. While as $H/\sigma \to \infty$, there is "mass concentration" at the point $(T^*, 1/2)$, which plays the role of a black hole. The mass density varies widely in the black hole, despite its radius being very small, in the order of $(H/\sigma)^{-1}$. Specifically, the mass density approaches zero from the centre to the outskirts of the black hole.

Boccotti defined as $EX(\alpha)d\alpha$ the expected number per unit time of waves whose height falls within a fixed small interval $\alpha, \alpha + d\alpha$. Through extended calculations it was verified that:

$$EX(\alpha) = \frac{2\left|K_1\left(T^*, \frac{1}{2}\right) K_2\left(T^*, \frac{1}{2}\right)\right|}{\pi\sqrt{M(T^*)K_\tau^* K_\xi^*}} a\, exp\left[-\frac{1}{4}\hat{f}\left(T^*, \frac{1}{2}\right)a^2\right], \qquad as\ H/\sigma \to \infty$$

(4.9a)

where

$$\left|K_1\left(T^*, \frac{1}{2}\right)\right| = \left|K_2\left(T^*, \frac{1}{2}\right)\right| = \frac{1}{2}\frac{1 + \ddot{\psi}_{T^*}}{1 - \psi_{T^*}}$$

(4.9b)

$$M(T^*) = \left(1 - \psi_{T^*}^2\right)\left(1 - \ddot{\psi}_{T^*}^2\right)$$

(4.9c)

$$\hat{f}\left(T^*, \frac{1}{2}\right) = \frac{1}{1 - \psi_{T^*}}$$

(4.9d)

$$K_\tau^* = \frac{\ddot{\psi}_{T^*}\left(1 + \ddot{\psi}_{T^*}\right)}{(1 - \psi_{T^*})^2\left(1 - \ddot{\psi}_{T^*}\right)}$$

(4.9e)

$$K_\xi^* = \frac{8}{1 + \psi_{T^*}}$$

(4.9f)

with:

$$\ddot{\psi}_{T^*} = \ddot{\psi}(T)/m_2$$

$$\psi_{T^*} = \psi(T)^4/m_0 = -\psi^*$$

And so, the probability $p(a)da$ that a wave height falls within a fixed small interval $(a, a+da)$ can be expressed as:

$$p(a)da = EX(\alpha)d\alpha/EX_+ \tag{4.10}$$

Where EX_+ is the expected number per unit time of zero up-crossings (0_+) of the surface displacement $\eta(t)$:

$$EX_+ = 1/2\pi \tag{4.11}$$

Finally, through eq. (4.9) – (4.11) the probability density function (pdf) is of the form:

$$p(a) = \frac{\left(1+\ddot{\psi}_{T^*}\right)}{\sqrt{2\ddot{\psi}_{T^*}(1-\psi_{T^*})}} \frac{a}{2(1-\psi_{T^*})} exp\left[-\frac{a^2}{4(1-\psi_{T^*})}\right], \qquad as\ H/\sigma \to \infty \tag{4.12}$$

And the total probability is:

$$P(a) = \frac{\left(1+\ddot{\psi}_{T^*}\right)}{\sqrt{2\ddot{\psi}_{T^*}(1-\psi_{T^*})}} exp\left[-\frac{a^2}{4(1-\psi_{T^*})}\right], \qquad as\ H/\sigma \to \infty \tag{4.13}$$

The constant before the exponential function of the formulas (4.12), (4.13)

$$K = \frac{\left(1+\ddot{\psi}_{T^*}\right)}{\sqrt{2\ddot{\psi}_{T^*}(1-\psi_{T^*})}} \tag{4.14}$$

can be taken to be 1 for the practical applications like those following in the next pages. On the contrary, the exact value of K must be applied for a careful test of the formula against the data from numerical simulations.

So, Boccotti (2000) defined the probability that a wave height occurs at some point, at some time, given the significant wave height H_s through the concept described in the previous paragraphs. Under the assumption of narrow bandedness spectrum and $H/\sigma \to$

[4] The autocovariance function arises. The previous chapter preludes this event.

∞, for $H/\sigma > 8$, which is commonly seen in the open sea, it can be verified that equation (4.13) can be expressed in a sequence of alternative equivalent equations (considering that $K = 1$) :

$$P(wave\ height > H\ |H_s = h) = exp\left[-\frac{4}{1+\psi^*}\left(\frac{H}{h}\right)^2\right] \tag{4.15a}$$

with $H_s = 4\sigma$ and $a \equiv H/\sigma$:

$$P(wave\ height > H\ |H_s = h) = exp\left[-\frac{a^2}{4(1+\psi^*)}\right] \tag{4.15b}$$

It can be easily verified that the probability density function (*pdf*), which proceeds from eq.(4.15a-b), is of the following form:

$$p(H\ |H_s = h) = \frac{8}{1+\psi^*}\ \frac{H}{h^2}\ exp\left[-\frac{4}{1+\psi^*}\left(\frac{H}{h}\right)^2\right] \tag{4.16}$$

For the mean JONSWAP spectrum ($\psi^* \to 0.73$), which will be used for all the applications of the current thesis, the above given equations are transformed to the much simplified form:

$$\begin{cases} P(wave\ height > H\ |H_s = h) = exp\left[-2.31\left(\frac{H}{h}\right)^2\right] \\ p(H\ |H_s = h) = 4.62\ \frac{H}{h^2}\ exp\left[-2.31\left(\frac{H}{h}\right)^2\right] \end{cases} \tag{4.17a-b}$$

Let us proceed in further investigation of the pair of equations (4.17a-b). Taking a closer look, one should notice at once the similarity with the common *Rayleigh distribution*, one of the very well-known probabilistic functions in ocean engineering which gives the probability of exceeding a wave height under the assumption of infinitely narrow spectrum.

$$P(wave\ height\ >\ H) = exp\left[-\frac{H^2}{8m_0}\right]\ if\ the\ spectrum\ is\ infinitely\ narrow \tag{4.18}$$

or expressed in an equivalent form as a set of equations with the associated probability density function given as:

$$\begin{cases} P(wave\ height > H\ |H_s = h) = exp\left[-2\left(\frac{H}{h}\right)^2\right] \\ p(H\ |H_s = h) = 4\frac{H}{h^2}\ exp\left[-2\left(\frac{H}{h}\right)^2\right] \end{cases}$$

(4.19a-b)

Longuet-Higgins (1952) established that in a stationary, Gaussian and extremely narrow banded process the wave heights may be regarded as twice the envelope amplitude and that these are distributed according a Rayleigh probability distribution function [eq. (4.19a-b)].

Boccotti verified this theory with the proposal of an improved expression of the Rayleigh distribution function given by eq. (4.17a-b). His approach gives the mechanics a more realistic depiction of the laws prevailing in ocean engineering.

In the following figure the differences between the common Rayleigh distribution and its alteration proposed by Boccotti are outlined.

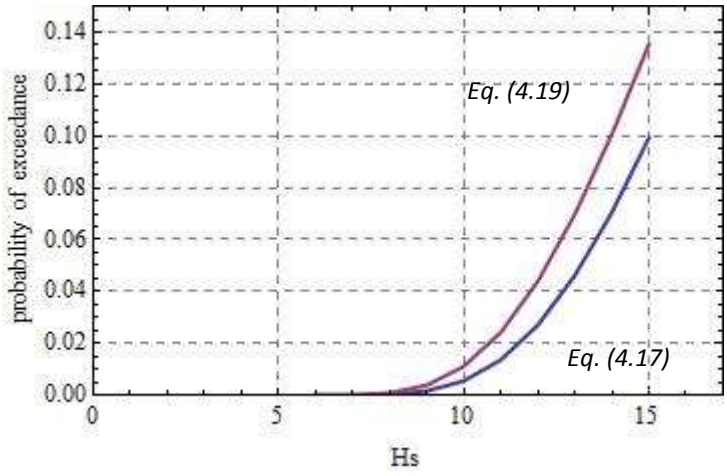

Figure 4.3: Comparative diagram of the probability of exceeding a specified wave height $(\boldsymbol{H = 15\ m})$ ***given by the sets of equations (4.17) and (4.19) with respect to the significant wave height***

From fig. *4.3*, it is obvious that for small H_s, the data points of the function (4.17) tend to be practically coincident with the function (4.19). From extended experiments in Reggio Calabria it is specified that for $H_s > 10\ m$, the obtained data points deviate gradually from (4.19) and move towards (4.17). This was the evidence that Boccotti's corrections on the Rayleigh distribution result in the establishment of an improved plus more realistic pdf.

Finally another interesting figure concerning the wave height distribution - only when the QD theory is employed - is fig. *4.4b*. With this depiction, the ratio h_{i+1}/h_i , $i = 1, \dots, n-1$ of the successive wave heights for the developing stage of the quasi-deterministic wave group is examined. This means that for $i = 1$ the ratio of the second wave height of the group to the first one (h_2/h_1) is obtained. So, the nth wave height is the central wave's height. Let us assume that we examine the case of $n = 6$ waves composing the semi-deterministic group [see fig. *4.4a*], with the following sea state conditions prevailing:

- $H_s = 12.04\ m$
- $T_p = 14.8\ sec$

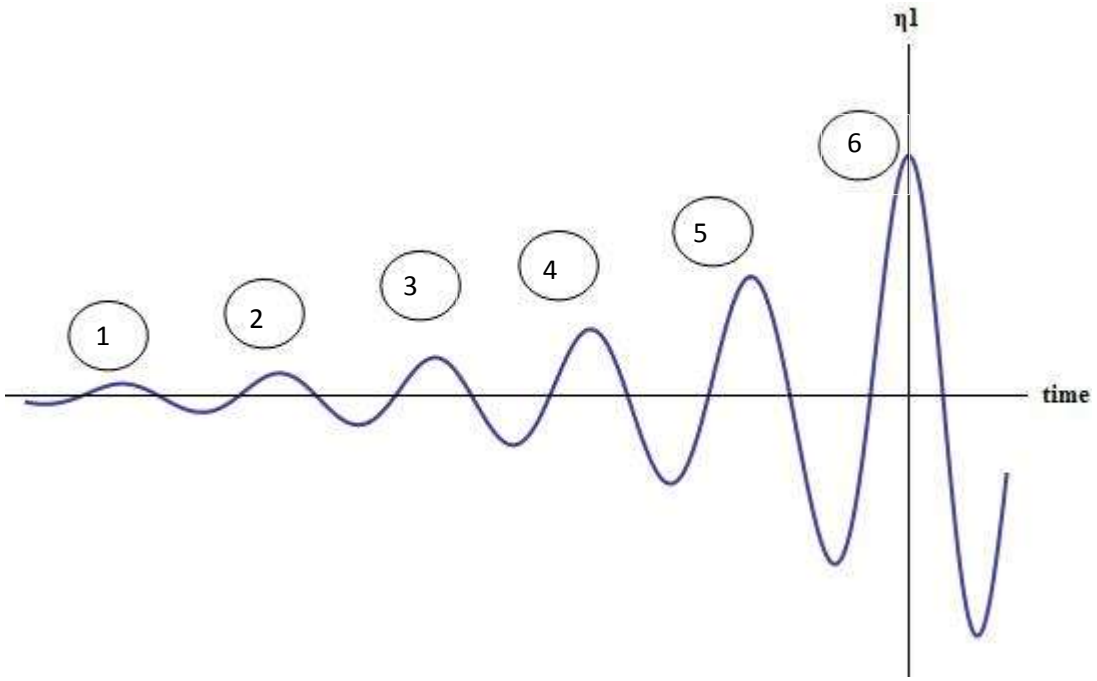

Figure 4.4a: Wave group train

Then, with the Quasi-Determinism theory applied, the arising wave height ratios are summed up into table 4.1a:

i	h_{i+1}/h_i	h_i
1	*1.60*	*1.56*
2	*1.69*	*2.50*
3	*1.87*	*4.21*
4	*1.82*	*7.85*
5	*1.67*	*14.32*
6	-	*23.91*

Table 4.1a

If the same procedure is repeated for a series of different sea states, we would notice that for all the obtained data points, the variation of h_{i+1}/h_i lays within the interval $[1.5\ ,1.9]$ with great concentration. The final results for a series of sea state scenarios are gathered in tables 4.1b-e[5] and figure *4.4b*.

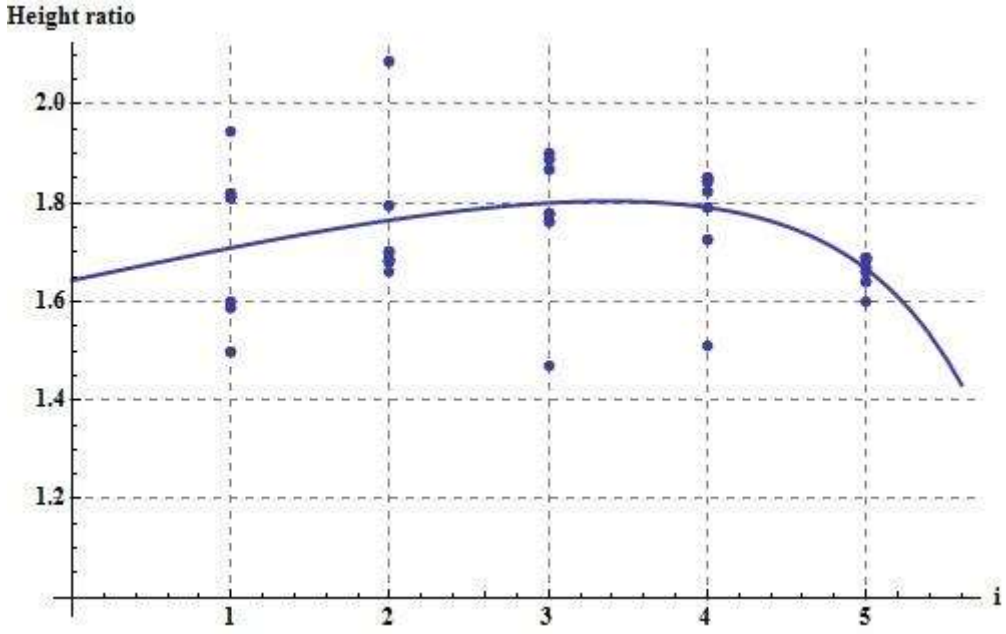

Figure 4.4b: Height ratio versus i^{th} wave height

$$H_s = 6.65\ m\ , T_p = 11\ sec$$

i	h_{i+1}/h_i	h_i
1	*1.82*	*1.24*
2	*1.70*	*2.26*
3	*1.76*	*3.85*
4	*1.84*	*6.79*
5	*1.69*	*12.51*
6	-	*21.13*

Table 4.1b

[5] Still the wave train sequence is considered for a run length $n = 6$ waves up to the central wave height with $H/\sigma > 8$. The selection of an appropriate group run length is a matter to be discussed in the following chapters.

$H_s = 9.29\ m\ , T_p = 13\ sec$

i	h_{i+1}/h_i	h_i
1	*1.81*	*1.27*
2	*1.68*	*2.31*
3	*1.78*	*3.88*
4	*1.85*	*6.90*
5	*1.69*	*12.77*
6	-	*21.52*

Table 4.1c

$H_s = 14.07\ m\ , T_p = 16\ sec$

i	h_{i+1}/h_i	h_i
1	*1.59*	*1.56*
2	*2.09*	*2.48*
3	*1.89*	*5.18*
4	*1.73*	*9.77*
5	*1.64*	*16.87*
6	-	*27.66*

Table 4.1d

$H_s = 12.56\ m\ , T_p = 18\ sec$

i	h_{i+1}/h_i	h_i
1	*1.94*	*2.40*
2	*1.66*	*4.66*
3	*1.47*	*7.75*
4	*1.51*	*11.37*
5	*1.60*	*17.17*
6	-	*27.45*

Table 4.1e

IV.3 *Applications on the theory*

IV.3.1 *First formulation ("New Wave")*

For this application section a very common sea state scenario has been considered $[H_s = 3.5\,m\,, T_p = 8\,sec\,,\ H_c/\sigma = 8\,, a_w = 0.01]$. Employing the QD theory, the specified waveform, for the time and the space domain respectively, is given in the following figures:

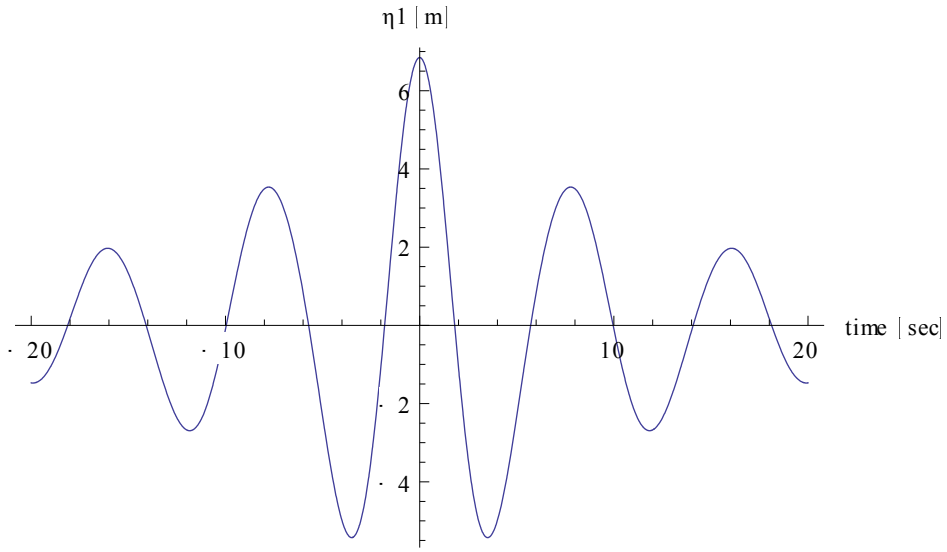

Figure 4.5: Linear component η_1 (m) as a function of time (sec) - "Record" - at $Y = 0\,m$

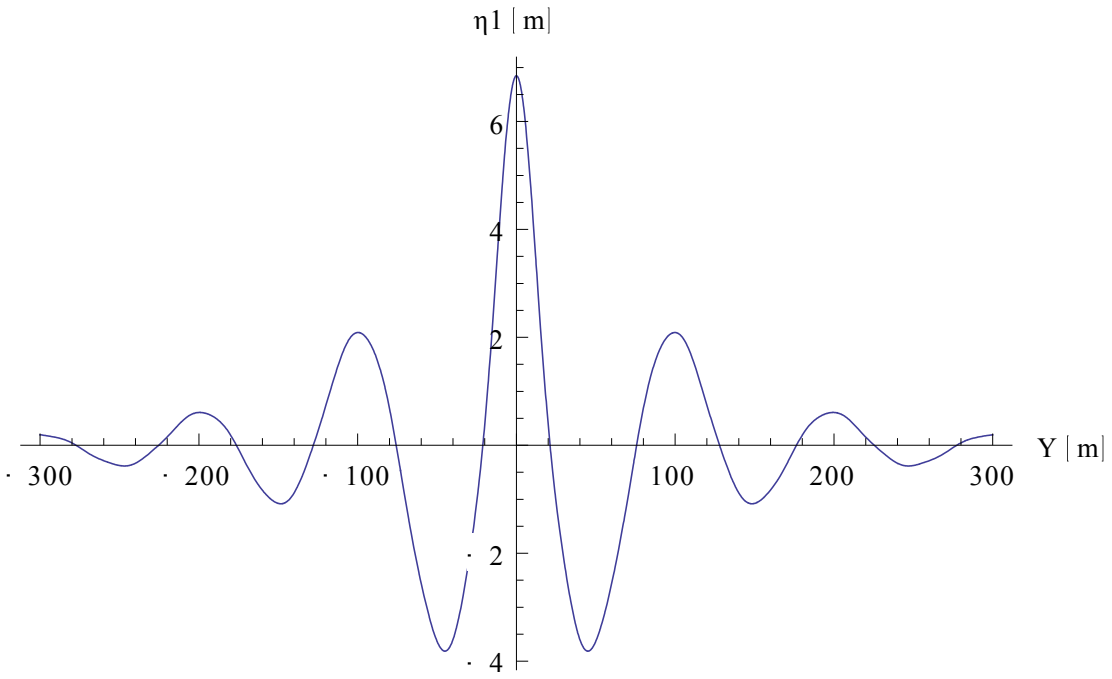

Figure 4.6: Linear component η_1 (m) as a function of space (m) - "Snapshot" - at $T = 0\,sec$

IV.3.2 *Second formulation*

Applying the previous sea state conditions $[H_s = 3.5\,m\,, T_p = 8\,sec\,,\ H^*/\sigma = 8\,, a_w = 0.01]$ the calculated spectral function is given in fig. *4.7*, whilst the form of the autocovariance function [see fig. *4.8*] denotes her impact on the shape and form of the linear solution η_1 [fig. *4.8*].

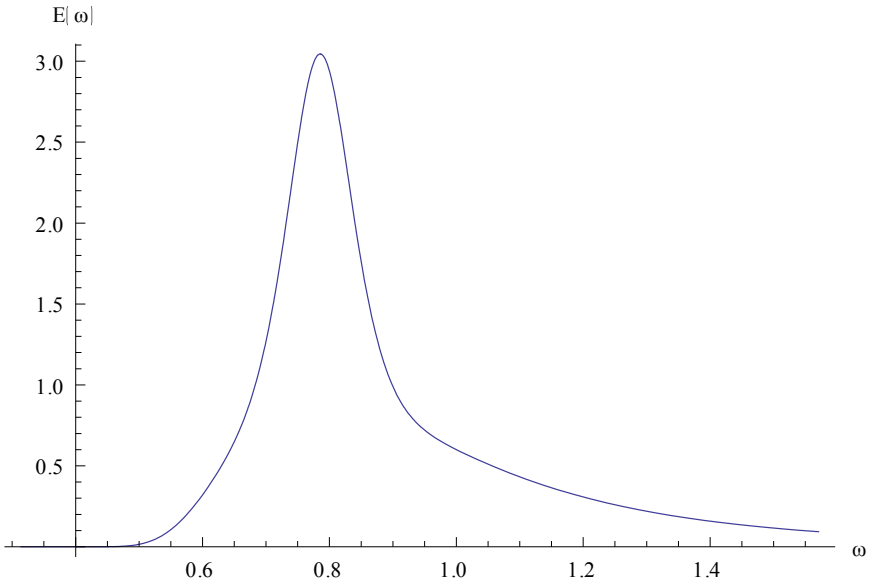

Figure 4.7: The arising mean JONSWAP spectrum

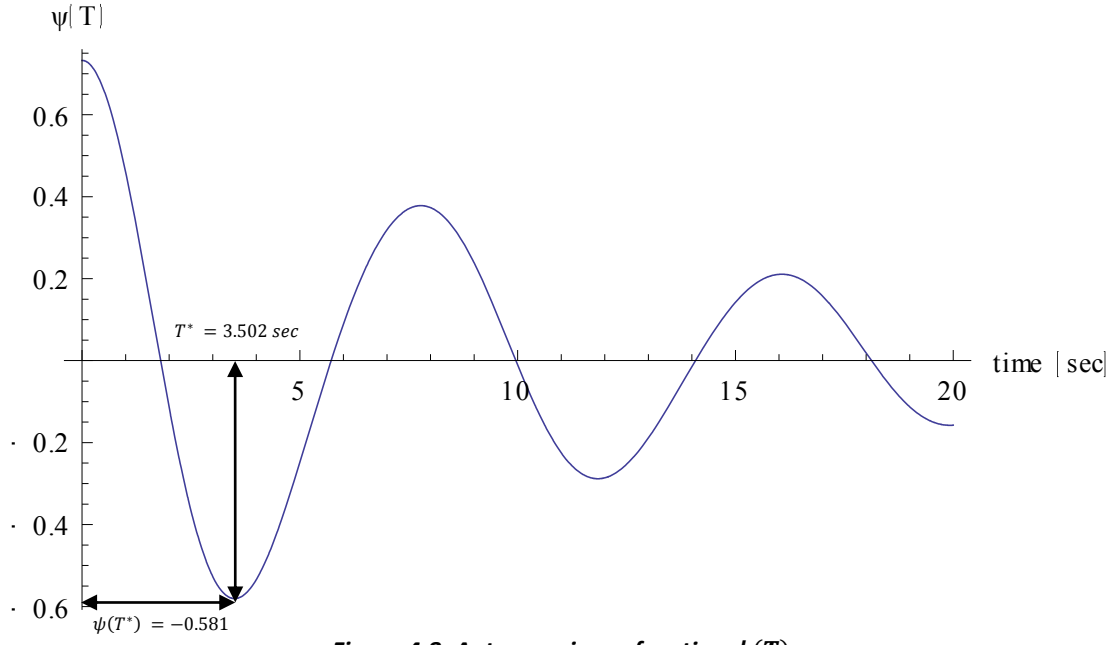

Figure 4.8: Autocovariance function $\psi(T)$

The final waveforms in the time and space domain are given respectively in fig. *4.9* and fig. *4.10*:

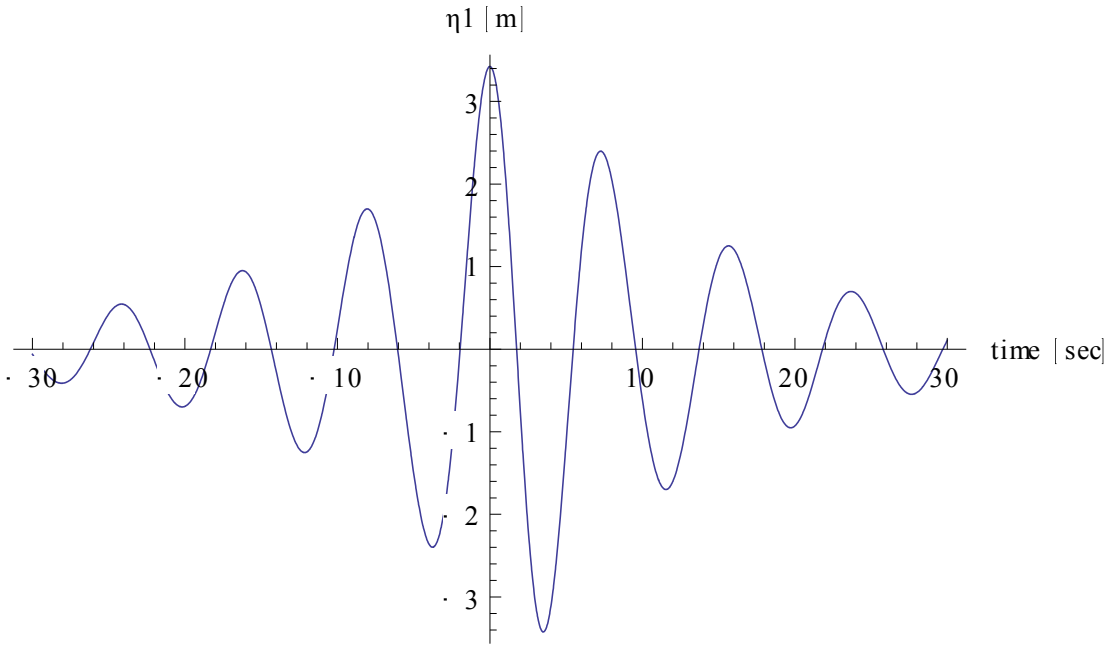

Figure 4.9: Linear component η_1 (m) as a function of time (sec) - "Record" - at $Y = 0\ m$

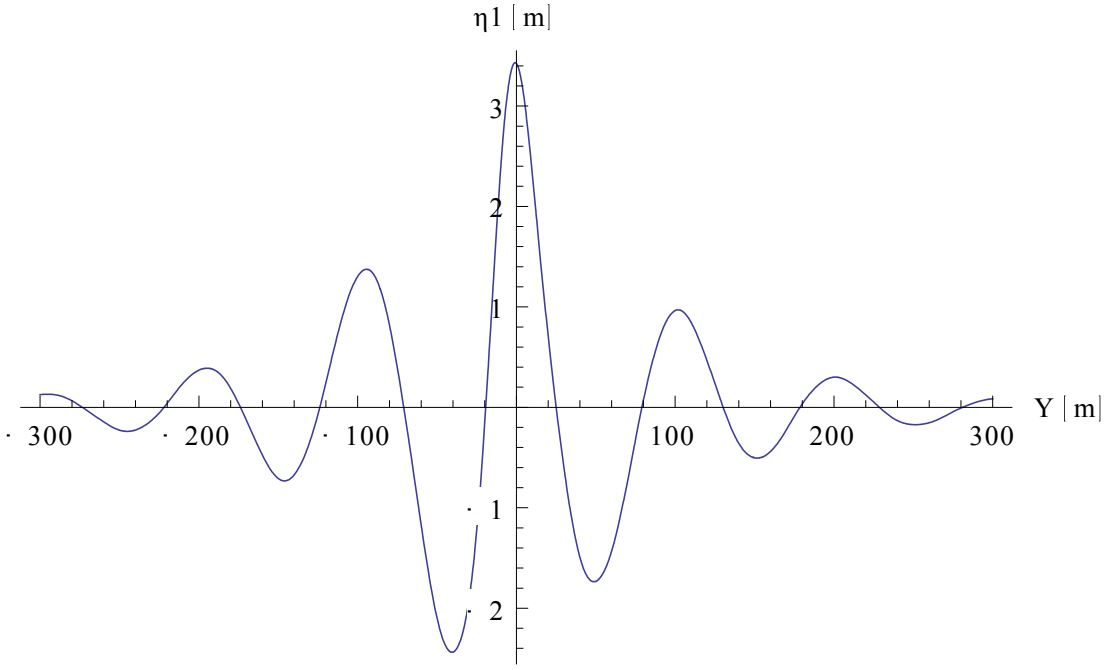

Figure 4.10: Linear component η_1 (m) as a function of space (m) - "Snapshot" - at $T = 0\ sec$

IV.4 *Quasi – Determinism theory and the second order corrections*

In 2005 Felice Arena gave the extension of the theory in both formulations and under the assumption of deep water. The second order corrections, exact to the second order in a Stokes expansion, satisfy a set of partial differential equations for an irrotational flow with an incompressible and inviscid fluid. The final expressions of the second order deterministic components of the free surface displacement for long-crested random waves, in an undisturbed field are given below:

IV.4.1 *First formulation – "New wave"*

If a wave crest with a given exceptionally large height H_c occurs at some point y_0 at a time instant t_0, during a sea storm, with probability approaching to 1, the second order correction for the random free surface displacement around point y_0 for a span of time before and after t_0, will be very close to the following deterministic function:

$$\eta_2 = \frac{{H_c}^2}{4\sigma^4}\int_0^\infty \int_0^\infty E(\omega_1)\cdot E(\omega_2) \cdot\{-|k_1-k_2|\cdot\cos(\varphi_1-\varphi_2)+(k_1+k_2)\cdot\cos(\varphi_1+\varphi_2)\}d\omega_2 d\omega_1 \tag{4.20}$$

Where

$$\sigma^2 = \int_0^\infty E(\omega)d\omega$$

is the variance of the random free surface displacement,

$E(\omega)$: is the frequency spectrum, with

$$\varphi_i(\omega, Y, T) = k_i Y - \omega_i T$$

IV.4.2 *Second formulation*

If a wave with a given exceptionally large crest-to-trough height H^* occurs at some point y_0 at a time instant t_0, during a sea storm, with probability approaching to 1, the second order correction for the random free surface displacement around point y_0 for a span of time before and after t_0, will be very close to the following deterministic function:

$$\eta_2 = \frac{(H^*)^2}{16 \cdot \left(\sigma^2 - \psi(T^*)\right)^2} \int_0^\infty \int_0^\infty E(\omega_1) \cdot E(\omega_2)$$
$$\cdot \{-|k_1 - k_2|$$
$$\cdot \left[\left(1 - \cos(\omega_1 T^*) - \cos(\omega_2 T^*) + \cos(\omega_1 T^* - \omega_2 T^*)\right) \cdot \cos(\varphi_1 - \varphi_2)\right.$$
$$\left. + \left(\sin(\omega_1 T^*) - \sin(\omega_2 T^*) - \sin(\omega_1 T^* - \omega_2 T^*)\right) \cdot sin(\varphi_1 - \varphi_2)\right]$$
$$+ (k_1 + k_2)$$
$$\cdot \left[\left(1 - \cos(\omega_1 T^*) - \cos(\omega_2 T^*) + \cos(\omega_1 T^* + \omega_2 T^*)\right) \cdot \cos(\varphi_1 + \varphi_2)\right.$$
$$\left. + \left(\sin(\omega_1 T^*) + \sin(\omega_2 T^*) - \sin(\omega_1 T^* + \omega_2 T^*)\right)\right.$$
$$\left. \cdot sin(\varphi_1 + \varphi_2)\right]\} d\omega_2 d\omega_1$$

(4.21)

where

T^* : is the abscissa of the absolute minimum of the autocovariance function.

IV.5 *Applications on the extended theory*

The following examples are developed for the same prevailing sea state conditions as in the previous paragraphs $[H_s = 3.5\,m\,, T_p = 8\,sec\,,\ H/\sigma = 8\,, a_w = 0.01]$.

IV.5.1 *First formulation ("New Wave")*

The total surface displacement, after the second-order corrections that equation (4.20) dictates, is given in fig. *4.11.* In fig. *4.12* a comparison between the linear and the total free surface displacement is displayed.

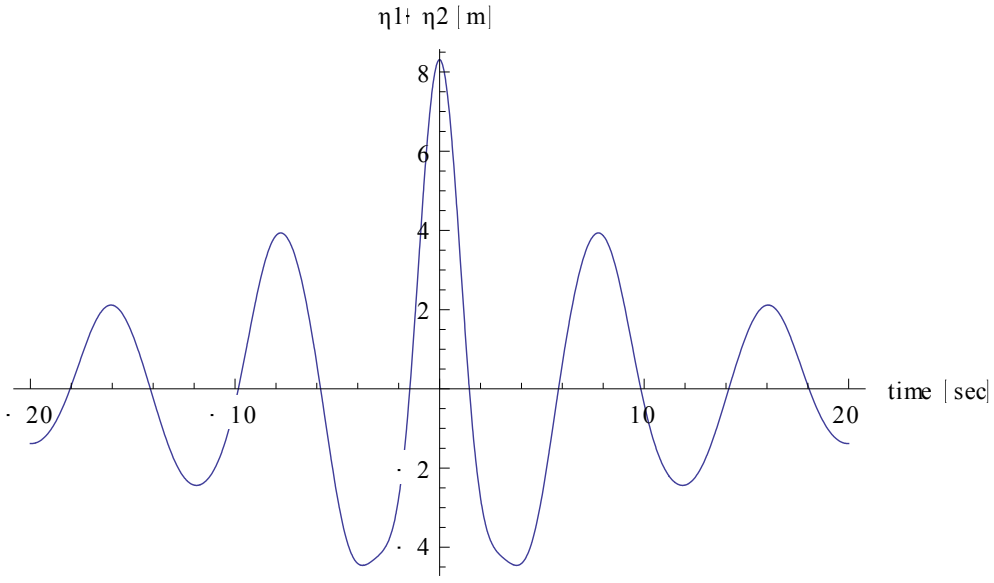

Figure 4.11: Total second-order free surface displacement $\eta_1 + \eta_2$ (m) as a function of time (sec) - "Record" - at $Y = 0\,m$

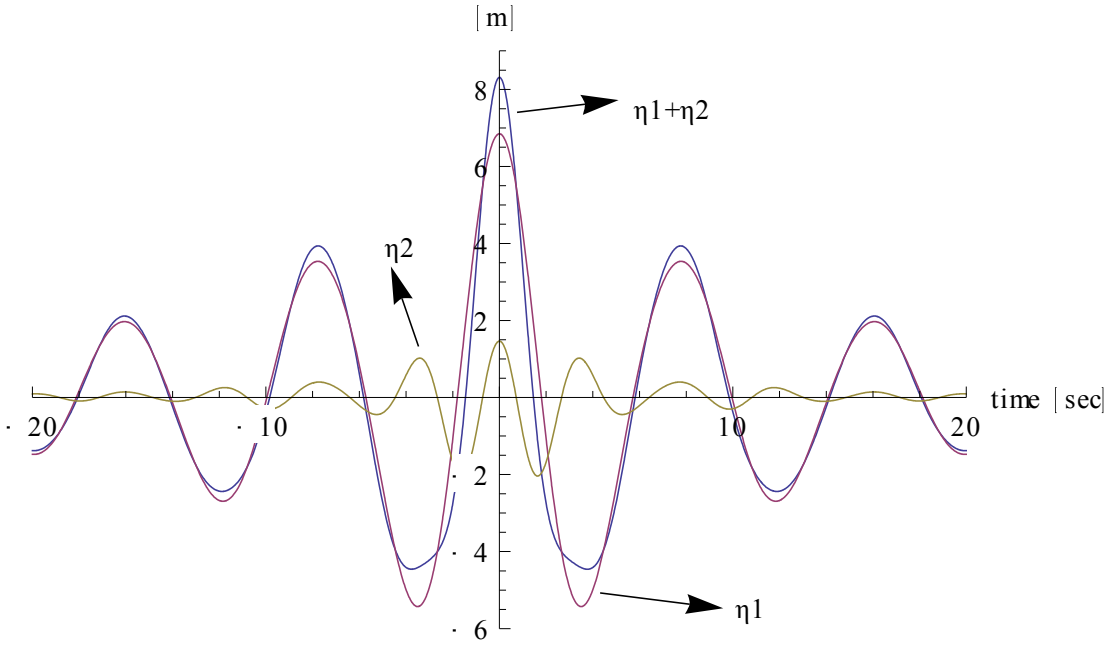

Figure 4.12: Comparison of the total second-order free surface displacement $\eta_1 + \eta_2$ (m) with the linear component η_1 (m) and the second-order correction η_2 (m) at the time domain $(Y = 0\ m)$

In fig. *4.13* we compare the calculated irregular waveform with the harmonic one generated from the central wave parameters of the QD theory: $= H_c Cos\left[\left(\omega_p^2/g\right)Y - \omega_p t\right]$.

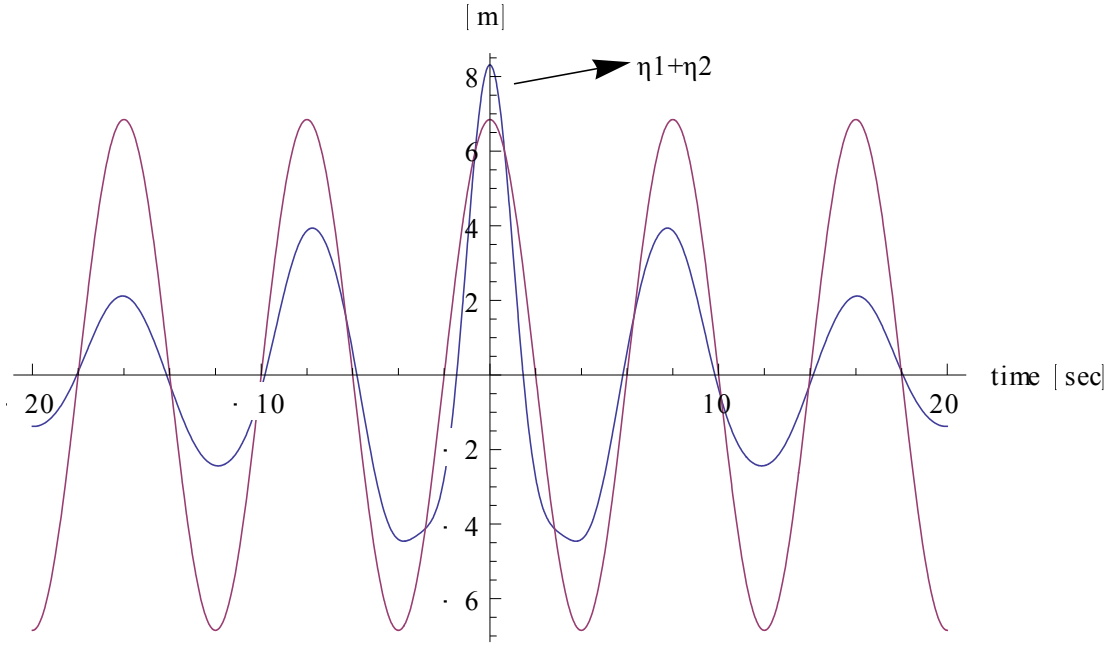

Figure 4.13: Comparison of the total second-order free surface displacement $\eta_1 + \eta_2$ (m) with the harmonic wave $y = H_c Cos\left[\left(\omega_p^2/g\right)Y - \omega_p t\right]$ (m) at the time domain$(Y = 0\ m)$

The final results in the space domain are given below in the same order:

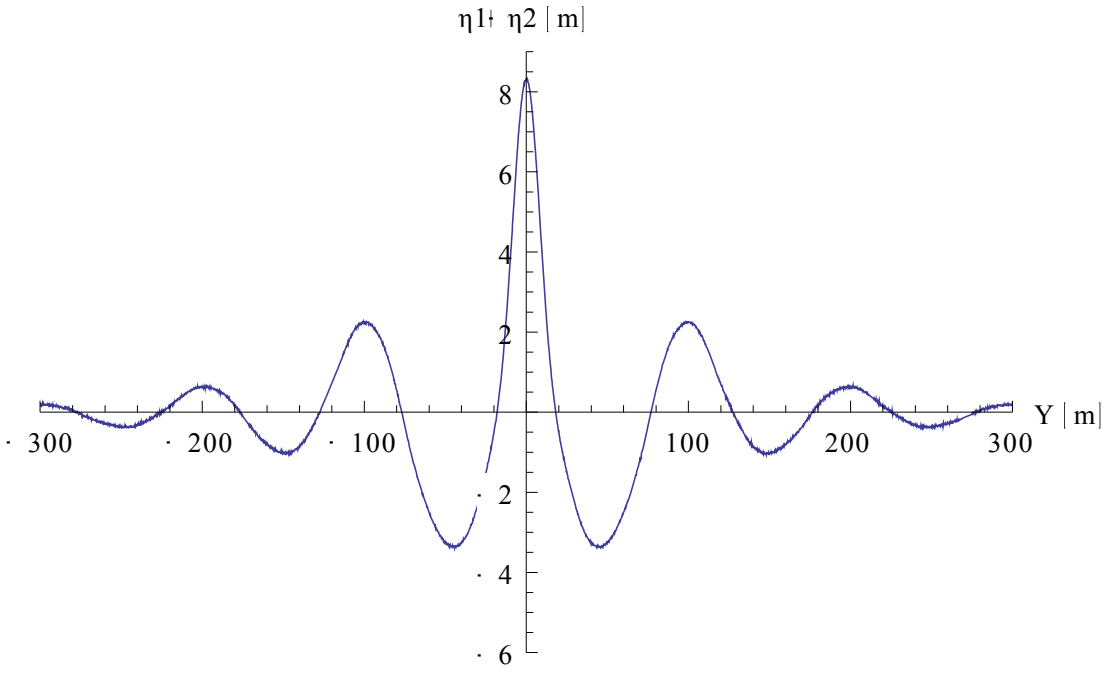

Figure 4.14: Total second-order free surface displacement $\eta_1 + \eta_2$ (m) as a function of space (m) - "Snapshot" - at $T = 0\ sec$

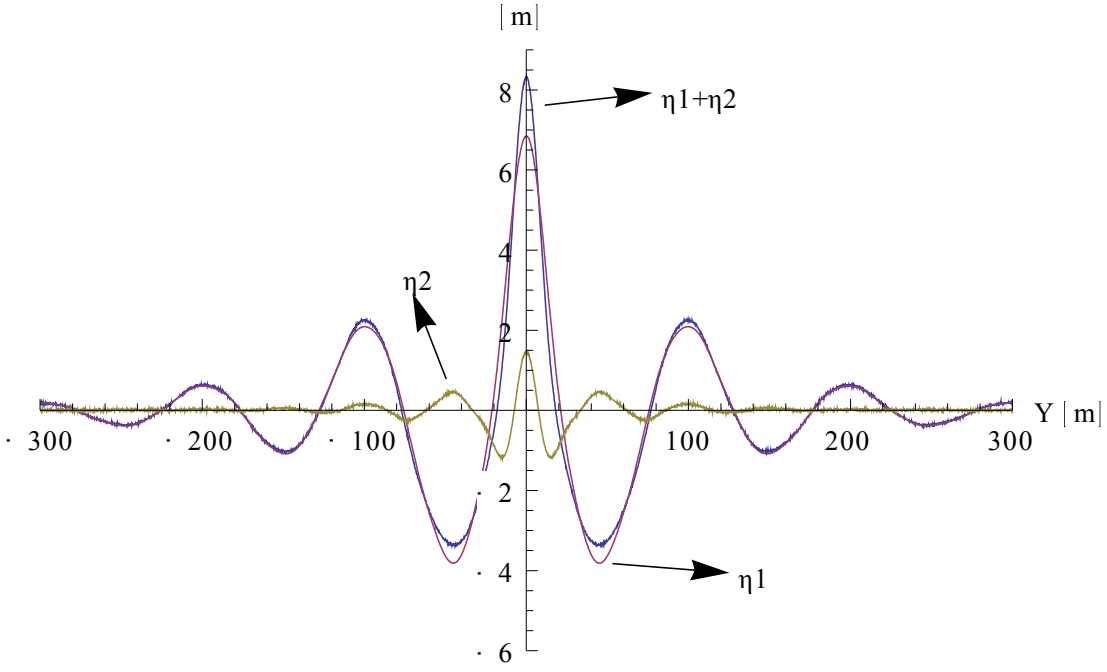

Figure 4.15: Comparison of the total second-order free surface displacement $\eta_1 + \eta_2$ (m) with the linear component η_1 (m) and the second-order correction η_2 (m) at the space domain$(T = 0\ sec)$

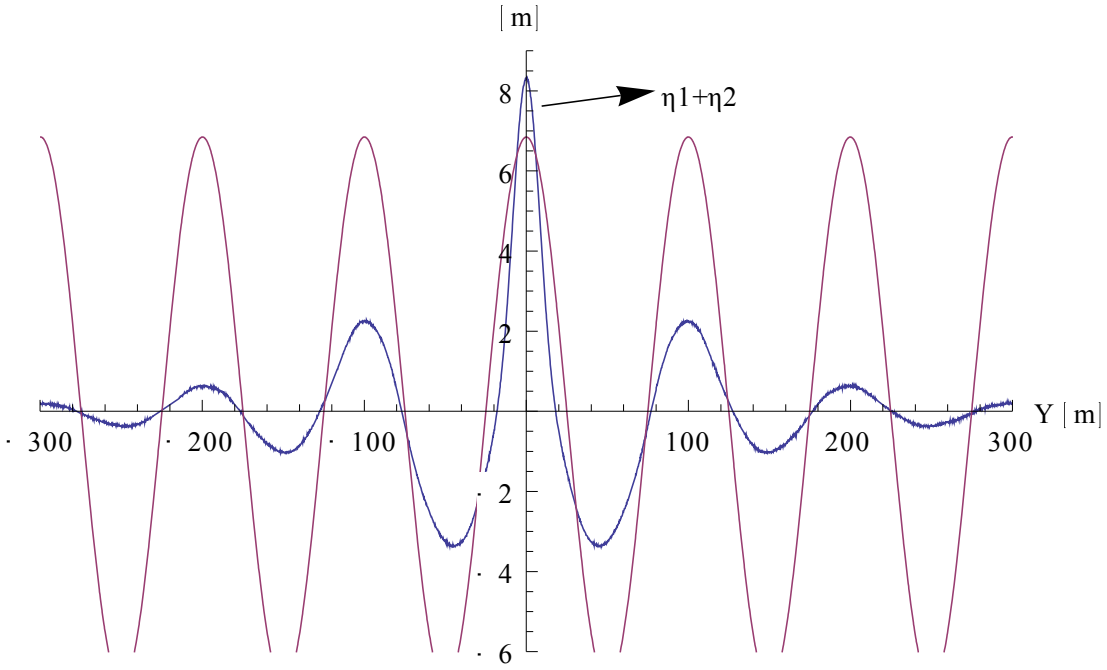

Figure 4.16: Comparison of the total second-order free surface displacement $\eta_1 + \eta_2$ (m) with the harmonic wave $y = H_c Cos\left[\left(\omega_p^2/g\right)Y - \omega_p t\right]$ (m) at the space domain $(T = 0\ sec)$

IV.5.2 *Second formulation*

The total surface displacement, after the application of the second-order corrections is depicted in the following graphics in the same order as in section IV.5.1:

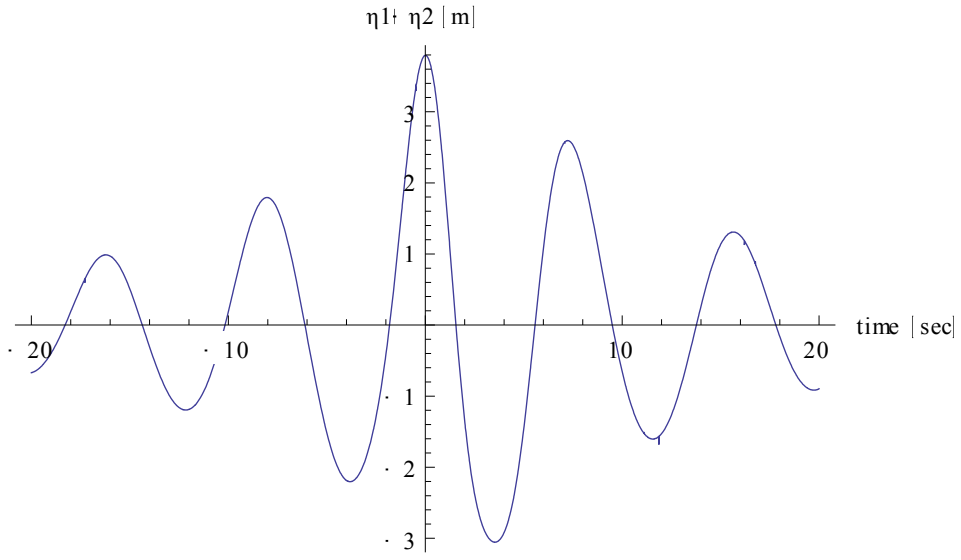

Figure 4.17: Total second-order free surface displacement $\eta_1 + \eta_2$ (m) as a function of time (sec) - "Record" - at $Y = 0\ m$

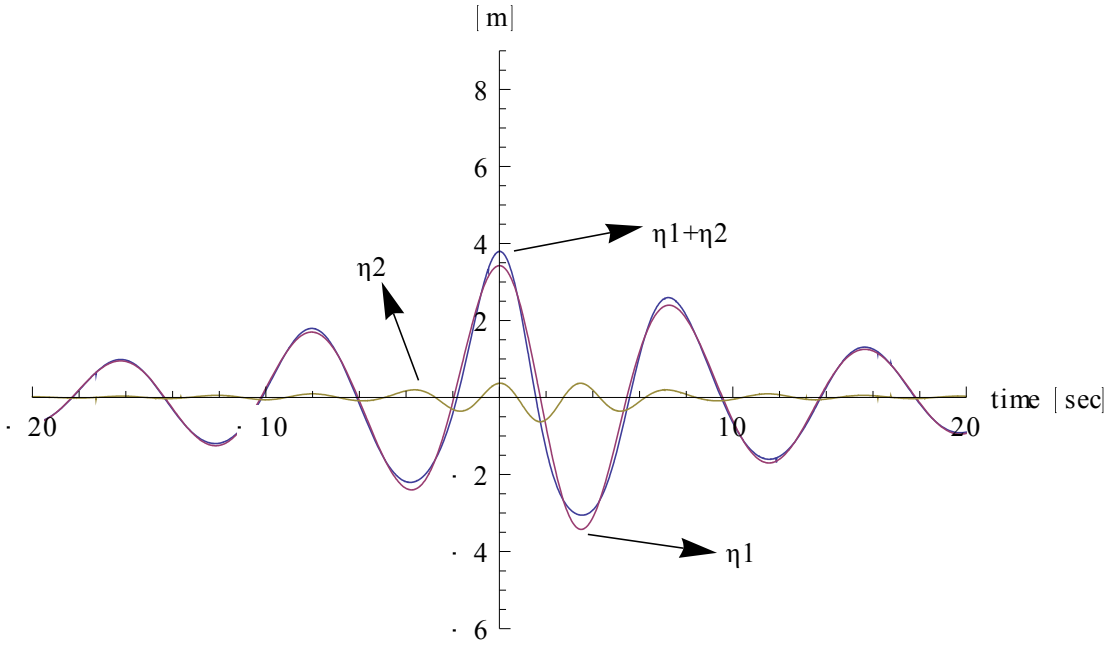

Figure 4.18 Comparison of the total second-order free surface displacement $\eta_1 + \eta_2$ (m) with the linear component η_1 (m) and the second-order correction η_2 (m) at the time domain $(Y = 0\ m)$

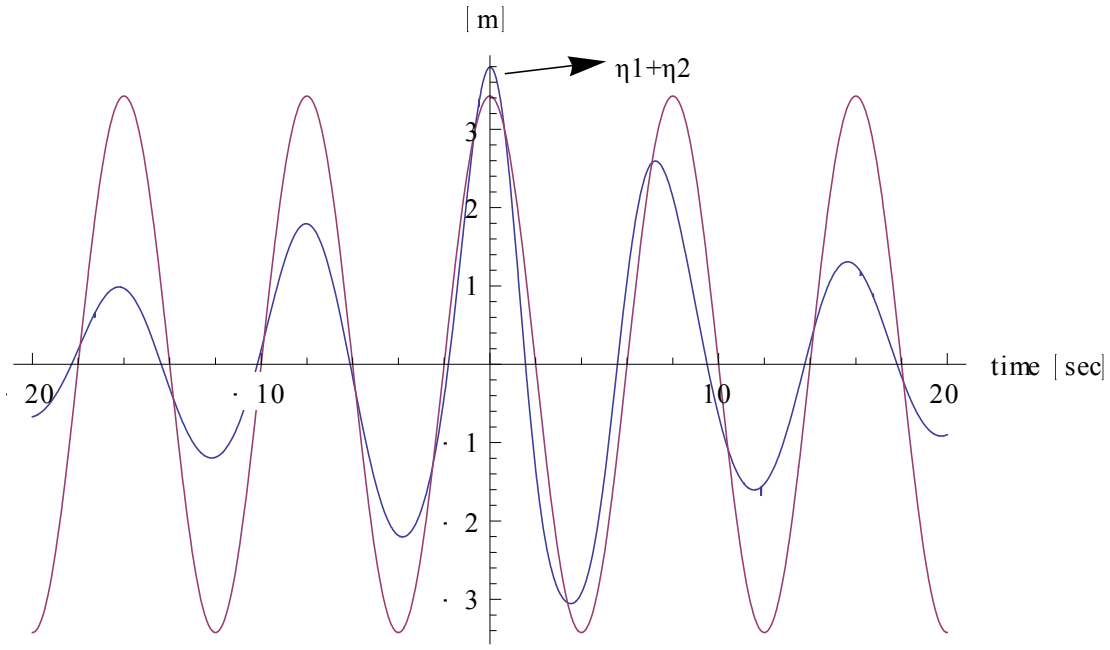

Figure 4.19: Comparison of the total second-order free surface displacement $\eta_1 + \eta_2$ (m) with the harmonic wave $y = (H^*/2)Cos\left[\left(\omega_p^2/g\right)Y - \omega_p t\right]$ (m) at the time domain$(Y = 0\ m)$

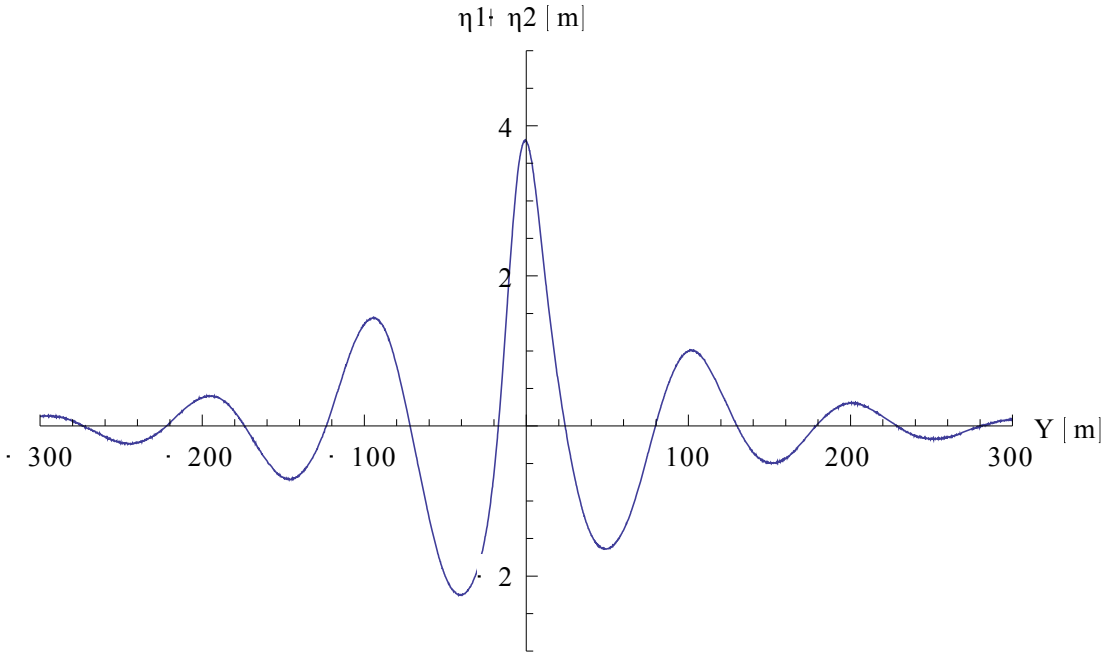

Figure 4.20: Total second-order free surface displacement $\eta_1 + \eta_2$ (m) as a function of space (m) - "Snapshot" - at $T = 0\ sec$

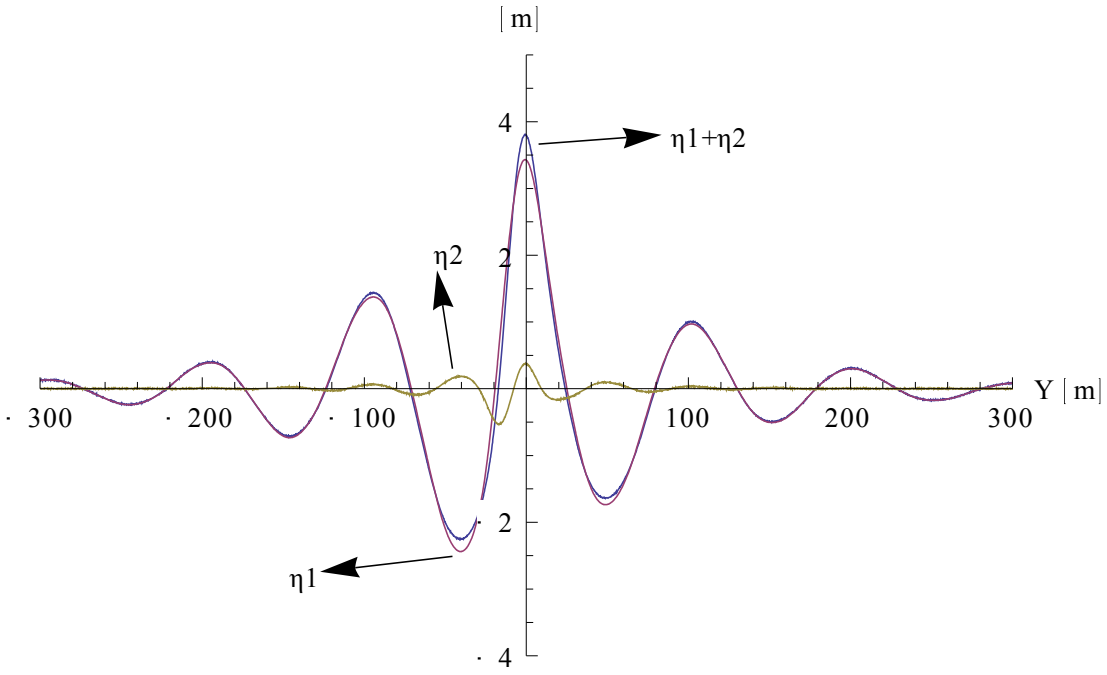

Figure 4.21: Comparison of the total second-order free surface displacement $\eta_1 + \eta_2$ (m) with the linear component η_1 (m) and the second-order correction η_2 (m) at the space domain$(T = 0\ sec)$

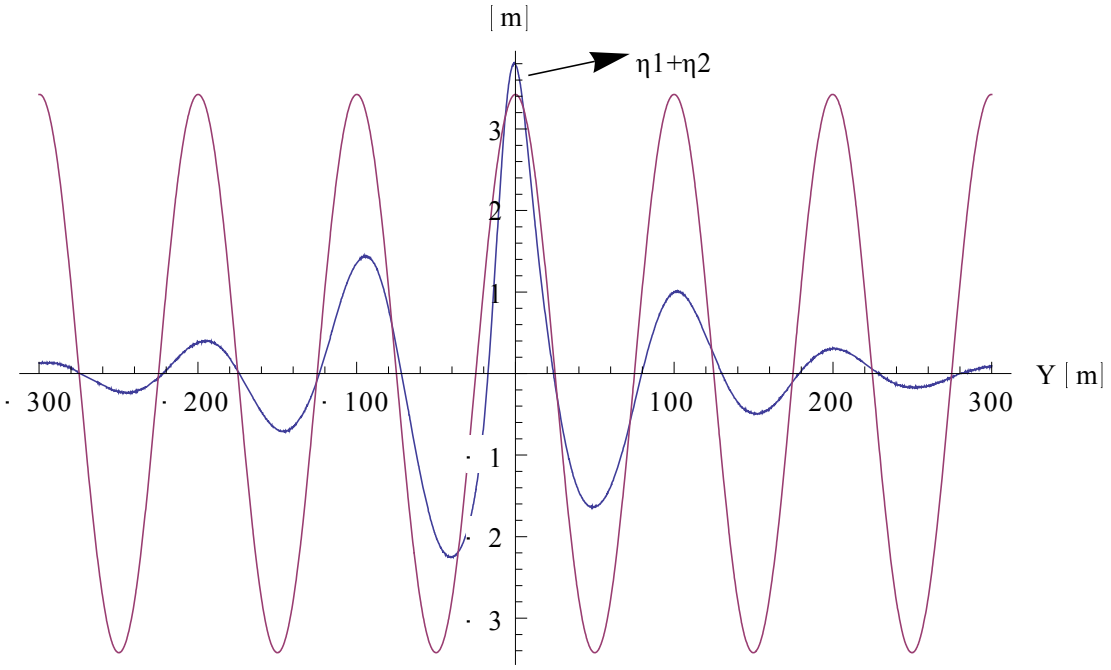

Figure 4.22: Comparison of the total second-order free surface displacement $\eta_1 + \eta_2$ (m) with the harmonic wave $y = H_c Cos\left[\left(\omega_p^2/g\right)Y - \omega_p t\right]$ (m) at the space domain $(T = 0\ sec)$

IV.6 *Concluding remarks*

The theory of Quasi-Determinism can be used in place of the periodic wave theory. It is valuable because it predicts what happens on the space-time domain just when the highest waves occur. As an example (x_0, y_0) could be the location of vessel and H the maximum expected wave height to be encountered during a specific route. Then the theory applicability allows one to predict the configuration of the water surface, the particle velocities and accelerations and finally the pressure fluctuations when this maximum wave height is affecting the specific structure.

It is an indisputable fact that non-linearity affects the crest elevation and the trough depth, but does not affect the crest-to-trough wave height. Similarly, the non-linearity shortens the wave crest and lengthens the wave trough, but does not affect the wave period. So, the second order corrections to the linear components of the QD theory that were given in Arena's calculations (2005), do not affect the crest-to-trough height for a narrow-band spectrum (though it may do so slightly for a finite bandwidth). According to extended studies carried out by Tayfun (1980) and Forristal (2000) it is confirmed that second-order corrections modify the distribution of crest heights (first formulation of the Quasi-Determinism theory). Under these circumstances, equations (4.17a-b) concerning the linear components of the theory, can be extended to the nonlinear wave height distribution of the total waveform $\eta_1 + \eta_2$ only in the case of the second formulation of the theory.

As for the period T_h it is obvious that the second-order effects do not provoke any modifications. A slight difference may be noticed in the crest and trough duration, which

are, respectively, equal to $0.43T_p$ and $0.49T_p$ (from the linear QD theory where they are both equal to $0.46T_p$).

Another observation on the nonlinearity effects that should be pointed out is that the crest height is increased by 16% (it is equal to $0.58H$), and the trough depth is decreased by 16% (the trough amplitude is equal to $0.42H$), with respect to linear predictions.

Special reference should be made at this conclusive point to the crucial parameter of the theory whose effects will come to light in the next chapters. Boccotti's research results in the minimum allowable value of this index so as the theory to be valid. Consequently, the settled condition is that if $a > 8$, as much as $a \to \infty$, the theory dominates over wave mechanics. However, with the increase of a the central crest-to-trough height increases dramatically with respect to H_s leading to unusually high waves out of interest for the study of ship rolling motions and further estimation of a capsizing risk level. In any case we deal with a specific identification index for every QD wave group.

At this point where the part of this thesis devoted to the wave mechanics is over, the final conclusions and benefits of the theory which will be essential for developing a ship stability probabilistic assessment framework should be gathered. The QD theory will be used as far as the second formulation is concerned due the discussed solidity to nonlinearity. Parameter a combined with the two consequences arising from the QD theory will possess a central role to the establishment of a new probabilistic approach on ship stability. Finally, the proposed improvements on the Rayleigh distribution function will be adopted in order to retain consistency with the QD theory.

In the Appendix more applications of the Quasi-Determinism theory are given for a variety of sea state parameters.

PART *II*

Probabilistic analysis of ship rolling

CHAPTER V:

A MATHEMATICAL MODEL OF SHIP ROLLING

This chapter aims to present the basic concepts of a well structured ship rolling oscillator that will take a central role in the development of the "Wave group theory" and the "Central wave theory" presented in chapter VI. Eventually, the calculation tools for the specification of "critical" wave groups[6] will be demonstrated. The ultimate goal is the subjection of such wave sets to a solid probabilistic analysis.

At this point, the deterministic character of a foreseen assessment methodology concerning ship dynamics comes to the scene. Numerical simulations performed in a *MATHEMATICA* environment will empower the prevalence of Quasi-Determinism theory over a founded ship stability model. However, certain weaknesses which occur in the context of the computational software program *MATHEMATICA* result in to a lower extent modeling procedure of the second QD formulation.

V.1 *A mathematical model of ship rolling in beam seas*

Let us consider a ship under the influence of regular (harmonic) waves that are generated in a direction vertical to the ship's longitudinal theoretical axis *x*, as it is shown in fig. *5.1*. Ship's motion can be modeled through the transverse rolling angle delimited by the center line vertical to the ship deck (*absolute rolling angle* χ) from an inclined to the upright position or the angle identified between the latter limit of angle χ and the vertical to the wave slope at midship (*relative rolling angle* φ). Both ways to identify the most appropriate rolling angle for our analysis have their pros and cons. In general terms, if it's about modeling ship rolling motions, it would be useful to record the time history of the absolute and the relative rolling angle as well. However, if one would be interested in avoiding capsizing, then he should focus on the relative rolling angle. On the other hand, if there is interest in the investigation of possible inertial excitation that can provoke critical cargo shift, then we should resort to the time history of the absolute rolling angle (Spyrou, NTUA 2009).

The subsequent analysis is based on Froude's experiments and calculations in about 1870. It should be noted that the ideas to be discussed, though approximate, are still popular internationally. Of course more sophisticated and complex hydrodynamic methods recently introduced in the field of ship dynamics can also be adopted. Nevertheless, the advantage of the followed approach is that a deeper insight is allowed in the matter of non linear effects as well as the limiting parameters that concern a ship stability concept.

Regarding the wave effect on ship's response, we will assume that the Froude-Krylov condition prevails. According to this assumption, the ship does not disrupt the form and scope of the incident pressures ripple (this assumption is more realistic as the ratio of the wavelength L to the ship's beam B tends to greater values, i.e., over 5). So, with the

[6] Wave groups leading to ship unsafe behavior.

condition of Froude-Krylov fulfilled and regarding a wave with extended wavelength, a linear approximation of the curve AOA' shown in fig. *5.1*, can be considered. Then, the hydrodynamic pressure isobars at the point where the wave is displaced by the ship hull will not differ from the standard hydrostatic condition and so, employing the relative rolling angle, we are able to simplify our analysis reaping the benefits of the stability parameters prevailing in calm water.

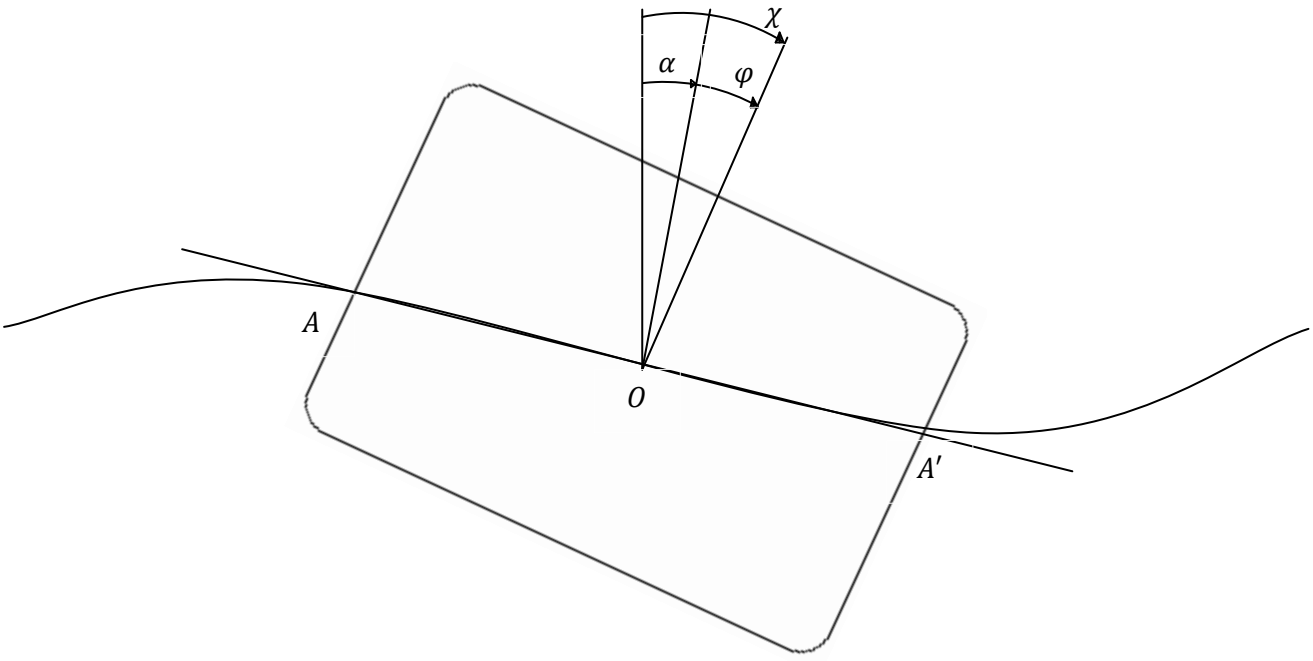

Figure 5.1: Ship rolling

In the case of wave excitation generated in beam seas (as defined fig. *5.2*), ship motion is affected by the system's inertial properties, resistance and tendecy to restore to the upright position. Starting from the latter, for a stable ship, the relative rolling angle will directly provoke a restoring moment. Therefore, a force yields from the system's stiffness, dependant on the time record of the relative rolling angle. In addition to this, there is a moment resisting to the ship motion owing to the rolling angular velocity. This is the damping moment, which is strongly connected with energy loss.

Equations of motion

At this point, let us introduce the critical parameters of our analysis and assign them to symbols:

- I, denotes the mass moment of inertia of the "dry" ship around her longitudinal axis *x* delimited from her centre of gravity if only one angular velocity acts upon the system

- $a = \pi \frac{H}{L}$, denotes the wave slope at midship, where H is the wave height and L is the wavelength

- $-\delta I(\ddot{\chi} - \ddot{a}) = -\delta I \ddot{\varphi}$, is the moment of inertia due to the surrounding fluid

- $-D(\dot{\varphi})$, is the damping moment and, as it was mentioned before, it is a function of the relative angular velocity

- $-R(\varphi)$, is the restoring moment as a function of the relative rolling angle

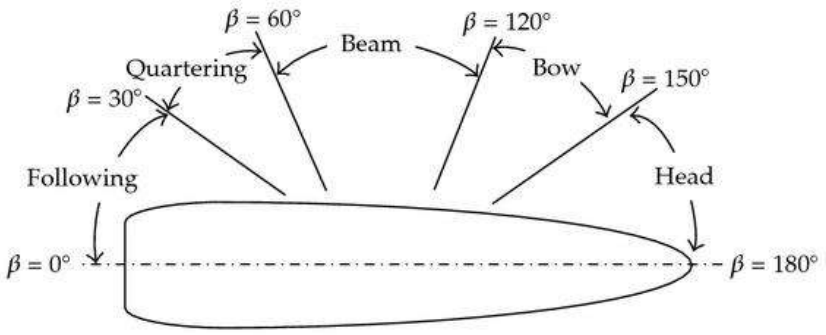

Figure 5.2: Definition of incident wave directions

In general, functions D, R are non linear and of odd order, with the effects of non linearity more obvious in the case of function $R(\varphi)$.

The equations of motion will be derived if the second law of Newton is applied (Spyrou, NTUA 2009):

$$I\ddot{\chi} = -\delta I \ddot{\varphi} - D(\dot{\varphi}) - R(\varphi) \tag{5.1}$$

and given that:

$$\chi = \varphi + a \tag{5.2}$$

equation (5.1) is formed as:

$$(I + \delta I)\ddot{\varphi} + D(\dot{\varphi}) + R(\varphi) = -I\ddot{a} \tag{5.3}$$

Note that ship excitation is proportional to the angular acceleration of the wave slope. In order to make equation (5.3) more specific, let us define functions D and R:

- ✓ *Damping moment:*

The following expressions are quite common in the case of the damping moment:

$$D(\dot{\varphi}) = B_1\dot{\varphi} + B_3\dot{\varphi}^3 \tag{5.4}$$

$$D(\dot{\varphi}) = B_1\dot{\varphi} + B_2|\dot{\varphi}|\dot{\varphi} \tag{5.5}$$

In fig. *5.3* the schematic representation of equations (5.4) – (5.5) is displayed:

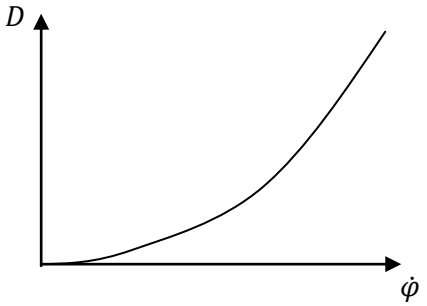

Figure 5.3: Function of damping moment $D(\dot{\varphi})$ according to equations (5.4), (5.5)

However, for the demonstration of the methodology described in chapter VI, and alternative and simplified approximation of the damping moment will be used:

$$D(\dot{\varphi}) = B_4\dot{\varphi} \tag{5.6}$$

where B_4 is the linear equivalent of the roll damping coefficient. Undoubtedly, the process can be followed without any modifications when equations (5.4) and (5.5) are to be employed. In fig. *5.4* the linear approximation of the damping moment function is depicted.

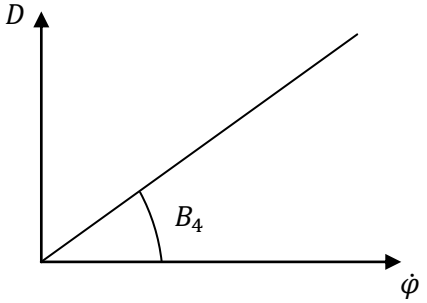

Figure 5.4: Function of damping moment $D(\dot{\varphi})$ according to equation (5.6)

✓ *Restoring moment:*

As far as the restoring moment is concerned, the following expression will be adopted:

$$R(\varphi) = \Delta g GM\varphi + \left(-\frac{\Delta g GM}{{\varphi_v}^2}\right)\varphi^3 \tag{5.7}$$

where Δ is the ship displacement, g is the gravity acceleration, GM is the metacentric height and φ_v is the critical angle of stability loss where $R(\varphi_v) = 0$. Fig. *5.5* shows a typical form of the equation (5.7):

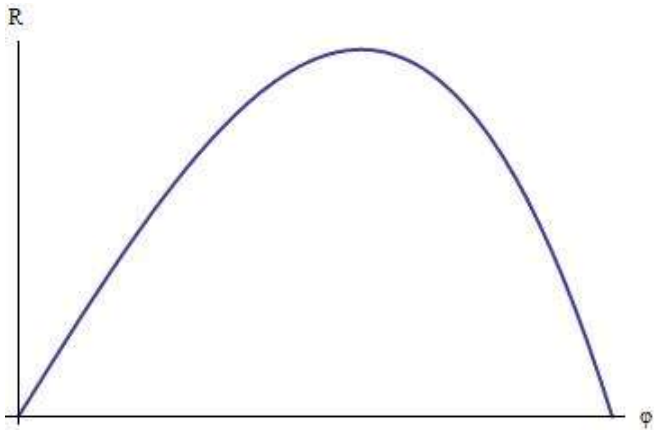

Figure 5.5: Function of restoring moment $R(\varphi)$ according to equation (5.7)

The greatest disadvantage of the representation of the restoring moment function and thus the righting arm through a cubic polynomial can be stated as follows: There are only two independent parameters that affect the function's form and thus, there are no many options if one would consider modifying the form of the restoring moment function. The parameters usually selected to be independent are: a) the metacentric height (GM) and b) the critical angle of stability loss (φ_v). The final result is that parameters that depict stability conditions, i.e., GZ_{max} , cannot be independently selected. Consequently, to overcome this drawback, it would be preferable to use polynomials of greater order (5th or 7th are sufficient) or splines and Bezier curves for the representation of the restoring moment function $R(\varphi)$. However, as the purpose of this thesis is to demonstrate a more realistic methodology concerning ship stability behavior, for practical applications the cubic approximation of the restoring moment function will be used. Without a doubt, the methodology is applicable for functions $R(\varphi)$ of higher order.

V.2 *Regular waves*

Let us consider the equation of a sinusoidal wave in deep water (see fig. *5.6*):

$$\xi = Asin(kx - \omega t) \tag{5.8}$$

where A, k, ω are the wave amplitude, the wave number and the angular frequency, respectively [see fig. *5.6*]. For the wave number it is indicated that:

$$k = \frac{2\pi}{L} \tag{5.9}$$

with L the wavelength as defined in fig. *5.6*.

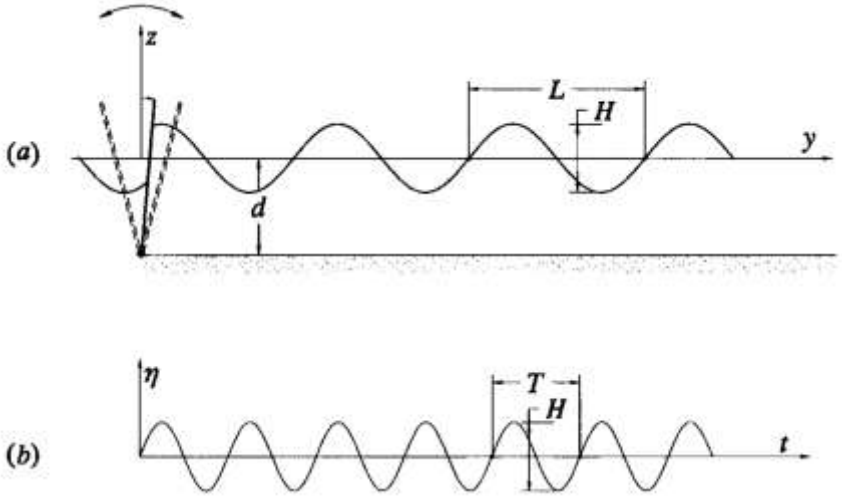

Figure 5.6: (a) Waves on the space domain, (b) Waves on the time domain

The wave slope a will be the derivative of ξ at the space domain:

$$a = \frac{\partial \xi}{\partial x} = Akcos(kx - \omega t) \tag{5.10}$$

Therefore, the maximum wave slope through equation (5.9) will be:

$$a_{max} = Ak = \frac{2\pi}{L}\frac{H}{2} = \pi\left(\frac{H}{L}\right) \tag{5.11}$$

For a specific ship position x (let us consider that $x = 0$ for the simplification of the process), we obtain:

$$\ddot{a} = -Ak\omega^2 cos(\omega t) \tag{5.12}$$

Combining equation (5.3) with (5.6),(5.7),(5.12) we conclude into the ship rolling equation in regular beam seas:

$$(I+\delta I)\ddot{\varphi}+B_4\dot{\varphi}+\Delta gGM\left(\varphi-\frac{1}{{\varphi_\nu}^2}\varphi^3\right)=IAk\omega^2cos(\omega t) \tag{5.13}$$

or in the dimensionless form:

$$\ddot{\varphi}+b_4\dot{\varphi}+{\omega_0}^2\left(\varphi-\frac{1}{{\varphi_\nu}^2}\varphi^3\right)=\frac{I}{(I+\delta I)}Ak\omega^2cos(\omega t) \tag{5.14}$$

where

$$b_4=\frac{B_4}{(I+\delta I)} \tag{5.15}$$

$$\omega_0=\sqrt{\frac{\Delta gGM}{(I+\delta I)}} \tag{5.16}$$

Through equations (5.14) and (5.16) the definition of the linear (concerning small amplitude stimulations) natural period for ship's rolling without damping, is defined.

V.3 *Irregular waves – The Quasi-Determinism theory is employed*

Under the consideration of the second formulation of the Quasi-Determinism theory the previous analysis regarding the effects of regular beam excitation can be extended. In more detail, in the previous chapter, the linear component of the quasi-deterministic wave group was given in the form:

$$\eta_1=\frac{{H^*}/{2}}{\sigma^2-\psi(T^*)}\int_0^\infty E(\omega)\cdot\{\cos[\ \varphi(\omega,Y,T)]-\cos[\varphi(\omega,Y,T)+\omega T^*]\}d\omega \tag{5.17}$$

Now, the wave slope a will be the derivative of η_1 at the space domain:

$$a=\frac{\partial\eta_1}{\partial x} \tag{5.18}$$

For a specific ship position x (let us consider that $x = 0$), it is finally given that:

$$\ddot{a} = \frac{\partial^2}{\partial t^2}\left[\frac{\partial \eta_1}{\partial x}\right]_{x=0} \tag{5.19}$$

Combining equation (5.3) with (5.6),(5.7),(5.19) the ship rolling equation in irregular beam seas is defined as:

$$(I + \delta I)\ddot{\varphi} + B_4\dot{\varphi} + \Delta g GM\left(\varphi - \frac{1}{{\varphi_v}^2}\varphi^3\right) = -I\frac{\partial^2}{\partial t^2}\left[\frac{\partial \eta_1}{\partial x}\right]_{x=0} \tag{5.20}$$

or in the dimensionless form:

$$\ddot{\varphi} + b_4\dot{\varphi} + {\omega_0}^2\left(\varphi - \frac{1}{{\varphi_v}^2}\varphi^3\right) = -\frac{I}{(I + \delta I)}\frac{\partial^2}{\partial t^2}\left[\frac{\partial \eta_1}{\partial x}\right]_{x=0} \tag{5.21}$$

Of course, one would prefer to add the effects of the second order corrections to the linear components of the QD theory. Then, eq. (5.21) would be formed as follows:

$$\ddot{\varphi} + b_4\dot{\varphi} + {\omega_0}^2\left(\varphi - \frac{1}{{\varphi_v}^2}\varphi^3\right) = -\frac{I}{(I + \delta I)}\frac{\partial^2}{\partial t^2}\left[\frac{\partial (\eta_1 + \eta_2)}{\partial x}\right]_{x=0} \tag{5.22}$$

where

$$\begin{aligned}\eta_2 = \frac{(H^*)^2}{16\cdot\left(\sigma^2 - \psi(T^*)\right)^2}\int_0^\infty\int_0^\infty & E(\omega_1)\cdot E(\omega_2)\\ &\cdot\{-|k_1 - k_2|\\ &\cdot\left[\left(1 - \cos(\omega_1 T^*) - \cos(\omega_2 T^*) + \cos(\omega_1 T^* - \omega_2 T^*)\right)\cdot\cos(\varphi_1 - \varphi_2)\right.\\ &\left.+\left(\sin(\omega_1 T^*) - \sin(\omega_2 T^*) - \sin(\omega_1 T^* - \omega_2 T^*)\right)\cdot sin(\varphi_1 - \varphi_2)\right]\\ &+ (k_1 + k_2)\\ &\cdot\left[\left(1 - \cos(\omega_1 T^*) - \cos(\omega_2 T^*) + \cos(\omega_1 T^* + \omega_2 T^*)\right)\cdot\cos(\varphi_1 + \varphi_2)\right.\\ &\left.+\left(\sin(\omega_1 T^*) + \sin(\omega_2 T^*) - \sin(\omega_1 T^* + \omega_2 T^*)\right)\right.\\ &\left.\cdot sin(\varphi_1 + \varphi_2)\right]\}d\omega_2 d\omega_1\end{aligned} \tag{5.23}$$

However, for the practical applications it was not feasible to reach a solution to the modified (according to the second order corrections) differential equation (5.22). In the *MATHEMATICA* environment, the powerful function ***NDSolve***, discussed in "*Numerical Differential Equations*", was the tool to approach numerical solutions to differential equations. `NDSolve` handles both single differential equations, and sets of simultaneous

differential equations. It can handle a wide range of *ordinary differential equations* as well as some *partial differential equations*. However, in the case of solving eq. (5.22) the function ended to no short-term results.

This fact should not be regarded as a weakness of the current analysis, though. The second formulation of the QD theory is not affected in its probabilistic aspect by second order corrections, as mentioned in the concluding remarks of the previous chapter. Consequently, a time consuming repetitive procedure such this of integrating the nonlinearity effects to the developed ship rolling model is eventually avoided for practical reasons.

V.4 *Concluding remarks based on a brief sensitivity analysis*

The concept of the procedure is given in this paragraph. Firstly, for five pre-defined sea state conditions (H_s, T_p) shown in tables 5.1a-b, the most probable non regular wave groups (with a certain central wave height H^*) were identified for the minimum possible value of index $a = 8$. Then, harmonic wave groups were generated in the form of eq. (5.24) and simulations were performed for the ship scenario of table 5.2. The idea to proceed in further analysis considering harmonic waves according to eq. (5.24), originates from the foundations laid from the QD theory.

$$\xi = \frac{H^*}{2} sin(kx - \omega_h t) \tag{5.24}$$

where $\omega_h = 2\pi/T_h$ and $T_h = 0.92T_p$. H^* is the quasi-deterministic central wave height.

Period scenario $T_p = 16\ sec$	$H_s\ [m]$
1	3.5
2	6.0
3	9.0
4	12.0
5	15.0

Table 5.1a

Height scenario $H_s = 3.5\ m$	$T_p\ [sec]$
1	8.0
2	11.0
3	13.0
4	16.6
5	18.0

Table 5.1b

$GM_{corrected}$	*2.08 m*
T_0 *(ship natural period)*	*15.26 sec*
$I + \delta I$	*1.965·10^9 kg·m^2*
B_4	*10^8 kg·m^2/sec*
φ_v	*1.15 rad*

Table 5.2: Ship stability particulars

When regular or irregular excitation simulations evolved, the maximum observed rolling angle was recorded. The final results of the calculations are shown in figures *5.7-5.8*:

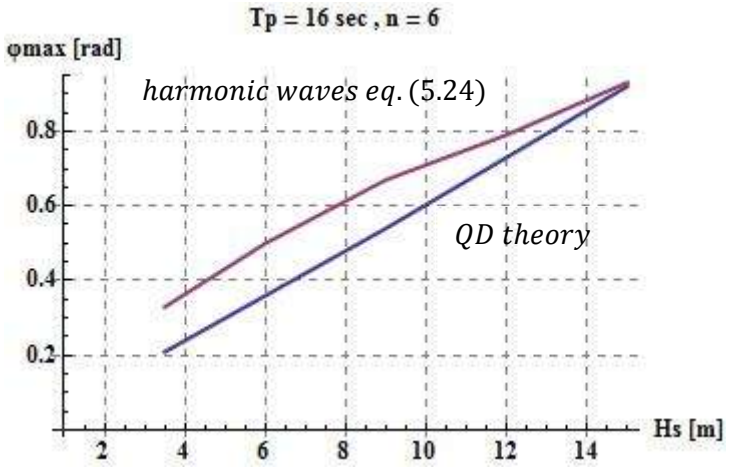

Figure 5.7: Sensitivity analysis with regard to H_s

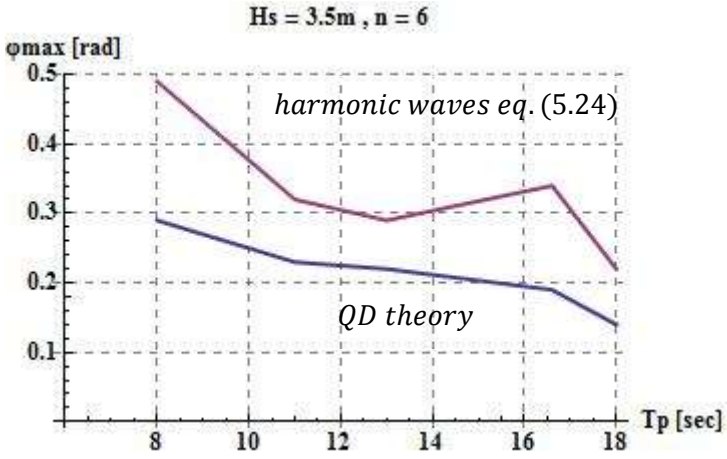

Figure 5.8: Sensitivity analysis with regard to T_p

The results verify that maximum rolling angle was reached in different time periods for each method. For example, in the case of regular modeling, maximum rolling angle was recorded during the time period of the first two successive waves' influence (transient response). Obviously, low group run lengths might result in ship capsizing. On the other hand, a QD wave group needed approximately 6 waves (till the central wave is encountered) to reach the maximum rolling angle, though it was definitely lower than the one observed in the regular case. This fact can be attributed to the lack of vessel's transient response to QD stimulation moments [see fig. *5.9a*]. Finally, as expected, regular models end up with a safe side prediction on the assessment of ship stability in beam seas. In figures *5-9a-d* are presented typical rolling history responses for the assumed scenarios given in tables 5.1a-b.

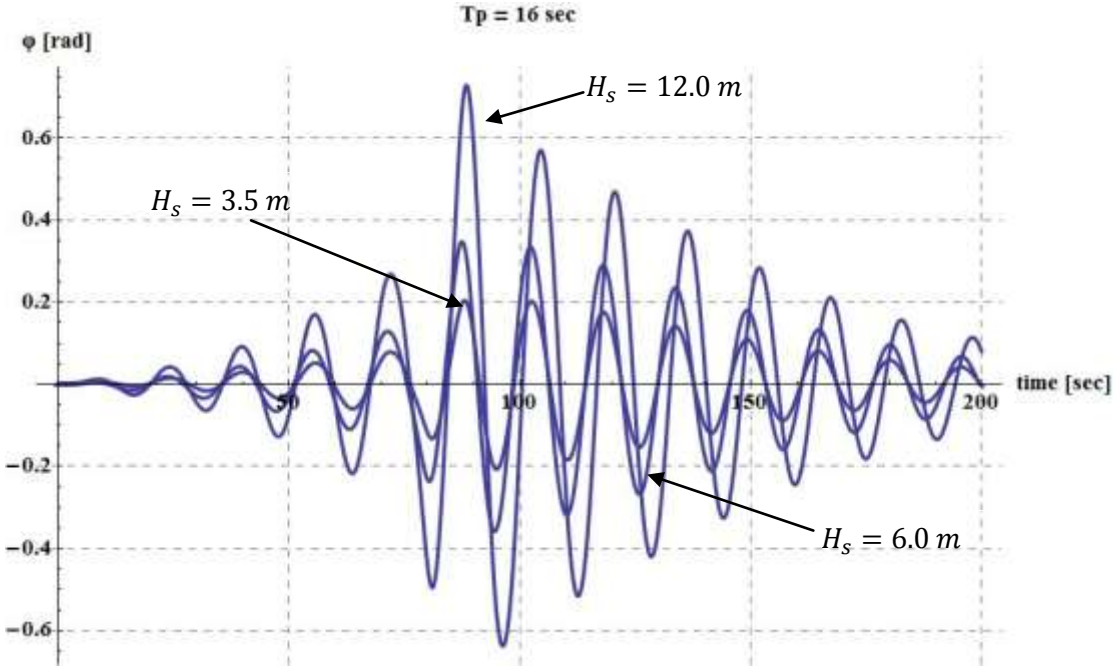

Figure 5.9a: Typical rolling history scenarios due to QD excitation

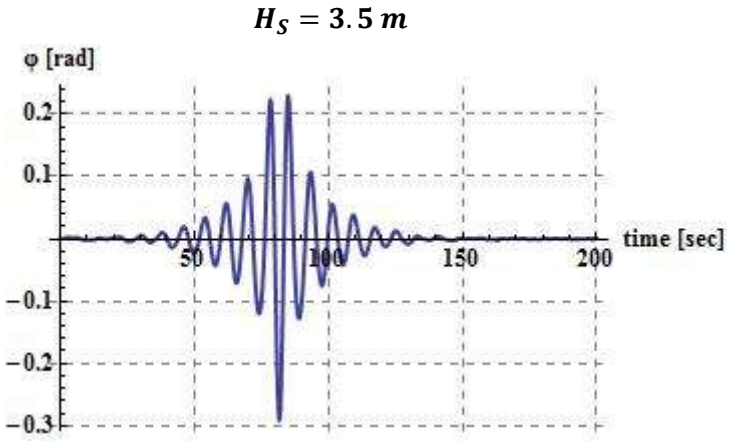

Figure 5.9b: Typical rolling history scenarios due to QD excitation $(T_p = 8\ sec)$

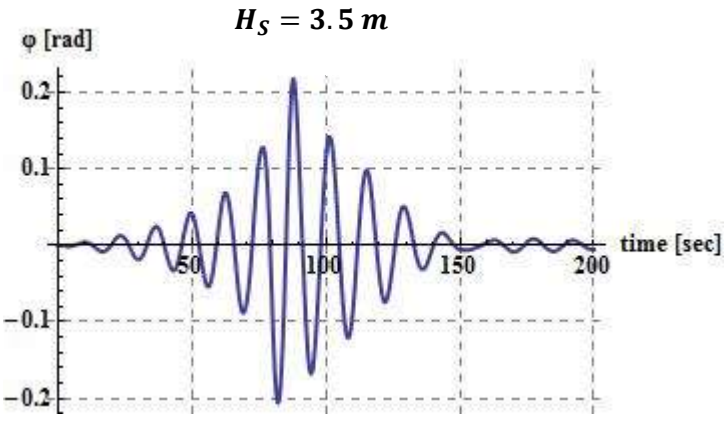

Figure 5.9c: Typical rolling history scenarios due to QD excitation $(T_p = 13\ sec)$

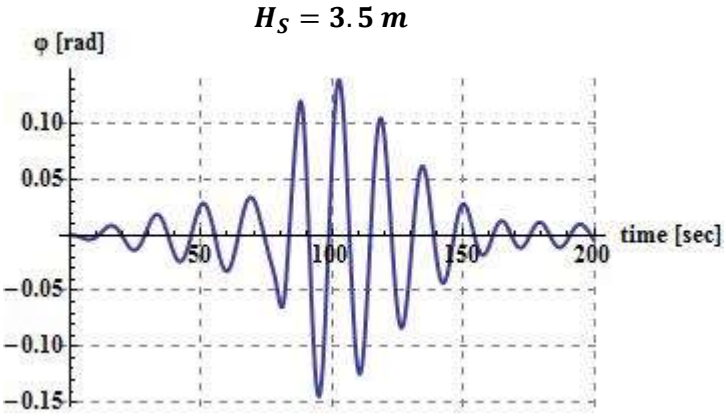

Figure 5.9d: Typical rolling history scenarios due to QD excitation $(T_p = 18\ sec)$

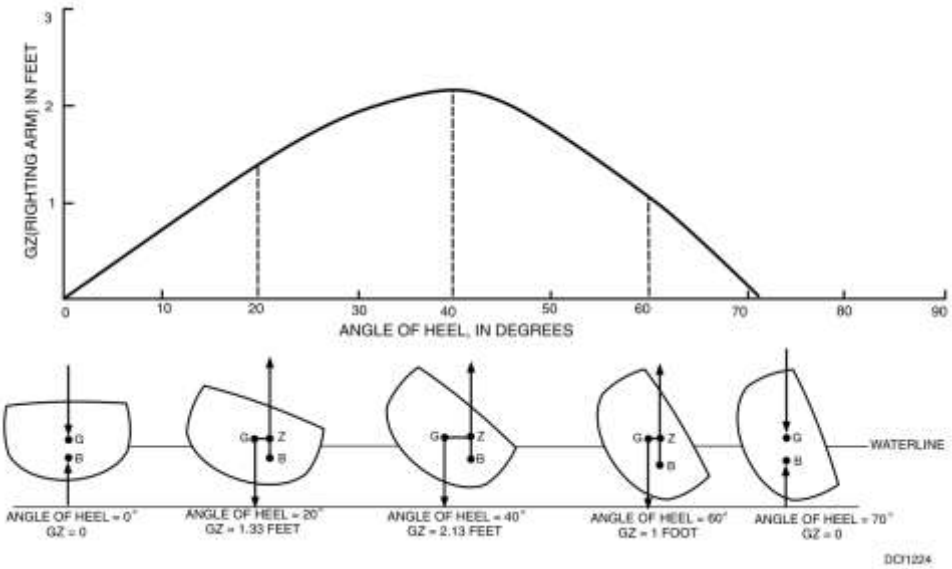

Figure 5.10: A typical example of the correlation between the curve of static stability and ship rolling potential (taken from "Ship stability for masters and mates" booklet)

CHAPTER VI:

A WAVE GROUP THEORY BASED ON THE QUASI DETERMINISM THEORY

The purpose of the current Chapter is to recommend a new modeling method, regarding the phenomenon of ship rolling in a more realistic and applicable way.

VI.1 *The concept of the methodology*

After the comprehensive description of the Quasi-Determinism (QD) theory followed by the establishment of a ship rolling mathematical model, the deterministic character of this thesis is over. As a consequence, the probabilistic aspect of the assessment methodology is to be presented. It is consisted of two different theories each one based on completely different principals concerning the structure of the wave groups. Structural differences amongst wave groups lead to modifications to the employed probabilistic methods. In other words, regular wave groups are to be treated in a different way than the non regular ones through the application of a certain probabilistic method.

In the case of the first theory called Wave Group (WG) theory, successive waves in a wave group are considered as a Markov Chain sequence. In words: *Markov Chain sequence is a stochastic process of events the probability for each of which depends only on the event immediately preceding it*. In more detail, we have to deal with a *"memoryless"* random process. Thus, each wave probability of occurrence in the group is strongly affected by the probability of occurrence for the wave firstly encountered in the sequence.

On the other hand, the second theory seems to be more consistent with the semi-deterministic foundations laid by Boccotti's QD theory [see chapter IV]. According to these, if a wave of a very large height (H^*) participating in a group occurs, the total group surface displacement is strongly connected with H^*. Thus, each wave of the set would occupy the centre of a well defined group that is the sum of a deterministic framework and a residual random noise of a smaller order. The form of the deterministic component was given in chapter IV as:

$$\eta_1 = (x_0 + X, y_0 + Y, t_0 + T) = \frac{\psi(X,Y,T) - \psi(X,Y,T-T^*)}{\psi(0,0,0) - \psi(0,0,T^*)}\frac{H^*}{2} \tag{6.1}$$

In consistency with such an approach, the probability of occurrence for each wave of the group sequence is dependent on the central wave's probability of occurrence. The central wave takes the central role in this approach and for this reason the Central Wave (CW) theory arises. Of course the validity of the theory will be empowered when parameter $a = H/\sigma \to \infty$, as already explained.

The principal aim of the theories applications presented in the next chapter will be to display the total probability rate of capsizing for each employed theory for a range of different sea state scenarios. Firstly, the familiar concept of Wave Group theory on regular wave groups will be applied. Then, the Wave Group theory on irregular waves will be considered and finally imposed on the Central Wave theory. In such a way, the total results based on irregular waveform methods will be clearly compared to the regular WG theory.

To determine norms of unsafe behavior for ship rolling motions, the "Weather Criterion" will be applied. Afterwards, the critical wave groups will be specified through simulation of the mathematical model developed in chapter V per sea state scenario. The ship will always be at the upright position. No initial inclination will be taken into consideration.

The final outcome of the procedure will be the total probability rate of instability for the considered sea state scenarios depending on the employed probabilistic method. Eventually, all three methodologies will be integrated into a united framework for the assessment of ship stability.

VI.2 *Regular wave groups and Wave Group theory*

Regular excitation is univocal for each ship and independent of the altering sea state parameters. So, according to the original concept of the WG theory, the realistic range of periods of ocean waves should been spanned [4-20 sec]. However, in order to be able to proceed in an immediate comparison of the results between regular and non regular based probabilistic theories, we should take a closer look into the regular time period span in the vicinity of $T_h = 0.92T_p$. This is the expected period of the central wave prevailing in a semi-deterministic wave group. In this way, we set equilibrium between regular and non regular groups so as to reach into comparable results. Moreover, in this way, the sea state affects regular waves indirectly.

With these in mind, the specification of the regular critical wave groups is limited to the determination of the critical wave group parameters. These are:

1. the wave height (H^*) which is the same for all the successive waves in the regular sequence,
2. the critical wave group period (T) and
3. the run length (n).

The final step of the procedure is the calculation of the probability for encountering the defined critical wave groups. The probability calculation procedure is based on the following concept (Themelis, 2008):

$$P_{encounter} = P_1 \cdot P_2 \tag{6.2}$$

$$P_1 = P(T_1, T_2, \dots, T_k | H_n > H_{cr}) = \int_{\tau_i}^{\tau_j} \underbrace{\int \dots \int}_{k} \int_{\tau_i}^{\tau_j} f(\boldsymbol{\tau} | h_n > h_{cr}) d\tau \,, n = 1, \dots, k$$

(6.3)

$$P_2 = P(H_1 > H_{cr}, \dots, H_k > H_{cr}) = \int_{h_{cr}}^{\infty} \int \dots \int_{h_{cr}}^{\infty} f(h_1, \dots, h_k) dh_1 \dots dh_k$$

(6.4)

where $\boldsymbol{\tau} = [\tau_1, \tau_2, \dots, \tau_k]^T$ and $\tau = T / T_m$, $h = H / H_{rms}$ are respectively the dimensionless wave period and height. T_m and H_{rms} stand for mean spectral period and root - mean - square wave height respectively. All the above calculations will be derived by the frequency spectra information. In more detail:

In the first probability [eq.(6.3)], the following multivariate conditional pdf of p -successive waves will be utilized:

$$f_{\boldsymbol{T}|\boldsymbol{H}}(\boldsymbol{\tau} | h_i > h_{cr}) = \frac{1}{(2\pi)^{p/2} \left| \Sigma_{\tau|h_{cr}} \right|^{1/2}} exp\left(-\frac{1}{2} \left(\boldsymbol{\tau} - \boldsymbol{\mu}_{\tau|\xi} \right)^T \Sigma_{\tau|h_{cr}}^{-1} \left(\boldsymbol{\tau} - \boldsymbol{\mu}_{\tau|\xi} \right) \right)$$

(6.5)

where

$\Sigma_{\tau|h_{cr}}$ is the covariance matrix given as:

$$\Sigma_{\tau|h_{cr}} = \begin{bmatrix} \sigma^2_{\tau|h_{cr}} & Cov[T_1, T_2 | H_{cr}] & Cov[T_1, T_p | H_{cr}] \\ \vdots & \dots & \vdots \\ Cov[T_1, T_p | H_{cr}] & \dots & \sigma^2_{\tau|h_{cr}} \end{bmatrix}$$

(6.6)

and $[T_i, T_j | H_{cr}] = \rho_{ij} \sigma^2_{\tau|h_{cr}}$. The mean values $\mu_{\tau|\xi}$ and the standard deviations $\sigma_{\tau|h_{cr}}$ are calculated from the below given formulas:

$$\mu_{\tau|\xi} = 1 + \nu^2 (1 + \nu^2)^{-3/2}$$

(6.7a)

$$\sigma_{\tau|\xi} = \frac{2\nu}{\sqrt{8}h(1+\nu^2)} \tag{6.7b}$$

with $h = H/\,H_{rms}$, $\tau = T/T_m$ and ν the well known bandwidth parameter.

The correlation coefficient ρ_{ij} corresponds to the correlation of wave periods whose sequence also forms a Markov Chain (Kimura 1980):

$$\rho_{ij} = (\hat{\rho}')^{j-1}, j \geq 2 \tag{6.8}$$

In a study carried out by Stansell et al (2002), time domain field data were compared in terms of group statistics with spectral prediction methods. According to the study an improved spectral estimate of the correlation parameter $\left(\hat{\kappa}_{f_2}\right)$ is given by:

$$\hat{\kappa}_{f_2}{}^2 \approx \hat{\rho}' - \frac{\hat{\rho}'}{16} - \frac{\hat{\rho}'}{128} \tag{6.9}$$

where

$$\hat{\rho}' = \frac{16-4\pi}{\pi}\hat{\rho}_{HHf} \tag{6.10}$$

$$\hat{\rho}_{HHf} = \frac{\rho_{HHf}\left(\hat{T}/2\right) + 2\rho_{HHf}\left(\hat{T}\right) + \rho_{HHf}\left(3\hat{T}/2\right)}{2 + 2\rho_{HHf}\left(\hat{T}/2\right)} \tag{6.11}$$

$$\rho_{HHf}(\tau) = \frac{\pi}{16-4\pi}\left(k^2(\tau) + \frac{k^4(\tau)}{16} + \frac{k^6(\tau)}{64}\right), for\ \tau = \hat{T}/2\,, \hat{T}, 3\hat{T}/2 \tag{6.12}$$

$$k(\tau) = \frac{1}{m_0}\left|\int_0^\infty E(\omega)\, e^{i2\pi\omega\tau} d\omega\right| \tag{6.13}$$

where $\hat{T}$ stands for T_m , the mean spectral period.

For the calculation of the second probability [eq.(6.4)], the multivariate joint pdf $f\ (\boldsymbol{h})$ or $f\ (h_1, \dots, h_k)$ will be estimated according to:

$$f\ (h_1, \dots, h_k) = f\ (h_k|h_{k-1}) \dots f\ (h_2|h_1) f\ (h_1) \tag{6.14}$$

where the conditional bivariate pdf are derived from:

$$f\ (h_{i+1}|h_i) = \frac{f\ (h_i, h_{i+1})}{f\ (h_i)} \tag{6.15}$$

The joint pdf $f\ (h_{i+1}|h_i)$ is estimated by the bivariate Rayleigh distribution for successive wave heights:

$$f(H_1, H_2) = \frac{4H_1H_2}{\left(1 - \left(\hat{\kappa}_{f_2}\right)^2\right) H_{rms}^4} e^{-\frac{\left(H_1^2 + H_2^2\right)}{\left(1-\left(\hat{\kappa}_{f_2}\right)^2\right)H_{rms}^2}} I_0\left(\frac{2\hat{\kappa}_{f_2} H_1 H_2}{\left(1 - \left(\hat{\kappa}_{f_2}\right)^2\right) H_{rms}^2}\right) \tag{6.16}$$

whilst for $f\ (h_i)$ the improved Rayleigh distribution is used [see chapter IV, eq.(4.19b)]. Therefore, the Markov chain concept allows for the estimation of the multivariate joint pdf through eq.(6.14) by the combination of the conditional bivariate pdfs.

Eventually, the total sea state scenario[7] probability rate of instability $\left(P_{wg}\right)$ will be calculated from the equation:

$$P_{wg} = \sum_{r=1}^{l} \sum_{n=2}^{k} P_{encounter_{r,n}} \tag{6.17}$$

where P_r corresponds to probabilities of different segments of the wave period range, while P_n represent probabilities of different run lengths. Probabilities for each segment are summed up. Events of wave-group-encounter in a range $r \in \left[T_i\ , T_j\ \right]$ with $n = 2,3, \dots, k$ successive waves are treated as independent but not mutually exclusive. The minimum run length (the minimum number of waves consisting a wave group) is obviously $n = 2$.

The followed procedure is developed in more detail by N. Themelis (“Probabilistic Assessment of Ship Dynamic Stability in Waves”). In fig. *6.1* the methodology is depicted in steps:

[7] A sea state scenario will be referred as “node” in the following sections.

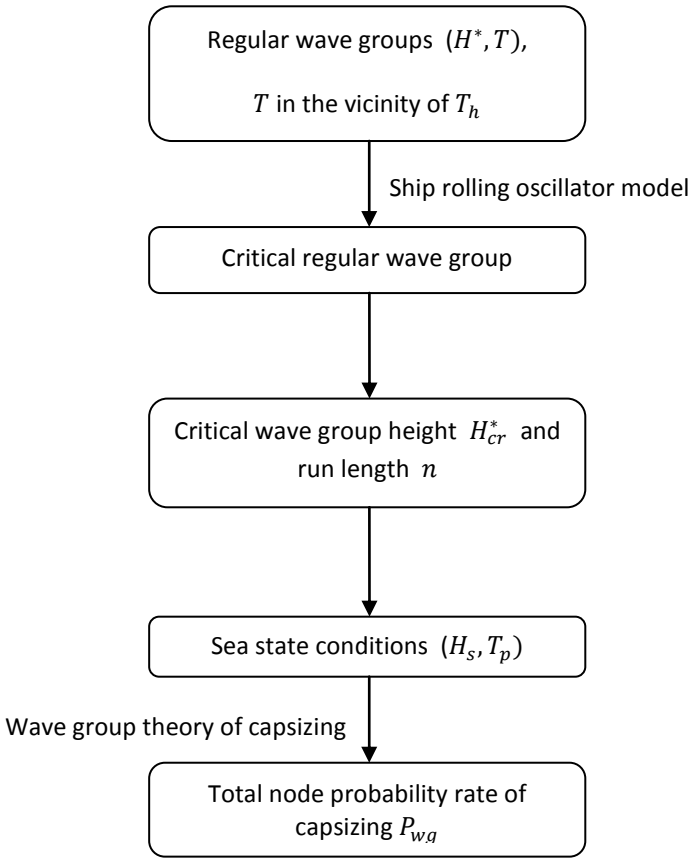

Figure 6.1: Flow-chart of the methodology concerning regular wave groups

VI.3 *Irregular wave groups and the Wave Group theory*

When we deal with irregular wave groups, essential modifications to the basic concept of the WG theory, have to be applied. These modifications are based on the conception of a united theory, in which the Quasi-Determinism theory is imposed on the Wave Group theory. In this method the specification of the non regular critical wave groups is limited to the specification of the critical wave group with the parameter a limited to the minimum value[8]. For this specific wave group, the important parameters to be noted are:

1. the critical wave height (H^*), defined in an indirect manner if the spectrum form and parameter a are given,
2. the critical wave group period (T_h), which is well defined through the consequences of the QD theory and
3. the run length (n)[9]

[8] $a > 8$ in any case so as the QD approach to be applicable.

[9] Usually in practical applications the number of waves constituting the group will be taken approximately at $n = 8$ waves because greater run lengths include waves with no defined period and of very low height (referred as "noise" in Boccotti's analysis).

Finally, the calculation of the total node probability rate $P_{wg,QD}$ is the same as in the regular case [see previous paragraph]. The only difference which implies a more realistic estimation of the risk effects upon ship instability is that in eq. (6.3) and (6.4) the critical wave heights (H_{cr}) differ for each wave of the set in a matter dictated into DQ theory.

VI.4 *Feasibility analysis on the integration of QD into WG theory*

Obviously, the WG theory is applicable and effective in the case of regular wave groups (see N. Themelis, "Probabilistic Assessment of Ship Dynamic Stability in Waves"). Thus, in order to embrace a united theory with the light of QD theory, it is of utmost importance to secure the feasibility of such a combined theory. Of course, the new theory should reach into reasonable conclusions and this fact will be investigated in the following pages. So, let us assume a certain peak period $T_p = 10$ sec while altering the significant wave height H_s in the way shown in table 6.1:

$Node$	$H_s\ [m]$
1	4.5
2	6.0
3	7.5
4	9.0

Table 6.1: Wave statistics (sea state parameters) per node

Now let us consider three regular plus three irregular wave groups noted as a, b, c and d, e, f, respectively, with their characteristics shown in table 6.2. The investigation procedure targets in the vicinity of the most probable (according to chapter IV) group period, $T_h = 0.92T_p = 9.2\ sec$. As far as the determination of the three irregular groups is concerned, the QD theory was not employed, as its validation through the application of the WG theory, is the object of our analysis. Thus, the individual successive wave heights were selected arbitrarily in a way so as to fulfill the QD assumption of > 8 . The group run length was selected as $n = 3$ for all the sets (regular or not).

For the calculation of the period[10] probability occurrence the integration methods were applied in the span of:

$$T_{cr} \in [T_{cr} - 0.5\ sec\ , T_{cr} + 0.5\ sec]$$

Now, employing the WG theory, the final results are given in tables 6.3a-b and fig. *6.2a-d*:

[10] Each wave is considered with its period approximately equal to the wave group period.

$wavegroup$	$h_i[m]$	$T_{group}\ [sec]$
$\boldsymbol{a}$	16.0	$0.92T_p - 1\ sec = 8.2\ sec$
$\boldsymbol{b}$	16.0	$0.92T_p = 9.2\ sec$
$\boldsymbol{c}$	16.0	$0.92T_p + 0.5\ sec = 9.7\ sec$
$\boldsymbol{d}$	$i\,th\,wave$ / $h_i[m]$: **1** 16.0; **2** 18.0; **3** 20.0	$0.92T_p - 1\ sec = 8.2\ sec$
$\boldsymbol{e}$	$i\,th\,wave$ / $h_i[m]$: **1** 16.0; **2** 18.0; **3** 20.0	$0.92T_p = 9.2\ sec$
$\boldsymbol{f}$	$i\,th\,wave$ / $h_i[m]$: **1** 16.0; **2** 18.0; **3** 20.0	$0.92T_p + 0.5 = 9.7\ sec$

Table 6.2: Characteristics of the considered wave groups

$H_s\ [m]$	$wavegroup\ a$ $0.92T_p - 1\ sec$	$wavegroup\ b$ $0.92T_p$	$wavegroup\ c$ $0.92T_p + 0.5\ sec$
4.5	$1.1393 \cdot 10^{-29}$	$1.3136 \cdot 10^{-28}$	$1.8842 \cdot 10^{-48}$
6.0	$7.2978 \cdot 10^{-18}$	$4.5241 \cdot 10^{-17}$	$4.6145 \cdot 10^{-29}$
7.5	$2.6739 \cdot 10^{-12}$	$1.1469 \cdot 10^{-11}$	$6.5361 \cdot 10^{-20}$
9.0	$\mathbf{3.2817 \cdot 10^{-9}}$	$\mathbf{1.1026 \cdot 10^{-8}}$	$\mathbf{7.9959 \cdot 10^{-15}}$

Table 6.3a: Application results

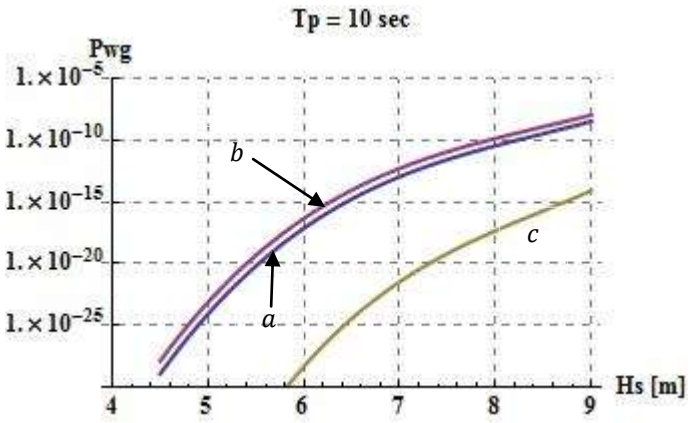

Figure 6.2a: Application results; groups a, b, c

Figure 6.2b: Application results; groups a, b, c

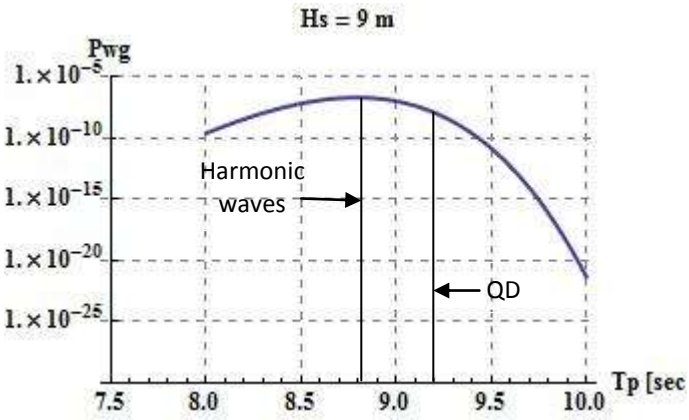

$H_s\ [m]$	$wavegroup\ d$ $0.92T_p - 1\ sec$	$wavegroup\ e$ $0.92T_p$	$wavegroup\ f$ $0.92T_p + 0.5\ sec$
4.5	$4.0539 \cdot 10^{-37}$	$6.3707 \cdot 10^{-36}$	$1.4587 \cdot 10^{-60}$
6.0	$4.1575 \cdot 10^{-22}$	$3.2373 \cdot 10^{-21}$	$5.6766 \cdot 10^{-36}$
7.5	$4.6348 \cdot 10^{-15}$	$2.3820 \cdot 10^{-14}$	$2.0596 \cdot 10^{-24}$
9.0	$\mathbf{3.6424 \cdot 10^{-11}}$	$\mathbf{1.4218 \cdot 10^{-10}}$	$\mathbf{5.1497 \cdot 10^{-18}}$

Table 6.3b: Application results

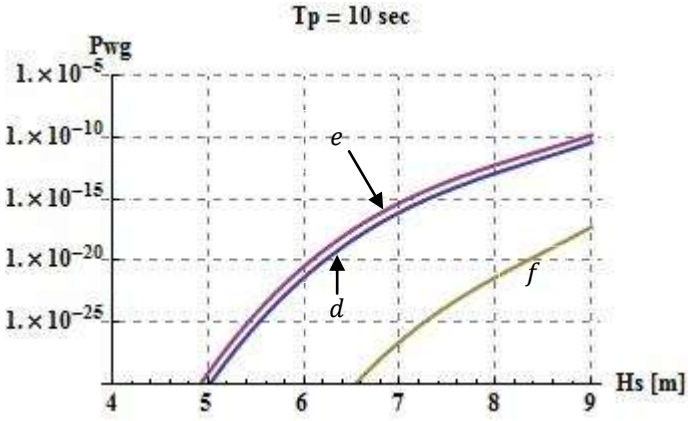

Figure 6.2c: Application results; groups d, e, f

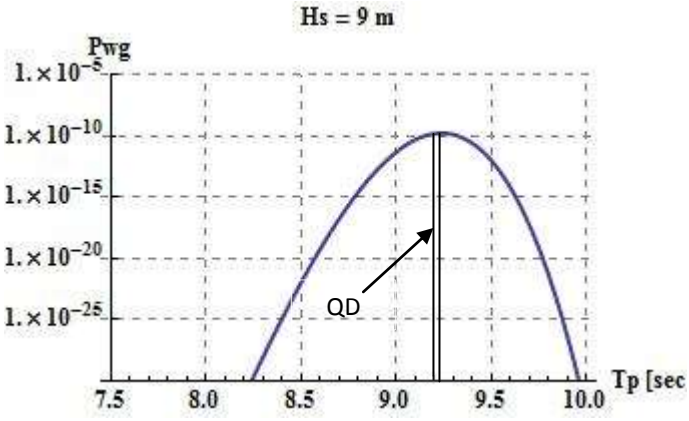

Figure 6.2d: Application results; groups d, e, f

Now let us repeat the procedure considering the regular wave groups shown in table 6.4a:

$wavegroup$	$h_i[m]$	$T_w\ [sec]$
a'	18.0	$0.92T_p - 1\ sec = 8.2\ sec$
b'	18.0	$0.92T_p = 9.2\ sec$
c'	18.0	$0.92T_p + 0.5\ sec = 9.7\ sec$

Table 6.4a: Characteristics of the considered wave groups

When the WG theory is applied the following results arise:

$H_s\ [m]$	$wavegroup\ a'$ $0.92T_p - 1\ sec$	$wavegroup\ b'$ $0.92T_p$	$wavegroup\ c'$ $0.92T_p + 0.5\ sec$
4.5	$8.9445 \cdot 10^{-37}$	$1.4119 \cdot 10^{-35}$	$4.1379 \cdot 10^{-60}$
6.0	$6.4499 \cdot 10^{-22}$	$5.0407 \cdot 10^{-21}$	$1.0087 \cdot 10^{-35}$
7.5	$6.1092 \cdot 10^{-15}$	$3.1492 \cdot 10^{-14}$	$2.9493 \cdot 10^{-24}$
9.0	$\mathbf{4.3968 \cdot 10^{-11}}$	$\mathbf{1.7206 \cdot 10^{-10}}$	$\mathbf{6.5650 \cdot 10^{-18}}$

Table 6.4b: Application results

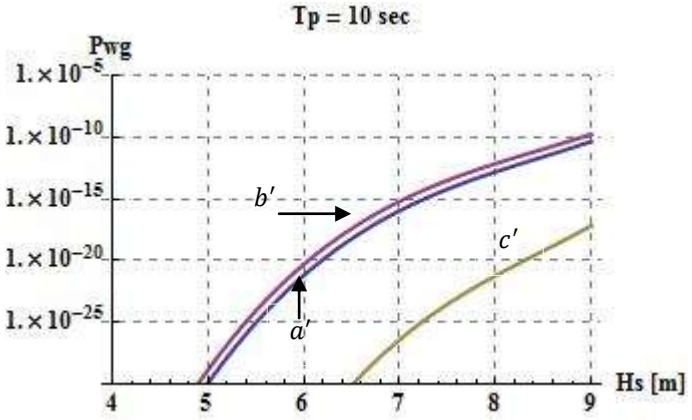

Figure 6.3a: Application results; groups a', b', c'

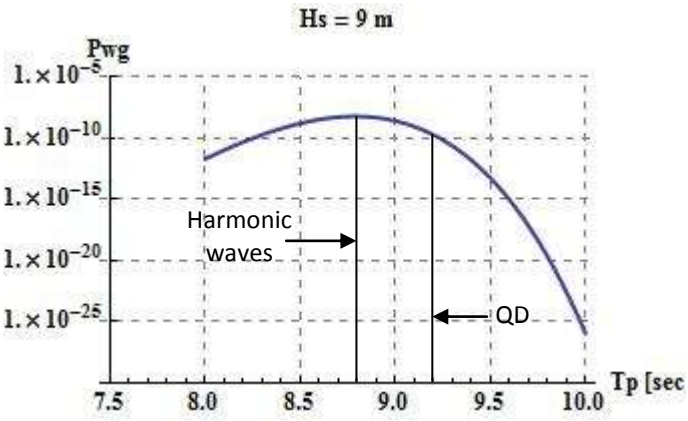

Figure 6.3b: Application results; groups a', b', c'

The same procedure is followed again considering the regular wave groups shown in table 6.4a:

$wavegroup$	$h_i[m]$	$T_w\ [sec]$
a''	20.0	$0.92T_p - 1\ sec = 8.2\ sec$
b''	20.0	$0.92T_p = 9.2\ sec$
c''	20.0	$0.92T_p + 0.5\ sec = 9.7\ sec$

Table 6.5a: The wave period scenarios

The final results are given below:

$H_s\ [m]$	$wavegroup\ a''$ $0.92T_p - 1\ sec$	$wavegroup\ b''$ $0.92T_p$	$wavegroup\ c''$ $0.92T_p + 0.5\ sec$
4.5	$1.0981 \cdot 10^{-44}$	$2.3801 \cdot 10^{-43}$	$4.3672 \cdot 10^{-73}$
6.0	$2.0318 \cdot 10^{-26}$	$2.0043 \cdot 10^{-25}$	$4.0905 \cdot 10^{-43}$
7.5	$7.2978 \cdot 10^{-18}$	$4.5241 \cdot 10^{-17}$	$4.6145 \cdot 10^{-29}$
9.0	$\mathbf{3.7810 \cdot 10^{-13}}$	$\mathbf{1.7251 \cdot 10^{-12}}$	$\mathbf{2.6157 \cdot 10^{-21}}$

Table 6.5b: Application results

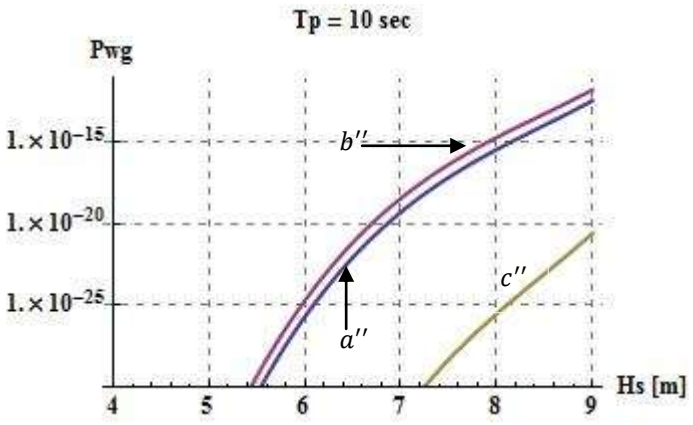

Figure 6.4a: Application results; groups a', b', c'

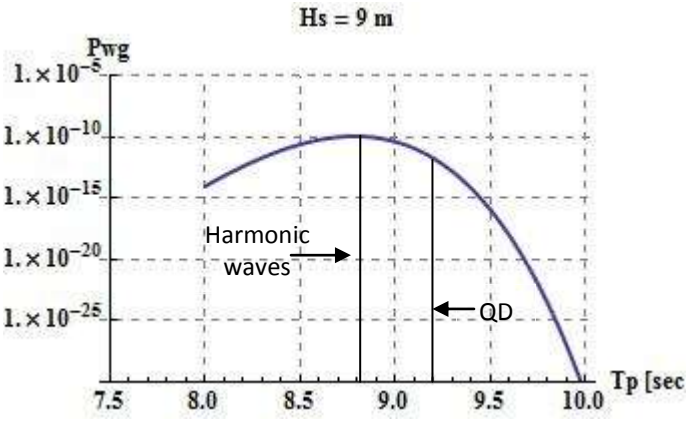

Figure 6.4b: Application results; groups a', b', c'

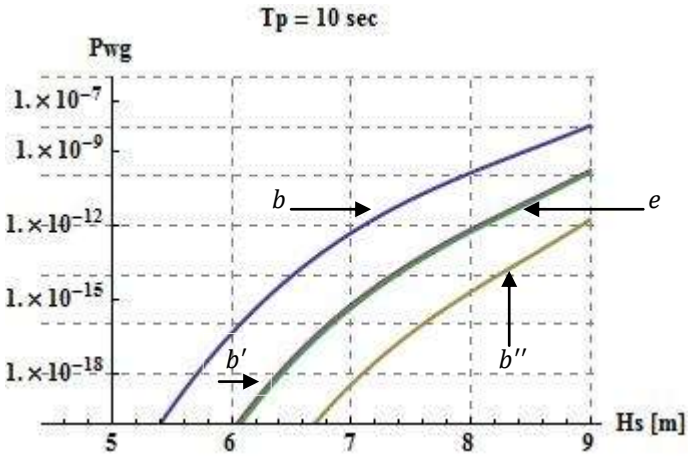

Figure 6.5a: Comparative figure

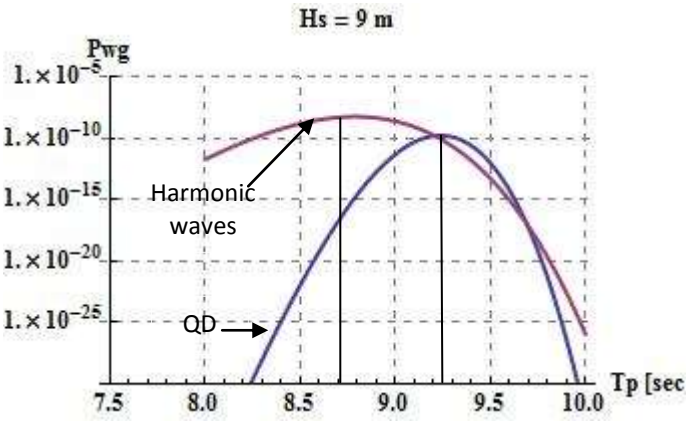

Figure 6.5b: Comparative figure

Important conclusions can now be reached, taking into consideration the following notes:

1. In the case of the irregular groups d, e, f, the critical period scenario occurs close enough to the period $T_{group} = 0.92T_p$.

This is the evidence that from a wide range of irregular wave groups, the greatest probability for ship instability occurs when the wave group period is approaching $T_h = 0.92T_p$. Consequently, WG theory consents to fact that the most probable non regular wave group approximately occurs when the period that the QD theory indicates, is met. In simple terms: *if the QD theory is employed, a critical wave group is defined whose period is approaching T_h. Then, WG theory verifies that this group is the most probable for ship capsizing* (fig. *6.2c-d*).

2. For all regular cases, WG theory tends to the most probable period scenario of $T_{group} = 0.87T_p$ as shown in figures *6.2b, 6.3b* and *6.4b*. However the differences in the final results shown in fig. *6.5b* vanish as long as the crucial QD parameter $a \to \infty$. In fig. *6.6,* it is confirmed through experiments in Reggio Calabria that for low values of a, the first consequence of the QD theory is not valid. However, a possible assumption of the most probable regular wave group period lying in the vicinity of T_h could come into force as the final results are still below the acceptable levels of deviation.

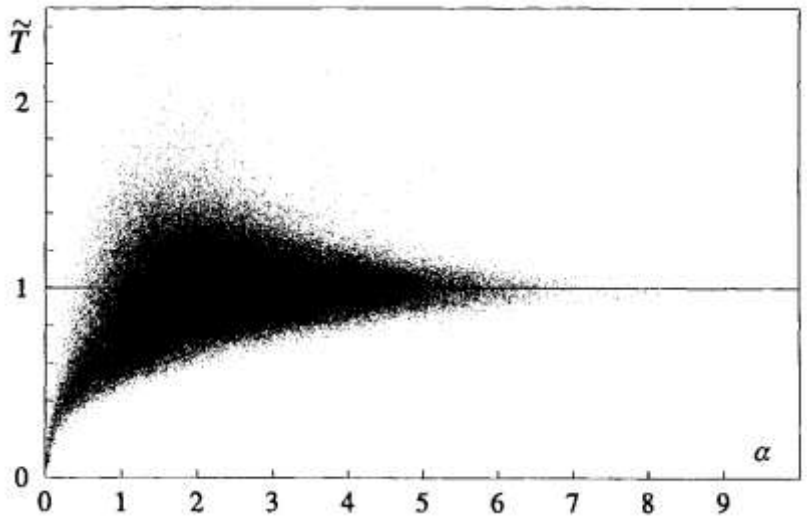

Figure 6.6: Data points $\alpha_i \equiv H_i/\sigma$, $\tilde{T}_i \equiv T_i/T_h$ obtained from the experiment RC 1990. We see that the $\tilde{T}$ of the highest waves are very close to 1 (Boccotti, 2000)

This analysis encourages a more substantial treatment of the WG theory. The united QD-WG theory preludes a more realistic depiction of wave mechanics.

VI.5 *The Central Wave Theory on Quasi-Deterministic waveforms*

Recalling the theory of Quasi-Determinism:

Given the condition (6.18) a wave of a very large given height H^*, with a very large probability, belongs to a wave group with the deterministic form of eq. (6.19). In more detail, eq. (6.19) gives the deterministic form of a wave group whose form and height is affected by the central wave height H^* [see fig. *6.7*].

$$\eta(x_0, y_0, t_0) = \frac{1}{2}H^* , \qquad \eta(x_0, y_0, t_0 + T^*) = -\frac{1}{2}H^* \tag{6.18}$$

$$\eta_1 = (x_0 + X, y_0 + Y, t_0 + T) = \frac{\psi(X,Y,T) - \psi(X,Y,T-T^*)}{\psi(0,0,0) - \psi(0,0,T^*)}\frac{H^*}{2} \tag{6.19}$$

So, the Central Wave theory is established on Boccotti's basic theorem which allows us to override the consideration of the wave group structure as a Markov chain. Each wave of the group will be closely connected to the central wave, whose modification will provoke changes to the whole structure of the group. So, a modification to each wave's height is allowed only if the central wave height is modified. In more detail, the wave group is treated as a deterministic framework depended on the central wave. A possible increase (or decrease) of a single wave height in the group will be proportional to a modification of the central wave height, ΔH^*, as it is stated in equation (6.19), [see fig. *6.8*].

Of vital importance for the validity of the CW theory, is obviously critical parameter a. As, $a \to \infty$, waveform (6.19) will be of great probability resulting in a powerful theory in the field of probabilistic ship stability analysis. Critical wave group period is obviously close to $T_h = 0.92T_p$ with probability approaching 1.

In order to employ the CW theory, the procedure to be followed is similar to the one of the WG theory but less complex. Of course, univariate pdfs will be used. More precisely, the associated probability rate of capsizing P_{cw} will be derived by the calculation of the following probabilities:

$$P_{encounter} = P_1 \cdot P_2 \tag{6.20}$$

$$P_1 = P(T_h | H^* > H^*_{cr}) = \int_{\tau_i}^{\tau_j} f(\tau | h_n > h_{cr}) d\tau \tag{6.21}$$

$$P_2 = P(H^* > H^*_{cr}) = \int_{h^*_{cr}}^{\infty} f(h^*) dh^* \tag{6.22}$$

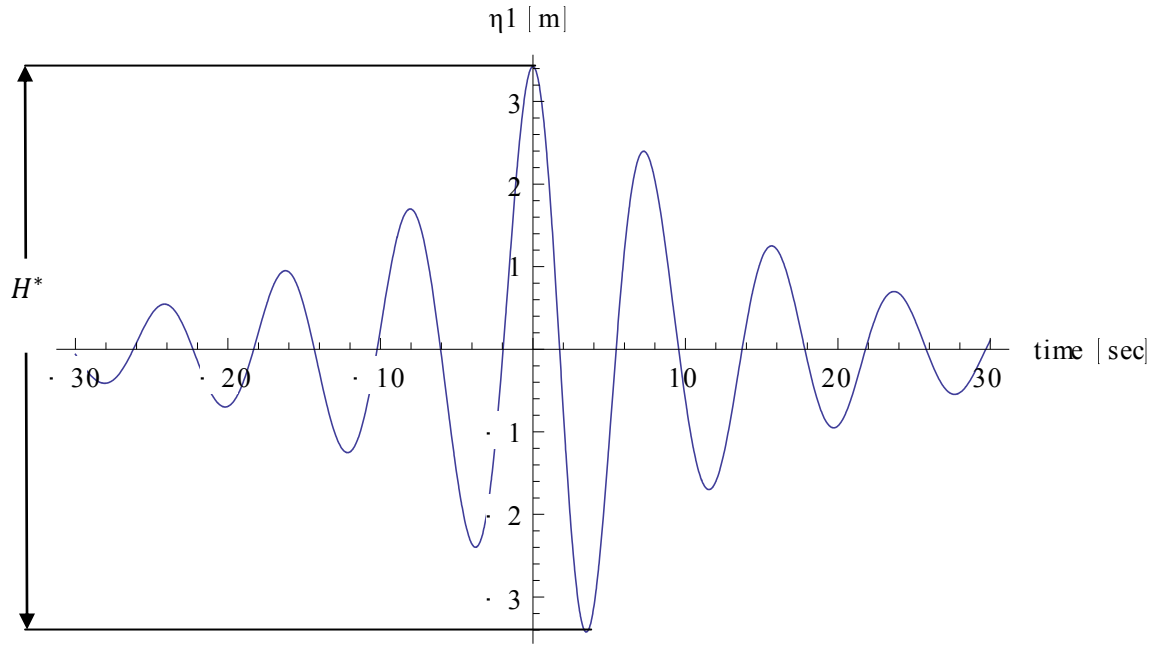

Figure 6.7: The most probable waveform according to the QD theory. At this point H^* is the characteristic value of this deterministic framework

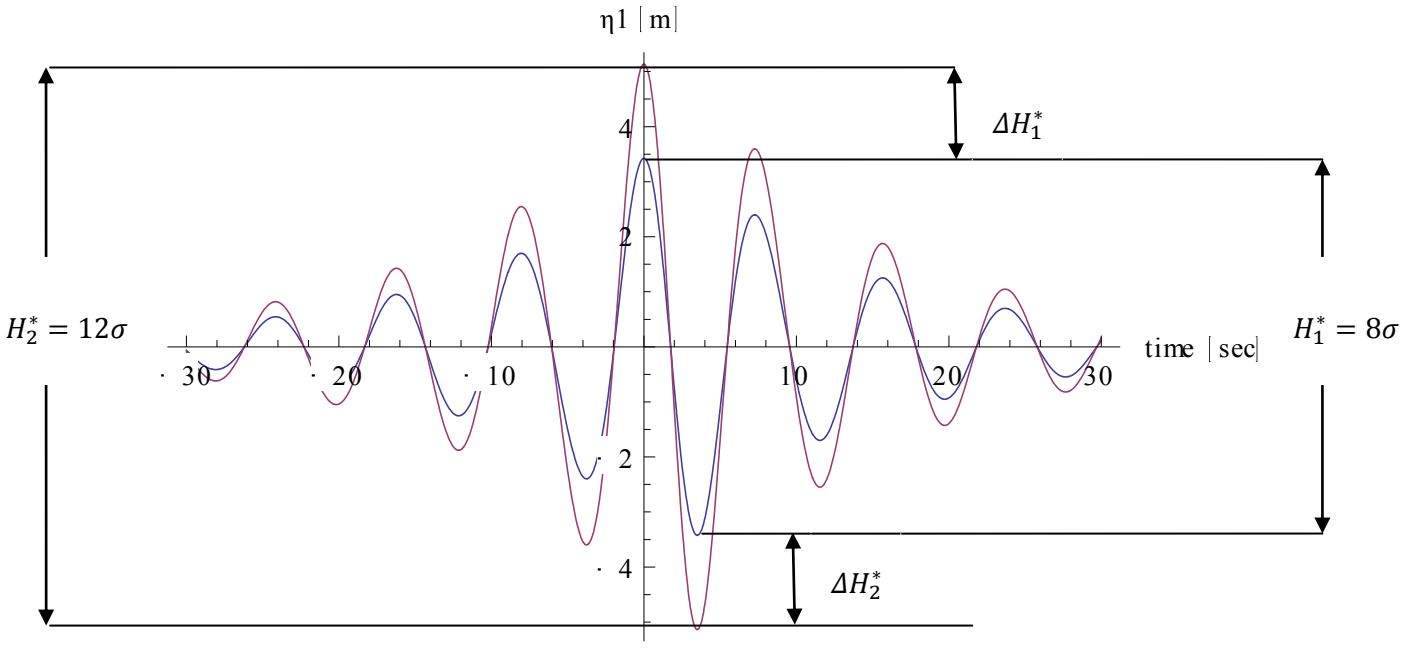

Figure 6.8: The schematic representation of the new concept, the Central Wave theory

In the first probability [eq. (6.21)], the following conditional pdf proposed by Tayfun(1990) is used:

$$f_{\tau|\xi} = C_1 exp\left(-\frac{1}{2}\left(\frac{\tau - \mu_{\tau|\xi}}{\sigma_{\tau|\xi}}\right)^2\right) \tag{6.23}$$

where C_1 is a parameter in order the following condition is satisfied:

$$\int_0^2 f_{\tau|\xi}\, d\tau = 1 \tag{6.24}$$

In eq.(6.23) the conditional mean and standard deviation are given by eq.(6.7a-b). According to eq.(6.24) the parameter C_1 approaches the value $C_1 \approx 1/\left(\sqrt{2\pi}\sigma_{\tau|\xi}\right)$.

For the calculation of the second probability [eq. (6.21)], concerning the univariate pdf $f\ (h^*)$, the modified Rayleigh distribution is used [see chapter IV, eq.(4.19b)].

In fig. *6.9* the applied methodology in the case of irregular excitation is depicted in steps:

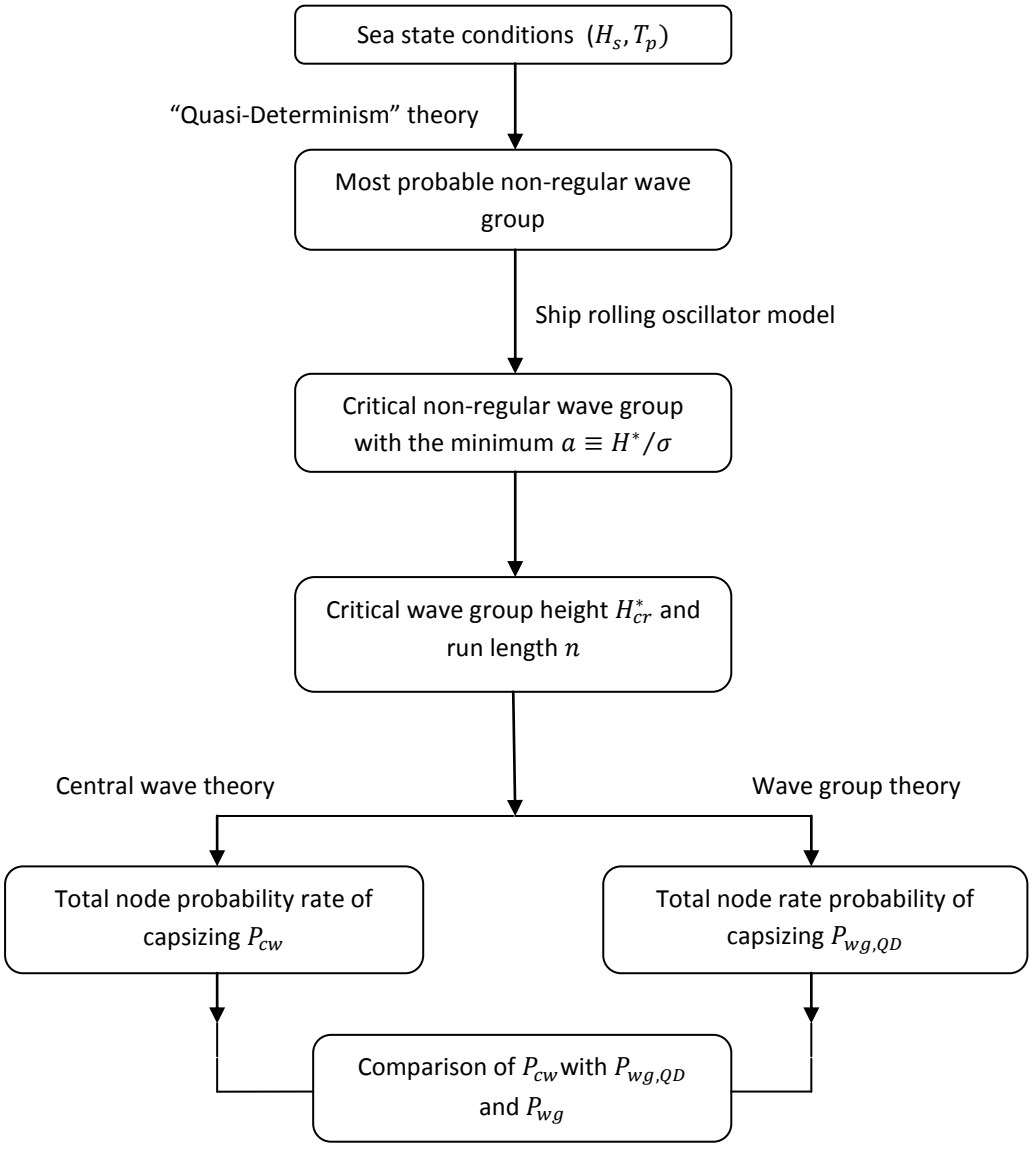

Figure 6.9: Flow-chart of the methodology concerning irregular wave groups

VI.6 *Concluding remarks*

These are included at the end of chap. VII.

CHAPTER VII:

APPLICATION OF THE ASSESSMENT METHODOLOGY

As the final chapter of this thesis is reached, the verification of the methodology described in the previous sections remains to be proved through extended calculations. It is reminded that the principal objective of the analysis is to settle a solid probabilistic assessment framework regarding ship stability in beam seas. The concept of this framework was briefly displayed in chapter VI, but more light is shed on this subject in the following pages.

To demonstrate the developed methodology, an extended application has been undertaken. In more detail, a ROPAX ferry has been examined in different sea state scenarios (*nodes*).

Probabilities of instability are calculated, leading to a series of new "probabilistic" diagrams for ship stability assessment. By these diagrams one can easily deduce which theory (Wave Group theory on regular waves, Wave Group theory on irregular waves and Central Wave theory) is more effective for ship stability analysis and the establishment of a widely accepted ship safety level against capsizing in beam seas. Moreover, if all three alternations of the same assessment methodology are carried out, then a complete probabilistic background for the stability assessment of a specific ship has been acquired.

VII.1 *Basic characteristics of the ROPAX ferry*

The examined ship is a recently built ROPAX ferry whose basic particulars are collected in table 7.1. In fig. *7.1* the ship's General Arrangement (GA) is displayed:

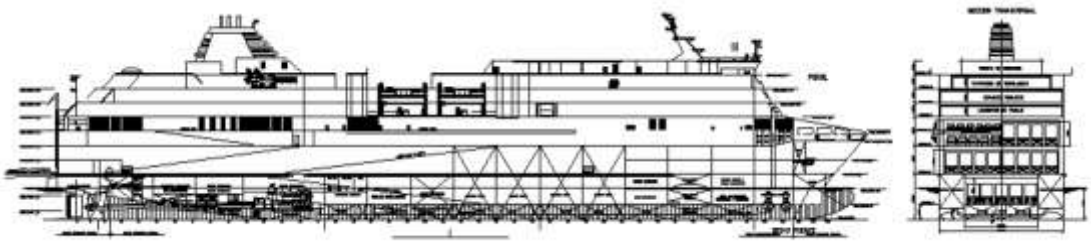

Figure 7.1: General arrangement of ROPAX

L_{BP}	*157 m*	C_B	*0.626*
B	*26.2 m*	V_s	*22.5 kn*
T_d	*6.2 m*	$GM_{corrected}$	*2.08 m*
D (to upper deck)	*15.37 m*	b_{BK}, l_{bk} *(breadth, length of bilge keels)*	*0.26 m* *60.9 m*

Table 7.1: Ship particulars

VII.2 *Sea state scenarios called "nodes"*

In order to assess ship stability, different scenarios of sea state conditions (nodes) are considered. The nodes were chosen in a way so as the entire range of realistic seaway periods to be spotted. However, as one would notice, in table 7.2 the selected peak periods (T_p) lay in the range of $[13,18]$sec. The reason why peak periods lower than 13 seconds were not determined is that for these cases the specified critical wave groups exceeded the Airy breaking limit. So, if individual waves in deep water break when the wave steepness exceeds about 0.17, the demonstration of the methodology will not be accurate. For all applied theories, the calculations for the probability of the critical wave group period occurrence were carried out for the time range:

$$T_{cr} \in [T_{cr} - 0.5\ sec\ , T_{cr} + 0.5\ sec] \tag{7.1}$$

The selection of the significant wave heights (H_s) were made according to eq.(3.18) resulting in three different values of the Phillips' parameter $\left(a_w = \begin{cases} 0.005 \\ 0.010 \\ 0.015 \end{cases}\right)$.

In total, 13 nodes were assumed. Tagged (per node) wave statistics are shown in table 7.2 and fig. *7.4*. The variation of the sea state parameters per node is given in figures *7.2-7.3*.

Node	$H_s\ [m]$	$T_p\ [sec]$
A	8.14	11
B	6.65	11
C	4.70	11
D	11.37	13
E	9.29	13
F	6.57	13
G	12.04	14.8
H	8.51	14.8
I	12.86	15.3
J	9.10	15.3
K	14.07	16
L	9.95	16
M	12.59	18

Table 7.2: Wave statistics (sea state conditions) per node

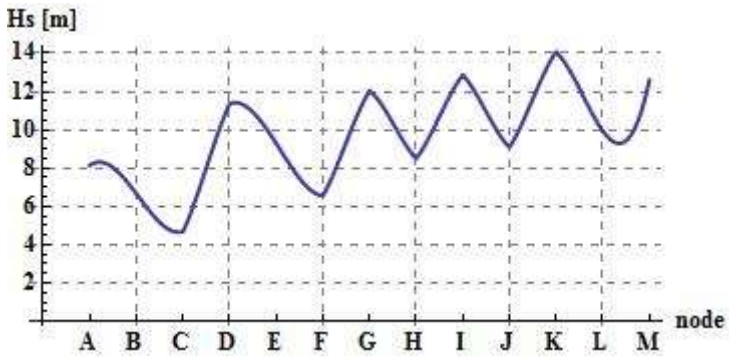

Figure 7.2: Variation of the mean value of H_s per node

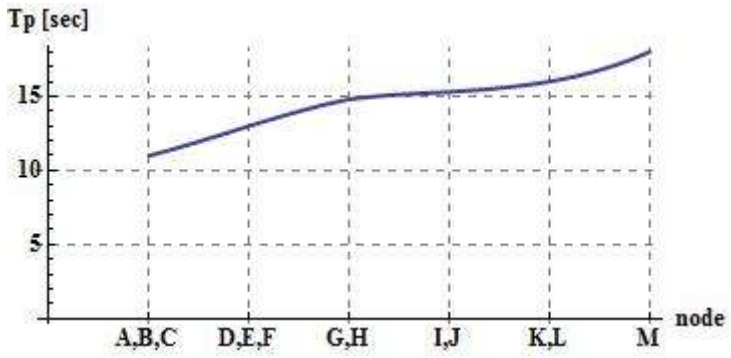

Figure 7.3: Variation of the mean value of T_p per node

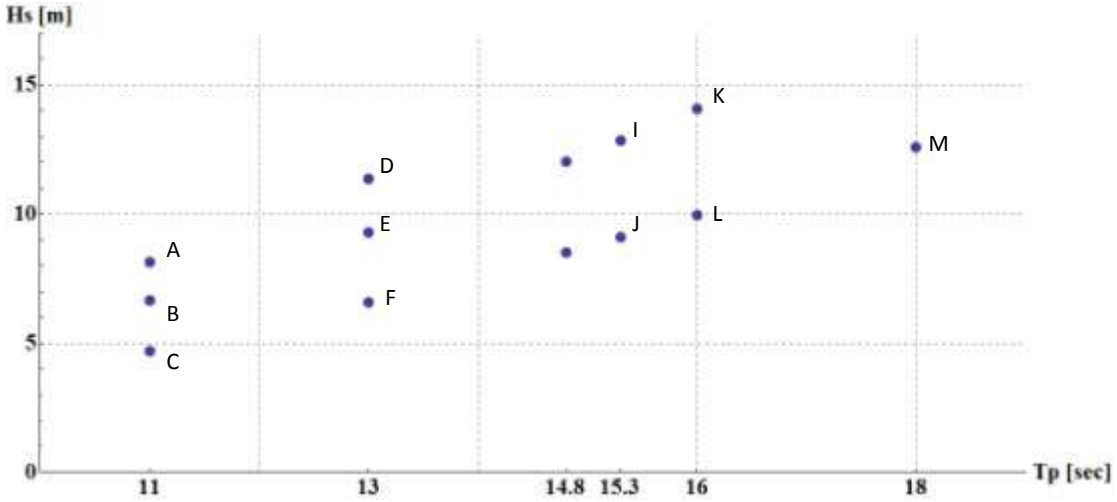

Figure 7.4: All the scenarios set to examination

For the applications following in the next paragraphs, the assumption of the mean JONSWAP spectrum is made (Hasselmann et al 1973):

$$E(\omega) = \alpha_w g^2 \omega^{-5} exp\left(-\frac{5}{4}\left(\frac{\omega}{\omega_p}\right)^{-4}\right)\gamma^{exp\left(-0.5\left(\frac{\omega-\omega_p}{\sigma\omega_p}\right)^2\right)} \tag{7.2}$$

where $\gamma = 3.3$ and $\sigma = 0.08$.

VII.3 *Ship natural period* (T_0)

The way ship characteristics are connected with T_0 is founded on a simple transformation procedure lying behind eq. (5.16):

$$\left.\begin{array}{l} \omega_0 = \sqrt{\frac{\Delta g GM}{(I+\delta I)}} \quad (5.16) \\ \\ T_0 = \frac{2\pi}{\omega_0} \end{array}\right\} \; T_0 = 2\pi\sqrt{\frac{(I+\delta I)}{\Delta g GM}} = \frac{1}{\sqrt{GM}} \cdot 2\pi\sqrt{\frac{(I+\delta I)}{\Delta g}} \tag{7.3}$$

where

$$I + \delta I = \sum_{\iota} m_i \cdot r_i^2 = \Delta \cdot \kappa^2$$

(7.4)

With κ the inertial moment radius expressed as a percentage of the ship beam:

$$\kappa = C \cdot B$$

(7.5)

Finally eq. (5.24) is transformed as:

$$T_0 = \frac{2\pi \cdot C \cdot B}{\sqrt{GM}} \cdot \frac{\pi}{g} \cong \frac{2\pi \cdot C \cdot B}{\sqrt{GM}}$$

(7.6)

Let us remember the IMO directive (IMO (MSC.1/Circ. 707)) to the ship master according to which the ship natural period is defined as:

$$T_R = \frac{2 \cdot C \cdot B}{\sqrt{GM}}$$

(7.7)

where

$$C = 0.373 + 0.023\frac{B}{T_d} - 0.043\frac{L}{100}$$

(7.8)

VII.4 *Norms of unsafe ship response – Application of the "Weather Criterion"*

At this point a limiting rolling angle must be determined so as to quantify unsafe responses. Exceeding this limit of ship rolling would cause ship capsizing. In this way, if wave groups resulting in critical ship inclination are identified they will be noted as "critical wave groups" and their characteristics will be recorded according to the methodology described in the previous chapter.

The specification of the critical rolling angle will be achieved through the application of the Weather Criterion for the considered ROPAX ferry. According to IMO the governing stability limit will be calculated if the following procedure is followed:

Calculation of rolling range φ_1

$$\varphi_1 = 109 \cdot k \cdot X_1 \cdot X_2 \cdot \sqrt{rs} \tag{7.9}$$

where

- for $B/T_d = 4.226 \rightarrow X_1 = 0.8$
- for $C_B = 0.626 \rightarrow X_2 = 0.96$
- T_0[11] $= 15.26\ sec \rightarrow s = 0.0473$
- $r_{calculated} = 0.73 + 0.6 \cdot \frac{KG - T_d}{T_d} = 1.361 \rightarrow r = 1\ \ if\ \ r_{calculated} > 1$
- $A_k = 0.26 \cdot 60.9 = 15.834\ m^3 \rightarrow k = 0.9923$

Thus

$$\varphi_1 = 0.3154\ rad = 18.07^o \tag{7.10}$$

Calculation of flooding φ_f

Let us assume that ship inclination leading in flooding of non-watertight openings occurs when the ship margin deck line is submerged. Thus critical angle φ_f can be calculated through a simple geometric calculation:

$$tan\varphi_f = \frac{D - T_d}{B/2} \rightarrow \varphi_f = 0.611\ rad = 35^o \tag{7.11}$$

According to IMO, as ship capsizing should be considered the exceedence of the minor of: the angle of vanishing stability determined as $\varphi_c = 62^o$; the flooding angle $\varphi_f = 35^o$; the perspective limit of $\varphi_a = 50^o$ that is prescribed in the application of the weather criterion for balancing work against potential energy.

Eventually,

$$\varphi_f = 0.611\ rad = 35^o \tag{7.11}$$

is the critical rolling angle.

The final results inferred from the application of the Weather Criterion are shown in fig. *7.5*.

[11] Eq. (5.16) was employed, according to the calculation procedure presented in section VII.3.

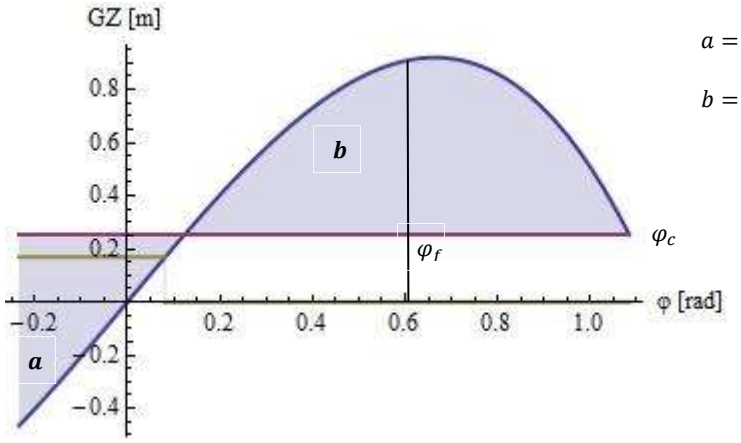

Figure 7.5: Application of the weather criterion

VII.5 *Regular waves – Wave Group theory application*

In the case of regular wave groups transient response was generally targeted. Repetitive simulations were carried out in order to specify which wave groups' impact on the ship response would lead to exceeding rolling angle φ_f. Figure *7.6a* presents a critical wave excitation in the time domain, while in fig. *7.6b* the provoked roll response time history is displayed.

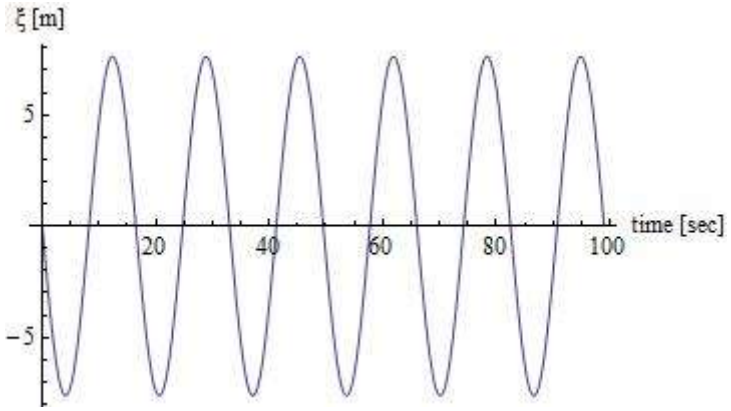

Figure 7.6a: A critical wave group $(\boldsymbol{T = 16.5\ sec, h = 15.23\ m, n = 6})$

According to the procedure, successive simulations were performed until wave groups producing critical ship inclination were identified. For a wide range of periods ($T \in [7.5,17.5]$sec), critical wave groups were specified. Groups consisting of $n = 2$ to 6 waves were considered. For obvious reasons (since the feasibility analysis carried out in the previous chapter allows us so), the critical wave groups occurring when $T = 0.92T_p$ were taken into consideration for each case of run length n. We should note however that, in general, the most probable regular wave groups did not occur exactly when $T = 0.92T_p$ but

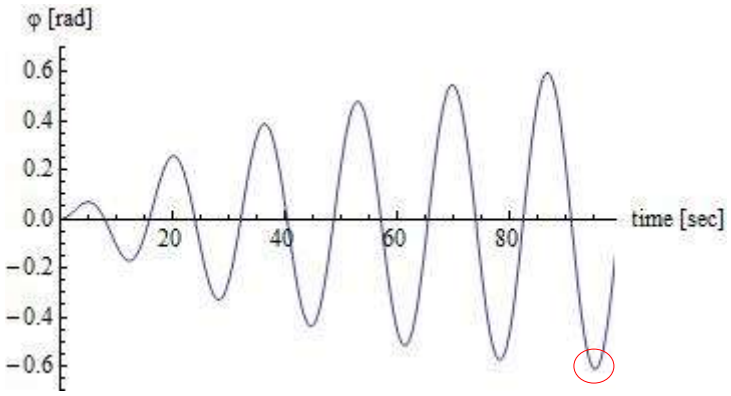

Figure 7.6b: Roll response simulation time history

in the narrow span of $[0.80T_p, 0.90T_p]$[12] . This result can be attributed to the fact that successive high waves have a strong impact on the calculation method of instability potential. A comparative diagram of WG theory of regular waves considered only when $T = 0.92T_p$ versus irregular wave groups will be presented in the following pages.

It should be noted however that, in the low range of periods (at about $T < 7.5\ sec$), it was not feasible to determine critical heights because the required steepness exceeded the wave breaking limit of Airy waves ($H/\lambda \cong 1/7$).

In figures *7.7-7.8* and tables 7.3a-e are summarized the obtained critical wave heights, parameterized with respect to wave period and run length.

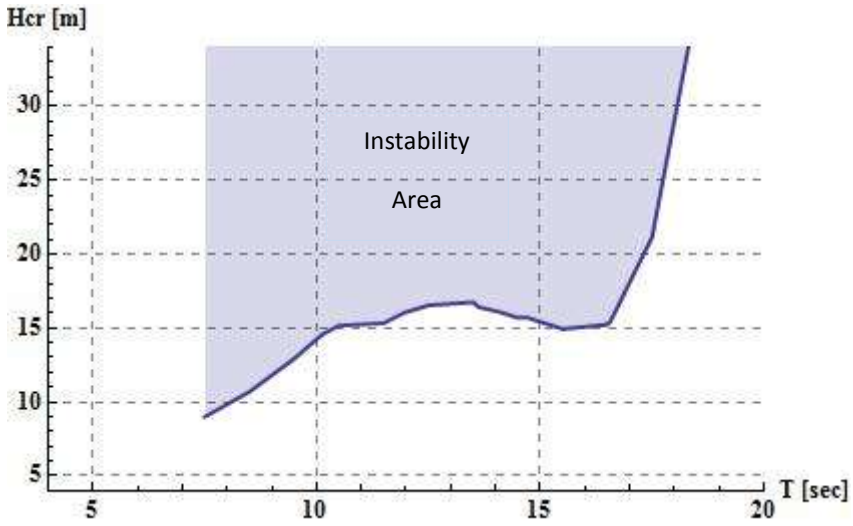

Figure 7.7: Ship's transient capsize diagram

[12] The reason for this fact was explained in detail in Chapter VI.

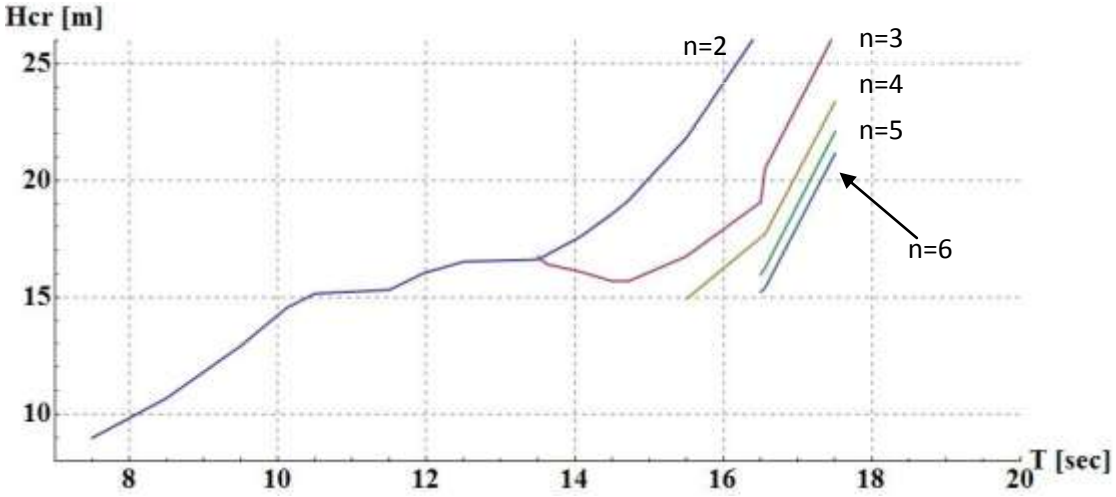

Figure 7.8: Wave groups resulting in critical ship inclination

$H_{cr}\ [m]$	$T\ [sec]$	
8.98	7.5	
10.68	8.5	
12.92	9.5	
14.55	10.12	$0.92T_{p_{A,B,C}}$
15.16	10.5	
15.32	11.5	
16.03	11.96	$0.92T_{p_{D,E,F}}$
16.53	12.5	
16.62	13.5	
16.82	13.62	$0.92T_{p_{G,H}}$
17.61	14.08	$0.92T_{p_{I,J}}$
18.58	14.5	
19.15	14.72	$0.92T_{p_{K,L}}$
21.83	15.5	
26.53	16.5	
26.92	16.56	$0.92T_{p_M}$
33.08	17.5	

Table 7.3a: The specified critical waves $(n = 2)$

$H_{cr}\ [m]$	$T\ [sec]$	
16.74	13.5	
16.42	13.62	$0.92T_{p_{G,H}}$
16.09	14.08	$0.92T_{p_{I,J}}$
15.69	14.5	
15.69	14.72	$0.92T_{p_{K,L}}$
16.76	15.5	
19.08	16.5	
20.53	16.56	$0.92T_{p_M}$
26.32	17.5	

Table 7.3b: The specified critical waves $(\boldsymbol{n = 3})$

$H_{cr}\ [m]$	$T\ [sec]$	
14.93	15.5	
17.56	16.5	
17.72	16.56	$0.92T_{p_M}$
23.37	17.5	

Table 7.3c: The specified critical waves $(\boldsymbol{n = 4})$

$H_{cr}\ [m]$	$T\ [sec]$	
15.97	16.5	
16.26	16.56	$0.92T_{p_M}$
22.08	17.5	

Table 7.3d: The specified critical waves $(\boldsymbol{n = 5})$

$H_{cr}\ [m]$	$T\ [sec]$	
15.23	16.5	
15.41	16.56	$0.92T_{p_M}$
21.15	17.5	

Table 7.3e: The specified critical waves $(\boldsymbol{n = 6})$

Total probability rate of capsizing per node is finally given in table 7.4:

Node	*Wave Group Theory regular waves*
A	$5.971 \cdot 10^{-5}$
B	$6.099 \cdot 10^{-7}$
C	$7.282 \cdot 10^{-13}$
D	$5.293 \cdot 10^{-4}$
E	$1.935 \cdot 10^{-5}$
F	$1.105 \cdot 10^{-9}$
G	$3.990 \cdot 10^{-4}$
H	$4.857 \cdot 10^{-7}$
I	$7.592 \cdot 10^{-4}$
J	$1.777 \cdot 10^{-6}$
K	$\underline{1.901 \cdot 10^{-3}}$
L	$1.497 \cdot 10^{-5}$
M	$1.454 \cdot 10^{-4}$

Table 7.4: Total probability rate of capsizing (P_{wg}) per node; The worst scenario for capsizing is underlined

In order to depict the variation of P_{wg} with the node sequence, fig. *7.9* is presented in logarithmic scale.

VII.6 *Irregular waves – Wave Group theory application*

Employing the Wave Group theory for irregular waves, the prescribed procedure was followed. Obviously transient response could not be identified as no steady excitation was imposed on the ship. Then, critical wave heights were estimated modifying the critical QD parameter a. In this part of the application, each node specifies a unique most probable quasi-deterministic wave period T_h. Figures *7.10a-c* present the critical wave excitations specified for Nodes A and L, whilst in figures *7.10b-d* the provoked roll response time histories are given, respectively.

In figure *7.11* and table 7.5 are summarized the obtained critical wave heights, parameterized with respect to wave period. It should be noted at this point that critical ship inclination was feasible to be identified only due to the central wave's excitation. In other words, ship instability was observed only when the central wave was encountered. Because the wave group with the minimum parameter a should be specified, capsizing could not be met due to wave preceding the central wave (of height H^*). If we would try to identify a wave group that could cause ship instability behavior under the influence of a wave not being in the center of the group, then we would notice that such a wave group is characterized from a very high value of parameter a. Thus, unusually high central waves occur $(H^* > 30\,m)$ in this case leading to violation of the Airy wave theory limit.

Figure 7.9: Probability rate of capsizing – Wave Group theory on regular waves

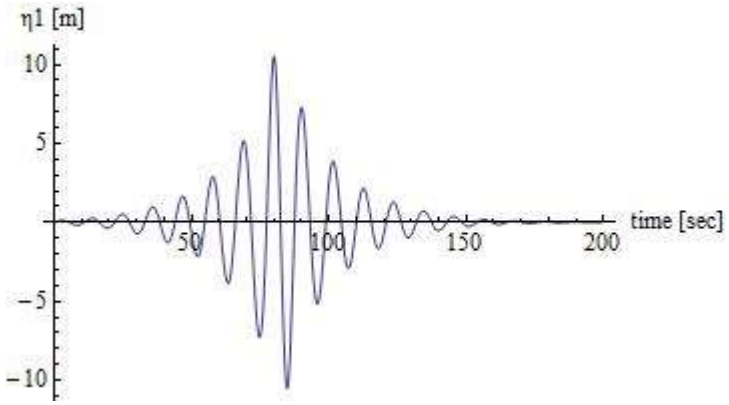

Figure 7.10a: The critical wave group identified in Node A

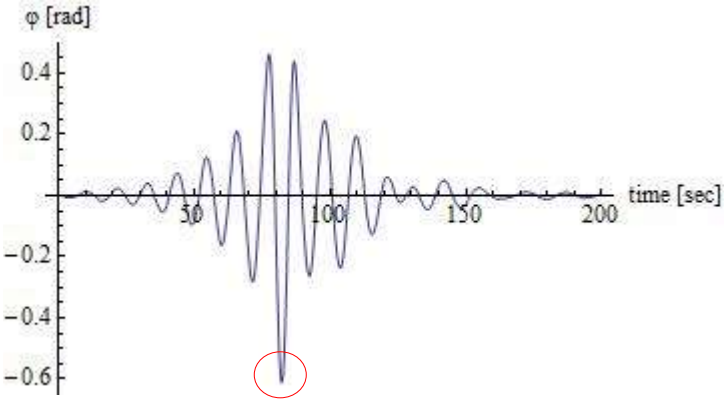

Figure 7.10b: The roll response simulation time history

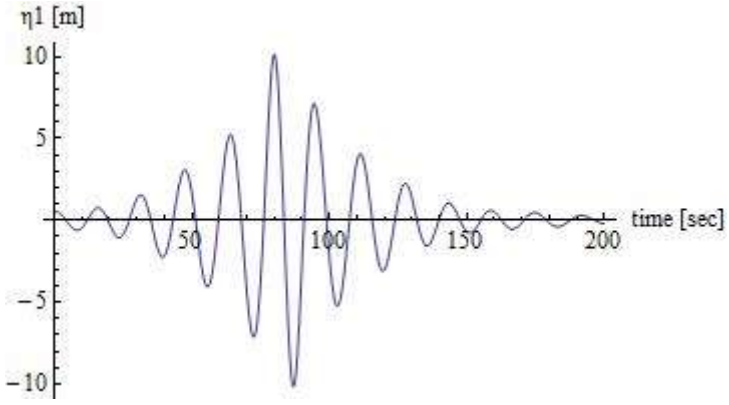

Figure 7.10c: The critical wave group identified in Node L

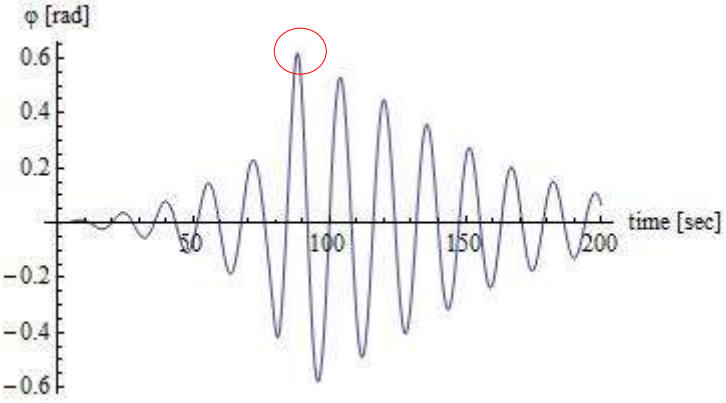

Figure 7.10d: The roll response simulation time history

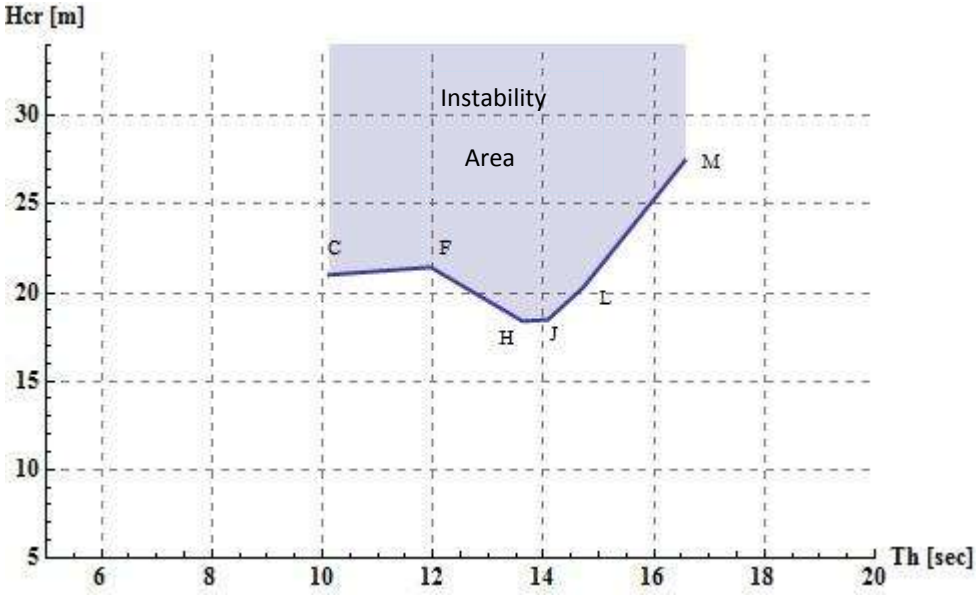

Figure 7.11: Ship's transient capsize diagram per node; Nodes with the minimum critical heights are spotted

Node	H^* $[m]$	T_h $[sec]$	*parameter a*
A	21.03	10.12	10.4
B	21.14	10.12	12.8
C	21.01	10.12	18.0
D	22.66	11.96	8.0
E	21.53	11.96	9.3
F	21.44	11.96	13.1
G	23.92	13.62	8.0
H	18.39	13.62	8.7
I	25.47	14.08	8.0
J	18.47	14.08	8.2
K	27.67	14.72	8.0
L	20.30	14.72	8.3
M	27.47	16.56	9.3

Table 7.5: The specified critical waves per node

Finally, the considered number of the waves the ship encounters (n), is an important factor. In the case of irregular groups, it was observed that the generated QD waveforms were usually consisted of eight to ten waves, with the first heights of the wave sequence always being lower than 1m. In figure *7.12a* we should notice that in a QD wave group very low heights accompanied by respectively high periods may occur. These waves have a strong impact on the probability formulas as they are quite unlikely to be met in a

realistic sea state. It is a factor that would lead in underestimated probabilities of occurrence for critical wave groups. Moreover, very low wave heights i.e., lower than 1m, are out of interest for a ship designer as the ship's depth is incomparably higher and without a doubt no additional ship tension to instability would be caused. For such reasons calculations were performed in two cases; in the first case, the QD group's effect on the vessel begins when the first wave with a well defined period is encountered. Thus $n = 8$ waves constitute these QD wave sequences. In the second case, waves with height lower than 1m mere neglected so as to reach in more realistic results regarding the excitation impact on the ship. For the latter procedure run length $n = 6$ was considered. Fig. *7.12b* shows a group of wave height trains in different nodes.

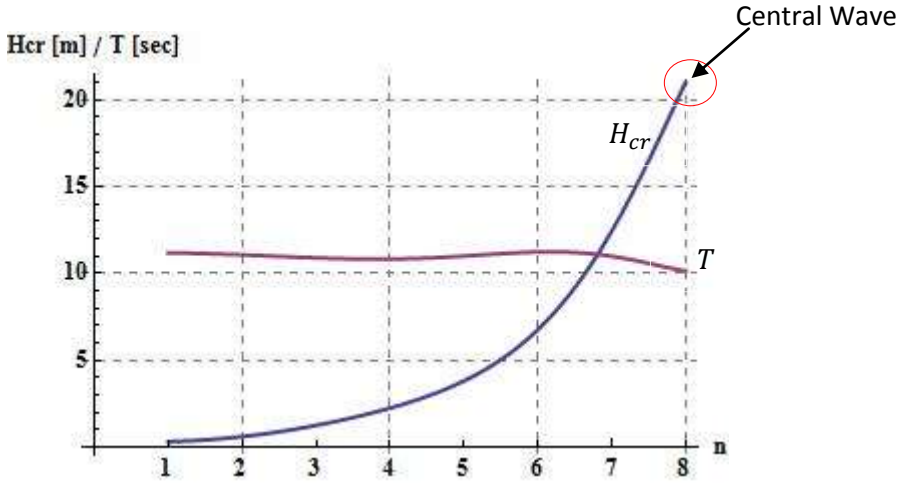

Figure 7.12a: Wave height and period sequence in node A

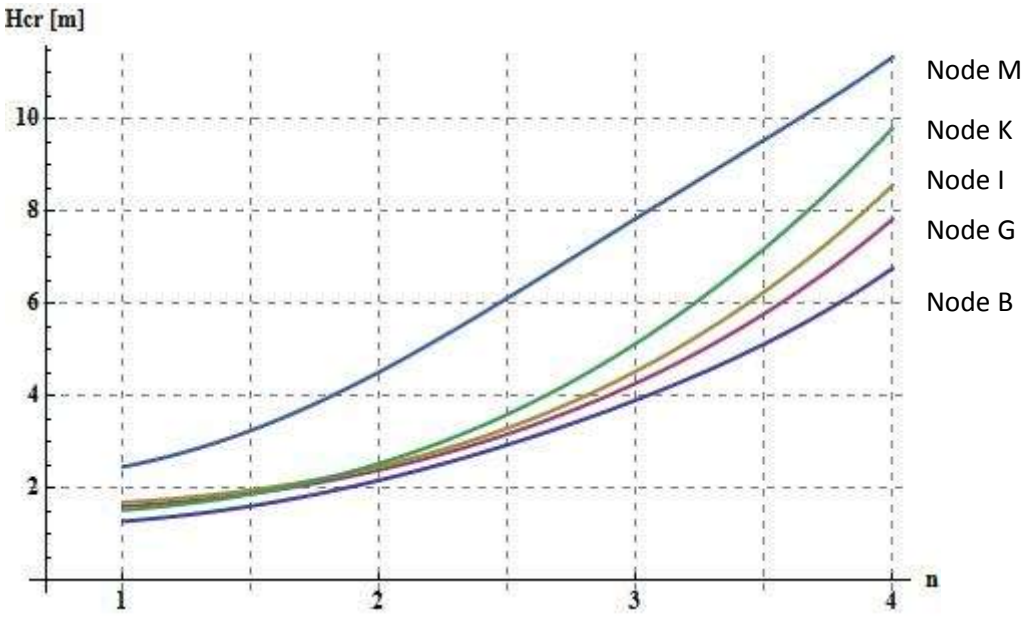

Figure 7.12b: Wave height sequence

Total probability rate of capsizing $(P_{wg,QD})$ per node is shown in table 7.6 and her variation in each node is given in fig. *7.13 -7.14* (logarithmic scale).

Node	*Wave Group Theory irregular waves* $n = 8$, $n = 6$		*parameter a concerning irregular waves*
A	$4.164 \cdot 10^{-20}$	$2.954 \cdot 10^{-18}$	10.4
B	$2.728 \cdot 10^{-26}$	$6.027 \cdot 10^{-24}$	12.8
C	$3.741 \cdot 10^{-44}$	$4.667 \cdot 10^{-42}$	18.0
D	$\underline{2.860 \cdot 10^{-15}}$	$\underline{3.941 \cdot 10^{-13}}$	8.0
E	$1.543 \cdot 10^{-18}$	$1.005 \cdot 10^{-15}$	9.3
F	$3.318 \cdot 10^{-28}$	$1.317 \cdot 10^{-25}$	13.1
G	$1.705 \cdot 10^{-16}$	$8.635 \cdot 10^{-14}$	8.0
H	$1.841 \cdot 10^{-18}$	$3.327 \cdot 10^{-15}$	8.7
I	$1.225 \cdot 10^{-17}$	$2.274 \cdot 10^{-14}$	8.0
J	$4.925 \cdot 10^{-18}$	$8.882 \cdot 10^{-15}$	8.2
K	$3.257 \cdot 10^{-18}$	$2.856 \cdot 10^{-15}$	8.0
L	$7.489 \cdot 10^{-19}$	$6.156 \cdot 10^{-16}$	8.3
M	$7.824 \cdot 10^{-24}$	$9.044 \cdot 10^{-21}$	9.3

Table 7.6: Total probability rate of capsizing $(P_{wg,QD})$ per node; The worst scenario for capsizing is underlined

It is important to notice for those Nodes where parameter $a = 8$, the defined critical central wave height H^* is much higher than the one really needed for capsizing. However, because $a_{min} = 8$, there was no other choice left but to set a equal to 8. So, in these cases the extracted probability rate of capsizing is underestimated.

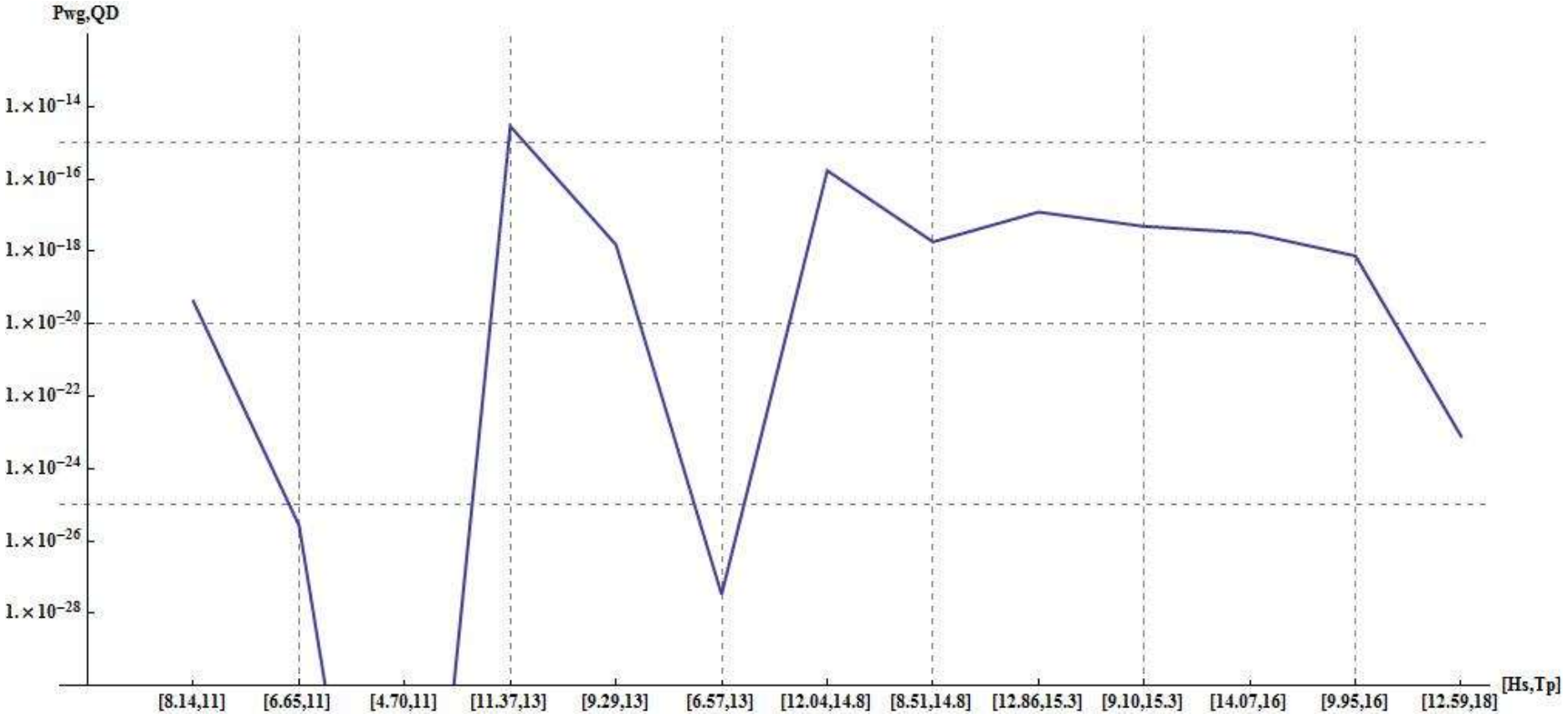

Figure 7.13: Probability rate of capsizing – Wave Group theory on irregular waves $(n = 8)$

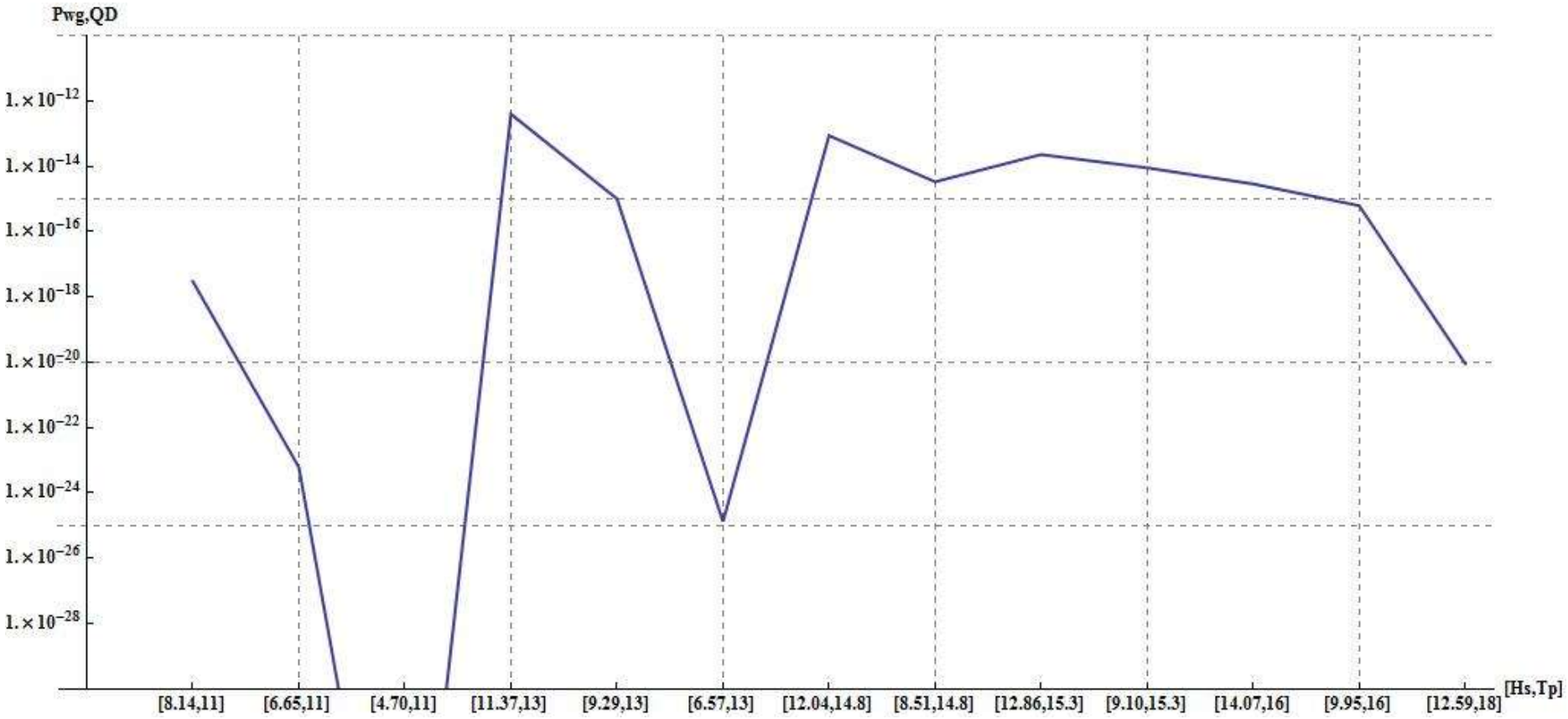

Figure 7.14: Probability rate of capsizing – Wave Group theory on irregular waves $(n = 6)$

VII.7 *Irregular waves – Central Wave theory application*

The procedure is followed by step as described in the previous chapter [see section VI.5]. The results are given in table 7.7 and fig. *7.15*. As one would observe, CW theory is an intermediate prediction of ship instability which lies between the probability estimation of the regular and irregular alternations of the WG theory.

Node	*Central Wave Theory irregular waves*	*parameter a concerning irregular waves*
A	$5.627 \cdot 10^{-8}$	10.4
B	$1.722 \cdot 10^{-11}$	12.8
C	$1.416 \cdot 10^{-21}$	18.0
D	$\underline{1.494 \cdot 10^{-5}}$	8.0
E	$4.494 \cdot 10^{-7}$	9.3
F	$8.515 \cdot 10^{-13}$	13.1
G	$7.913 \cdot 10^{-6}$	8.0
H	$1.163 \cdot 10^{-6}$	8.7
I	$3.968 \cdot 10^{-6}$	8.0
J	$3.453 \cdot 10^{-6}$	8.2
K	$5.419 \cdot 10^{-6}$	8.0
L	$2.388 \cdot 10^{-6}$	8.3
M	$8.832 \cdot 10^{-8}$	9.3

Table 7.7: Total probability rate of capsizing (P_{cw}) per node; The worst scenario for capsizing is underlined

VII.8 *Probability rate of "instability" in beam seas – Comparing the theories*

At this point the three applied theories will be set into comparative procedures. The final results for each theory are summarized in table 7.8 and fig.*7.16*.

Generally, all employed theories agree on the matter of which nodes are of "high risk". Probability variation for each node reaches into the same conclusions.

In the case of WG theory on regular waves, the probability rate of instability is increased, as expected. It is a common belief that using regular waves a "safe-side" ship stability prediction is provided. The reason is that transient ship response causes unexpected high rolling motions so as the critical rolling angle is exceeded.

In the case of WG theory on irregular waves, it is obvious that probability of encountering critical waves is significantly decreased. As expected, a more realistic approach is achieved through the Quasi-Determinism theory and lower risk levels are proposed.

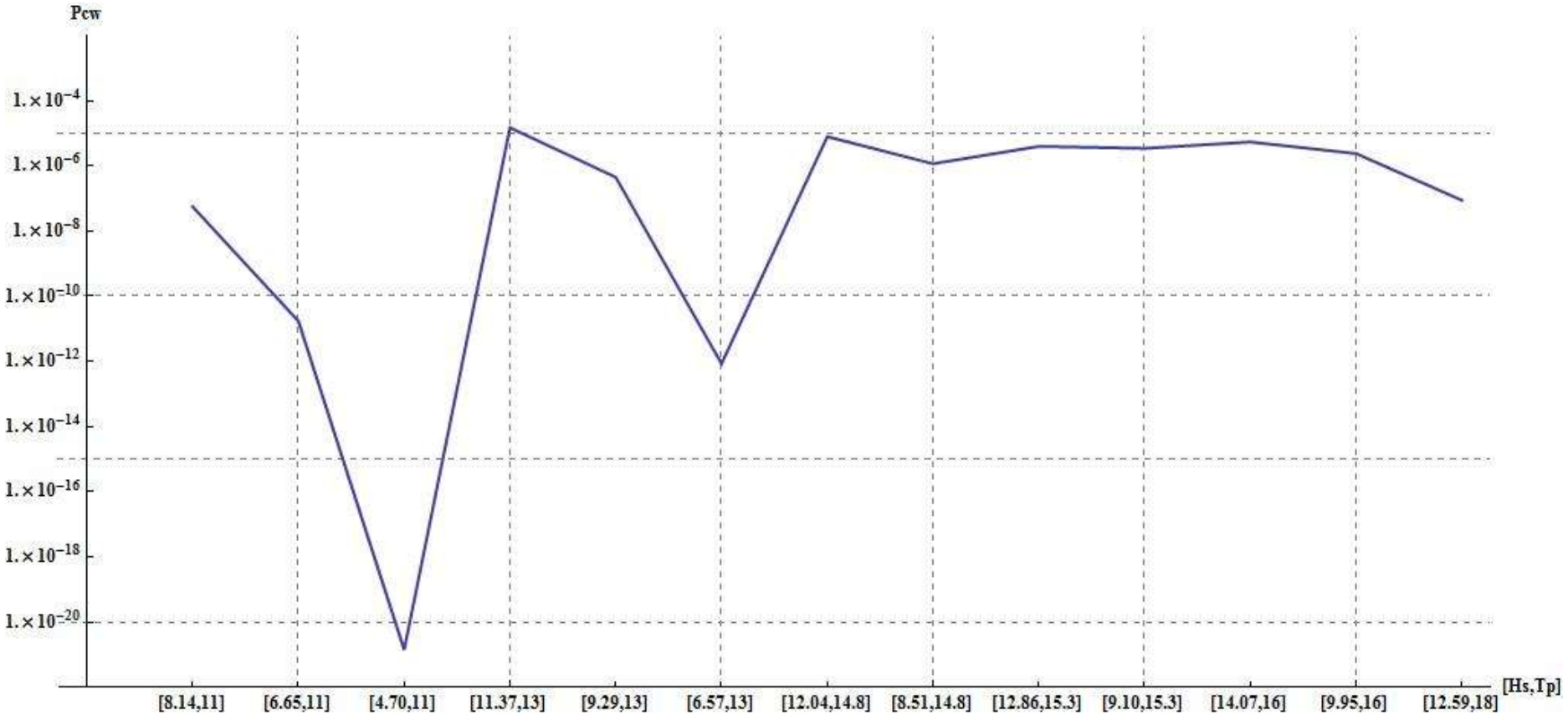

Figure 7.15: Probability rate of capsizing – Central Wave theory on irregular waves (logarithmic scale)

Node	*Wave Group Theory regular waves*	*Wave Group Theory irregular waves* $n=8$	$n=6$	*Central Wave Theory irregular waves*	*parameter a concerning irregular waves*
A	$5.971 \cdot 10^{-5}$	$4.164 \cdot 10^{-20}$	$2.954 \cdot 10^{-18}$	$5.627 \cdot 10^{-8}$	10.4
B	$6.099 \cdot 10^{-7}$	$2.728 \cdot 10^{-26}$	$6.027 \cdot 10^{-24}$	$1.722 \cdot 10^{-11}$	12.8
C	$7.282 \cdot 10^{-13}$	$3.741 \cdot 10^{-44}$	$4.667 \cdot 10^{-42}$	$1.416 \cdot 10^{-21}$	18.0
D	$5.293 \cdot 10^{-4}$	$\underline{2.860 \cdot 10^{-15}}$	$\underline{3.941 \cdot 10^{-13}}$	$\underline{1.494 \cdot 10^{-5}}$	8.0
E	$1.935 \cdot 10^{-5}$	$1.543 \cdot 10^{-18}$	$1.005 \cdot 10^{-15}$	$4.494 \cdot 10^{-7}$	9.3
F	$1.105 \cdot 10^{-9}$	$3.318 \cdot 10^{-28}$	$1.317 \cdot 10^{-25}$	$8.515 \cdot 10^{-13}$	13.1
G	$3.990 \cdot 10^{-4}$	$1.705 \cdot 10^{-16}$	$8.635 \cdot 10^{-14}$	$7.913 \cdot 10^{-6}$	8.0
H	$4.857 \cdot 10^{-7}$	$1.841 \cdot 10^{-18}$	$3.327 \cdot 10^{-15}$	$1.163 \cdot 10^{-6}$	8.7
I	$7.592 \cdot 10^{-4}$	$1.225 \cdot 10^{-17}$	$2.274 \cdot 10^{-14}$	$3.968 \cdot 10^{-6}$	8.0
J	$1.777 \cdot 10^{-6}$	$4.925 \cdot 10^{-18}$	$8.882 \cdot 10^{-15}$	$3.453 \cdot 10^{-6}$	8.2
K	$\underline{1.901 \cdot 10^{-3}}$	$3.257 \cdot 10^{-18}$	$2.856 \cdot 10^{-15}$	$5.419 \cdot 10^{-6}$	8.0
L	$1.497 \cdot 10^{-5}$	$7.489 \cdot 10^{-19}$	$6.156 \cdot 10^{-16}$	$2.388 \cdot 10^{-6}$	8.3
M	$1.454 \cdot 10^{-4}$	$7.824 \cdot 10^{-24}$	$9.044 \cdot 10^{-21}$	$8.832 \cdot 10^{-8}$	9.3

Table 7.8: Final probability rate of capsizing per node and employed theory; maximum probability per method is underlined

Finally, as far as the CW theory is concerned, an intermediate risk level is obtained. Because of the fact that this theory overleaps the effect of the lower waves of the group on the occurrence probability of the critical group period, the above given results are justified. However, it is important to notice that in nodes H and J a higher risk level is proposed than the safe-side prediction of regular WG theory. This is a matter of issue as it is proved that harmonic waveforms might lead to underestimations concerning ship safety!

All in all nodes C and F are definitely the ones of lowest risk level. The node of highest risk is not easily distinguished, though. Irregular theories agree to the fact that node D is the most probable for capsizing, whilst in regular WG theory node K is proposed. However, even in this case, node D is of the highest risk nodes. Theories deviations in the final results are limited and in within the acceptable level.

Figure 7.16: Probability rate of capsizing – Comparative diagram (logarithmic scale)

Finally, the WG theory for irregular groups is compared with the regular one when $T = 0.92T_p$ considering a run length of $n = 3$ [see table 7.9 and fig. *7.18*]. Method convergence is reinforced:

Node	*Wave Group Theory regular waves* $T = 0.92T_p$ $n = 3$	*Wave Group Theory irregular waves* $n = 3$	*Central Wave Theory irregular waves*	*parameter a concerning irregular waves*
G	$1.687 \cdot 10^{-7}$	$\underline{9.891 \cdot 10^{-11}}$	$\underline{7.913 \cdot 10^{-6}}$	8.0
H	$1.675 \cdot 10^{-12}$	$3.521 \cdot 10^{-12}$	$1.163 \cdot 10^{-6}$	8.7
I	$7.037 \cdot 10^{-7}$	$2.968 \cdot 10^{-11}$	$3.968 \cdot 10^{-6}$	8.0
J	$2.877 \cdot 10^{-11}$	$1.126 \cdot 10^{-11}$	$3.453 \cdot 10^{-6}$	8.2
K	$\underline{3.090 \cdot 10^{-6}}$	$6.095 \cdot 10^{-12}$	$5.419 \cdot 10^{-6}$	8.0
L	$5.432 \cdot 10^{-10}$	$1.248 \cdot 10^{-12}$	$2.388 \cdot 10^{-6}$	8.3
M	$1.206 \cdot 10^{-13}$	$5.669 \cdot 10^{-16}$	$8.832 \cdot 10^{-8}$	9.3

Table 7.9: Final probability rate of capsizing per node and employed theory; maximum probability per method is underlined – Regular waves with $\boldsymbol{T = 0.92T_p}$

The purpose of table 7.9 and fig. *7.18* is to scale under the same conditions the WG theory if regular and irregular waves are considered. Eventually, comparative conclusions are more obvious: Node M is the one of lowest risk level. Node G is indisputably of very high risk for capsizing[13]. In general, one would notice as long as parameter $a \gg 8$ the WG methods seem to result in the same estimation for probability rate of capsizing.

Figures *7.17a-d* are to be used as a supplement for comparing procedures. In these figures the wave height train is shown in the case of irregular waves for different run lengths. The fixed regular height is also noted. For the defined run length $n = 3$, method convergence is met as $H_{harmonic} \to H^*$. In simple words, comparable results are produced as far as the standard wave height of the regular waves reaches the central wave height of a QD irregular set.

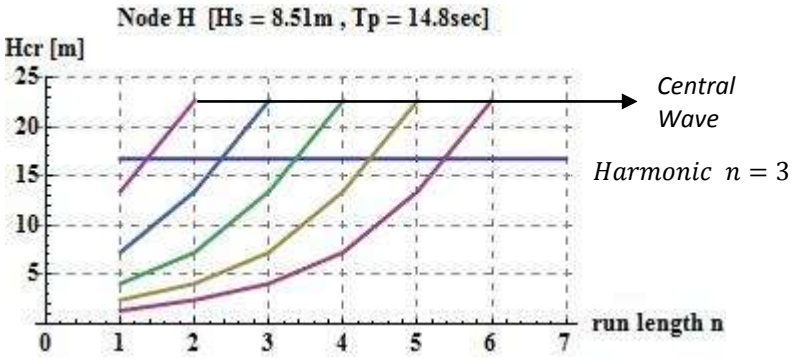

Figure 7.17a: Wave height train variation, Node H

[13] The specification of regular critical wave groups for Nodes A,B,C,D,E and F was not feasible as ship capsizing was met only for run length $n = 2$.

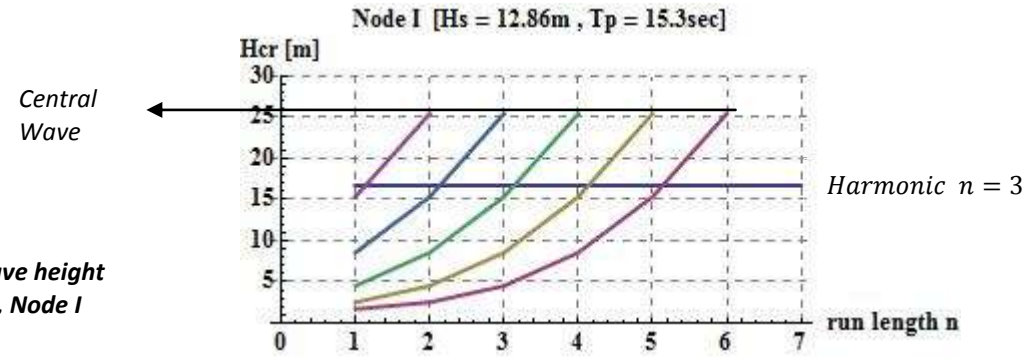

Figure 7.17b: Wave height train variation, Node I

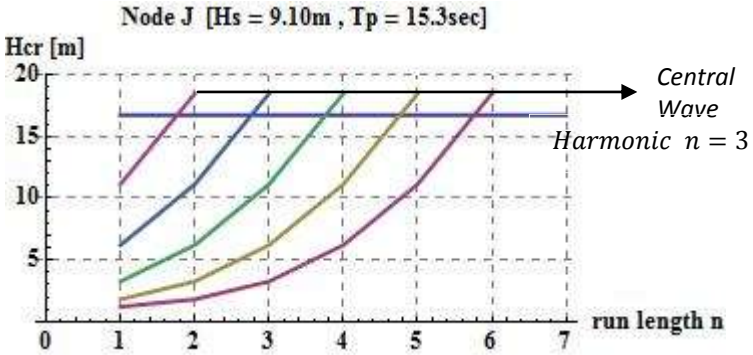

Figure 7.17c: Wave height train variation, Node J

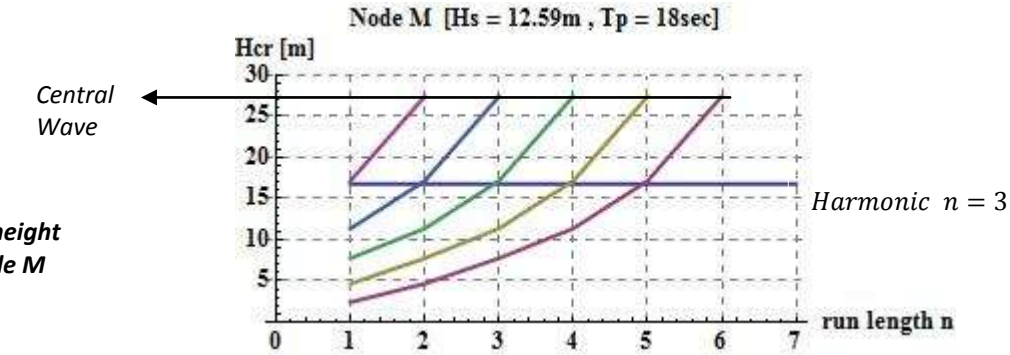

Figure 7.17d: Wave height train variation, Node M

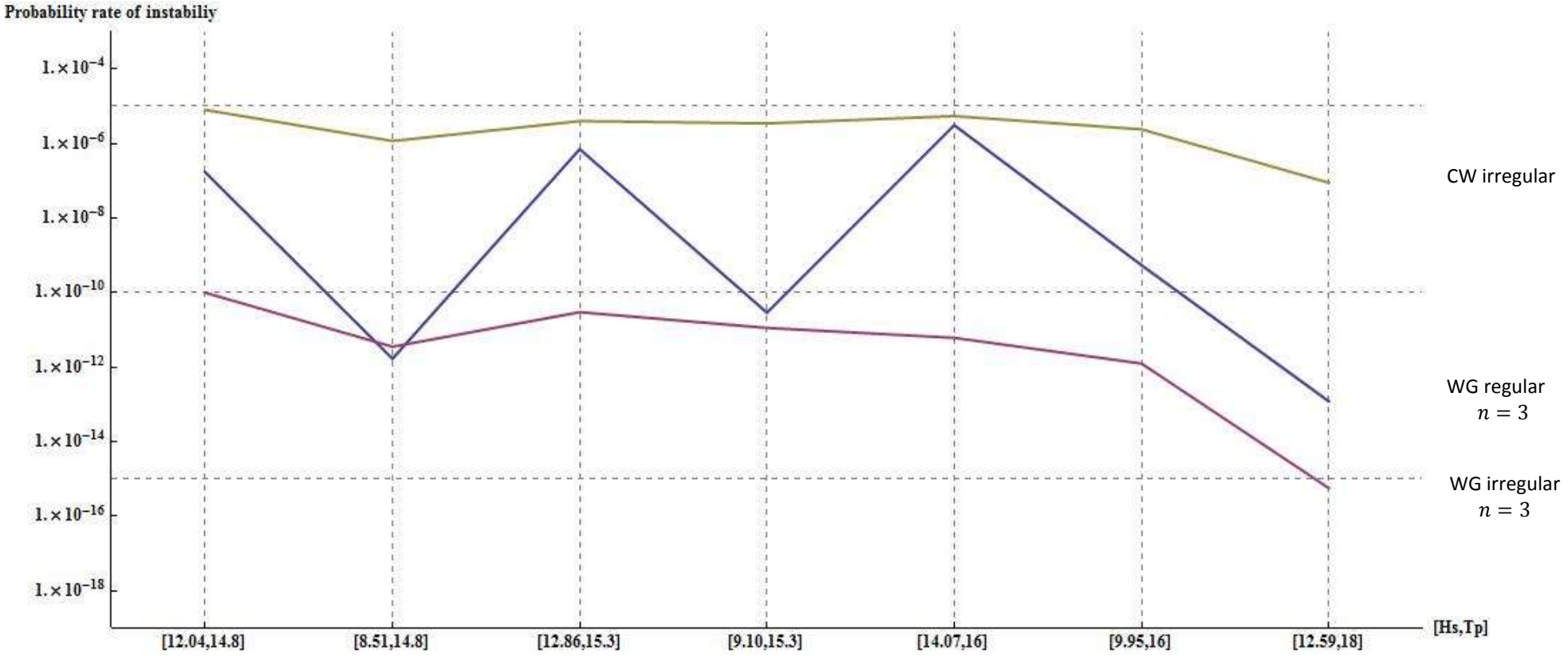

Figure 7.18: Probability rate of capsizing – Comparative diagram; Regular waves with $T = 0.92T_p$ (logarithmic scale)

Finally, of significant importance to depict the effects of the QD theory on the probability rate of ship instability are the following diagrams:

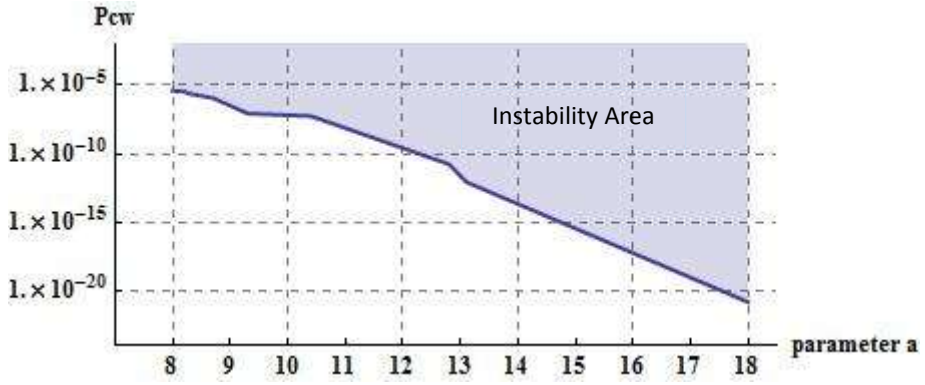

Figure 7.19a: Effect of the QD theory on the CW probability rate of capsizing $(\boldsymbol{n = 6})$

Figure 7.19b: Effect of the QD theory on the WG probability rate of capsizing $(\boldsymbol{n = 6})$

In the above given diagrams, the minimum parameter a which results in a specific risk level, is presented. Figures *7.19a-b* constitute a useful tool if the risk level is defined and the maximum value of a has to be calculated. Then, a quick and approximate answer to the matter if a generated wave group is critical can be given without proceeding in numerical simulations.

VII.9 *Probability rate of "instability" in beam seas if initial rolling angle is set – QD theory applications*

After a series of repetitive simulations, the final conclusion on this matter was that such an analysis would be meaningless. As no transient response occurs, the ship will reach the maximum rolling angle when the central wave is encountered. Because of the fact that a few waves intercede to the central wave encounter, system's extra stored energy has time

to be damped. Thus no difference to the upright position case will be observed, even though the wave period T_h approaches ship's natural period T_0.

VII.10 *Probability rate of "instability" if GM is modified*

The effects of the GM upon the ship natural period through the mathematical model presented in chapter V are a matter of discussion as the final GM value of a specific ship design is a result of compromise.

In general, if the metacentric height is high, the developed righting arms, in small heel angles, are increased. Then a "stiff" ship design resistant to rolling motions is secured. Otherwise, the provoked righting arms are insufficient for stability establishment and then we deal with a ship tender to slow rolling.

However, when a ship design project is undertaken, careful mapping of the possible sea states that the vessel would encounter is essential. It is an important matter to avoid tuning areas that lead to increased rolling amplitude. In more detail, if we take the first consequence of the QD theory under consideration, ship's natural period (T_0) should be set in a span of periods far from the most probable wave period T_h. As one could imagine, if $T_0 \to T_h$, the most probable wave of Boccotti's established theory becomes the most dangerous one, as well. In simple words, if a specific sea state is identified by a peak period over T_0, a possible increase of GM would lead in an increased probability rate of capsizing, as eq. (5.16) implies.

Now, let us examine the case in which GM is modified for the ROPAX ferry described in the previous sections. In the case of node F and run length of $n = 3$, the final results are shown in fig. *7.20a-b*:

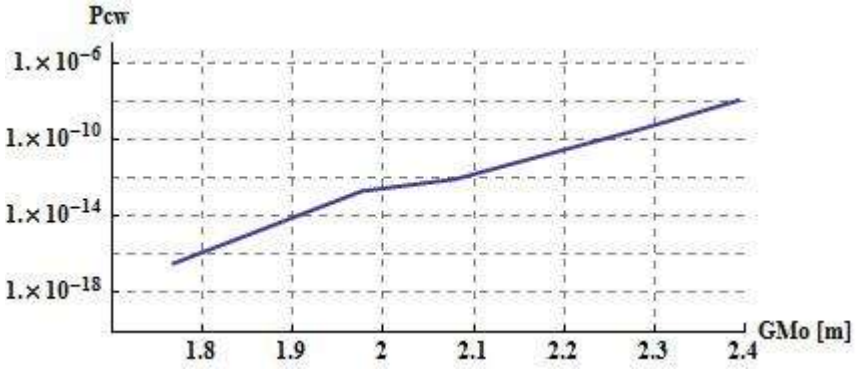

Figure 7.20a: Effect of the variation of GM to the probability rate of capsizing WG theory on non regular

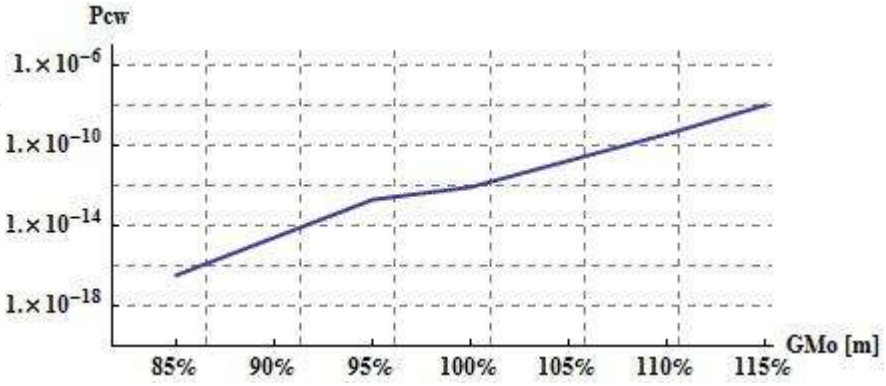

Figure 7.20b: Effect of the variation of GM to the probability rate of capsizing WG theory on non regular

VII.11 *Concluding remarks*

All in all there seems to be excellent agreement between the Quasi-Determinism and the Wave Group theory based on Kimura's approach in the field of the critical group period. The latter theory estimates that the most probable period to occur in a realistic seaway, is the one proposed by the Quasi-Determinism theory. The fact that this probability overdominates the probability of exceeding critical wave heights results in the effective combination of the aforementioned theories so as to evaluate ship stability.

In general the probability rate of capsizing is overestimated if regular treatment of wave groups is regarded. Of course one should expect this. However, when irregular waveforms are generated from the Quasi-Determinism theory, the mechanics of prevailing wave laws are given in a more realistic way. The final outcome is that the total risk levels are definitely lower, depending though on the group run length. After a brief investigation into the matter of the appropriate run length considered in probability calculations, the conclusion is that by discarding the lower heights of the sequence, increased risk levels are met. For these reasons, if irregular waves are to be examined, the Central Wave theory should be taken seriously into consideration. This method gives the upper limit of the probability range of the Wave Group theory.

Obviously, the recommended probability rate of instability cannot be univocal in the case of irregular wave groups. The interpretation of ship unsafe behaviors lies within a range of probability values defined from the Central Wave (high probabilities) and the Wave Group theory of run lengths $n > 3$ (lower limit). Yet, this particular range gives a more realistic depiction of capsizing phenomena.

As a recommendation for future work, a coupled roll-sway model could be adopted. An oscillator of this kind would definitely improve the applied methodology in the field of ship dynamics. Moreover, Monte Carlo simulations could be carried out so as to verify the Wave Group theory's results. Finally, other instability modes could also be investigated (i.e., parametric rolling and pure loss of stability) under the scope of the Quasi-Determinism theory.

APPENDIX

ADDITIONAL APPLICATIONS ON THE QUASI DETERMINISM THEORY

This section aims to present more applications of the employed Quasi-Determinism theory for various sea state conditions. Calculations were carried out for the first and the second formulation of the theory under the assumption of deep water for the time and space domain. The Phillips' parameter was assumed to take on the most usual design value of $a_w = 0.01$.

A.1 *First formulation – "New Wave"*

A.1.1 *Sea state conditions*

$T_p = 15\ sec$, $H_s = 12.35\ m$, $H_c = 8\sigma$

Time domain

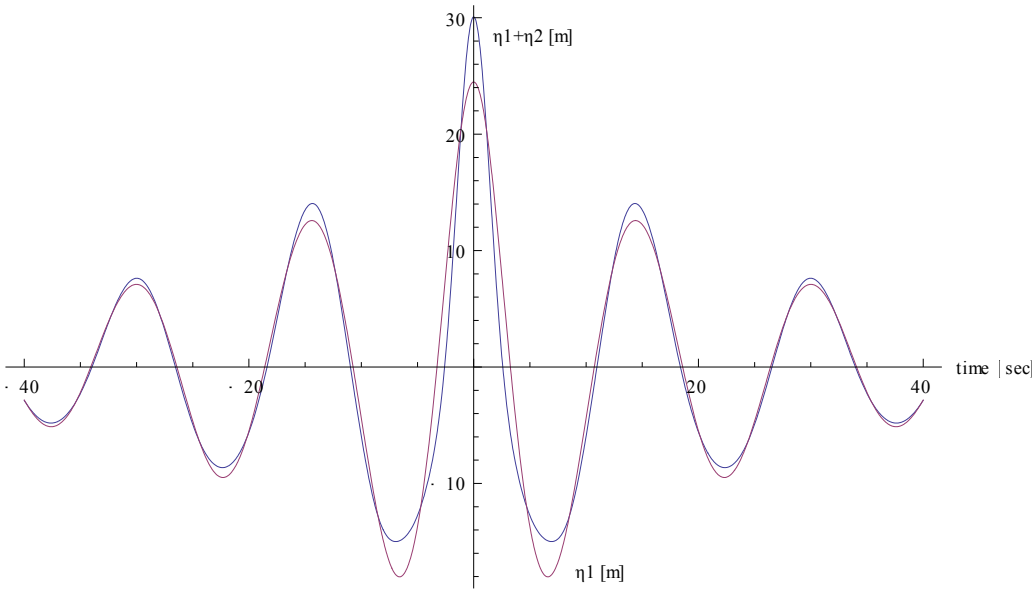

Figure A.1a: Linear component $\eta_1[m]$ compared with the total second-order surface displacement $\eta_1 + \eta_2$ [m] as a function of time (sec))

Space domain

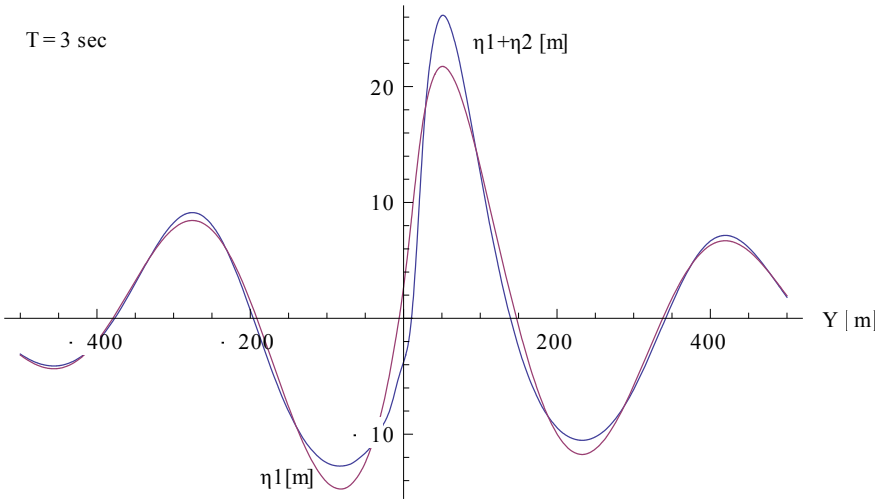

Figure A.1b: Linear component $\eta_1[m]$ compared with the total second-order surface displacement $\eta_1 + \eta_2$ [m] in the space domain

A.2 *Second formulation*

A.2.1 *Sea state conditions*

$T_p = 12\ sec$, $H_s = 7.9\ m$, $H^* = 8\sigma$

Time domain

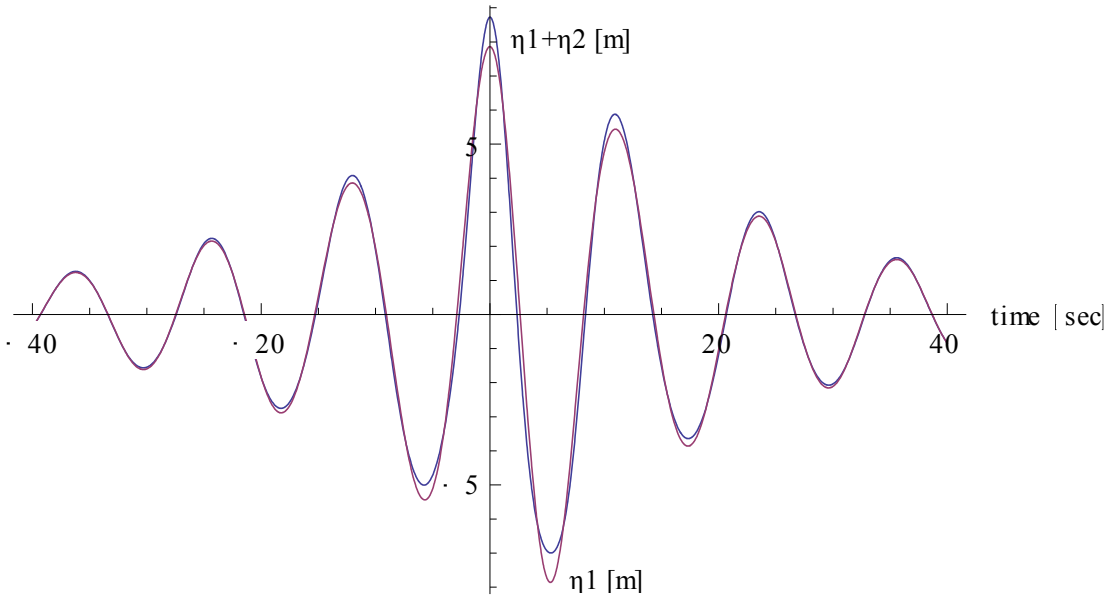

Figure A.3a: Linear component $\eta_1[m]$ compared with the total second-order surface displacement $\eta_1 + \eta_2$ [m] as a function of time (sec)

Space domain

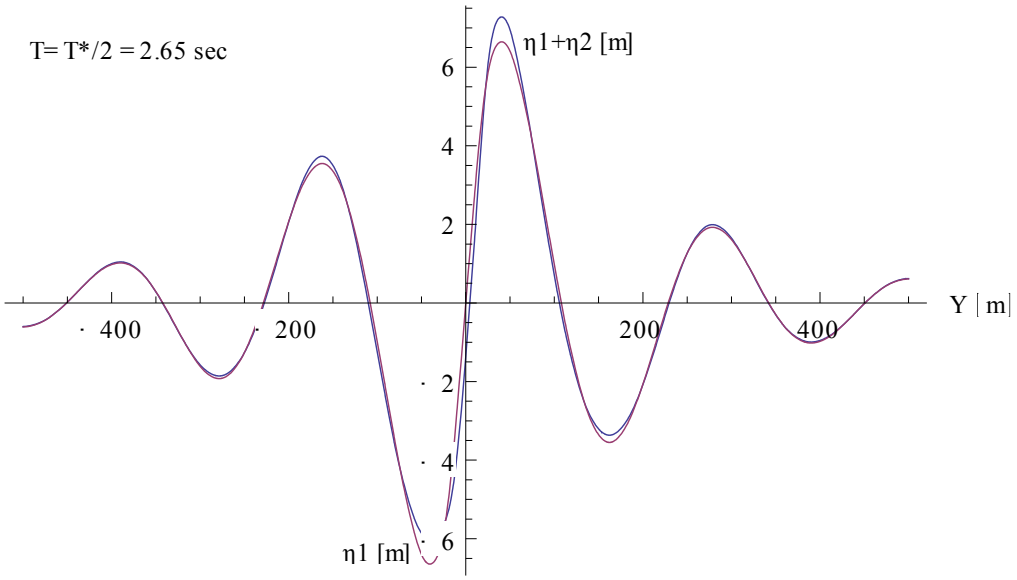

Figure A.3b: Linear component η_1[m] compared with the total second-order surface displacement $\eta_1 + \eta_2$ [m] in the space domain

REFERENCES

- Arena, F., "On non-linear very large sea wave groups", *Paper, ELSEVIER*, Italy (2005).
- Arena, F., Ascanelli, A., Nava, V., Pavone, D. and Romolo, A., "Three dimensional nonlinear random wave groups in intermediate water depth", *Paper, ELSEVIER*, Italy (2008).
- Atahanssoulis, G.A., "Wind Generated Sea Waves", *Course notes, NTUA,* Athens (2007).
- Belenky, V. and Sevastianov, N., "Stability and safety of Ships: Risk of Capsizing", 2nd Edition, *Society of Naval Architects and Marine Engineers (SNAME)*, New Jersey, USA, 2007, ISBN 0-939773-61-9.
- Boccotti, P., "Wave mechanics for ocean engineering", *Paper series, ELSEVIER*, Italy (2000).
- Gemmrich, J. and Garrett, C., "Dynamical and statistical explanations of observed occurrence rates of rogue waves", *Paper, Natural Hazards and Earth System Sciences*, Canada (2011).
- Hasselmann, K., Barnett, T.P., Bouws, E., Carlson, H., Cartwright, D.E., Enke, K., Ewing, J.A., Gienapp, H., Hasselmann, D.E., Kruseman, P., Meerburg, A., Muller, P., Olbers, D.J., Richter, K., Sell, W., and Walden, H., "Measurement of Wind-Wave Growth and Swell Decay During the Joint North Sea Wave Project (JONSWAP)", *Report, German Hydrographic Institute*, Hamburg (1973).
- Holmes, P.: "Coastal processes: Waves", University of West Indies, *Professional Development Programme: Coastal Infrastructure Design, Construction and Maintenance*, West Indies, (2001).
- Malara, G., Arena and F., Spanos, P.D, "On the interaction between random sea waves and a floating structure of rectangular cross section", *Sustainable Maritime Transportation and Exploitation of Sea Resources – Rizzuto & Guedes Soares (eds) © 2012 Taylor & Francis Group*, London, ISBN 978-0-415-62081-9.
- Spyrou, K.J., "Ship Rolling Stability and Regulation Background", *Course notes, NTUA,* Athens (2009).
- Stansell, P., Wolfram, J. and Linfoot, B., "Statistics of wave groups measured in the northern North Sea: comparisons between time series and spectral predictions", *Paper, ELSEVIER*, Edinburgh (2002).
- Themelis, N.I., "Probabilistic Assessment of Ship Dynamic Stability in Waves", *Doctoral Thesis, NTUA*, Athens (2008).